Foundations of Future Nuclear Power:

Legacy Reactor Antineutrino Monitoring and Fuel Security

A Dissertation Presented for the

Doctor of Philosophy

Degree

The University of Tennessee, Knoxville

Robert Jacob Carter

December 2024

Copyright © 2024 by Robert Jacob Carter

All rights reserved.

ACKNOWLEDGEMENTS

In a letter to Robert Hook, Sir Isaac Newton wrote, “If I have seen further, it is by standing on the shoulders of giants (Cleick, 2004).” The scientists, engineers, and educators from Oak Ridge National Laboratory (ORNL) and the University of Tennessee have encouraged me to see far beyond the horizon of my limited vision. I can’t possibly thank everyone individually, but I would be sorely remiss if I didn’t credit those who have been most helpful and supportive in my journey to understand physics better.

Gary Alley and Dan Archer are at the top of the list. Without their support, ORNL would not likely have hired a 55-year-old military retiree. Fifteen years later, I still owe my loyalty and gratitude to these two men who allowed this old airman to work in the laboratory I had dreamed of as a young man growing up in nearby Knoxville.

Irakli Garishvili allowed me to participate in his vision, the Compact HIFR Antineutrino Monitoring Platform (CHAMP). Dr. Garishvili has provided an unending stream of support and direction. Likewise, James Matta was a critical hardware and software contributor to CHAMP. Jason Nattress unselfishly donated his time to help set up a dedicated Linux Ubuntu computer for Geant4 experimentation. Mica Folsom designed and presented an excellent course in Geant4, C plus plus [C++] programming.

Nance Ericson and Bruce Warmack have been constant positive role models and sources of helpful information. I sincerely appreciate their mentorship and guidance.

I appreciate my committee’s time and valuable suggestions - Howard Hall (chair), Lawrence Heilbronn, Irakli Garishvili, and Jason Newby. I was about thirty percent complete on a separate topic under Jason Hayward when funding concerns and personal

health brought my dissertation effort to an abrupt halt. I'm deeply indebted to Dr. Hayward in the University's Nuclear Engineering Department for his support and encouragement. Howard Hall, Lawrence Heilbronn, and Eric Lukosi taught critical tools required to understand nuclear science aspects relevant to my previous work and this dissertation. Each mentored me in educator and academic excellence. In the aftermath of my previous attempt, Dr. Garishvili selflessly offered me the opportunity to manage his project and consult.

The University of Tennessee Science and Engineering (ESE) Department in the Bredesen Center allowed me to step out of my electrical engineering world and see the physical sciences from a new perspective. Lee Riedinger, then ESE program director, made this possible by granting me the department's first-ever part-time student status in a cohort-only program. My advisor, Allie Burnes, stood beside me against all odds through my cancer treatment to complete my degree. Without her, I doubt I would have made it. Abby Sherman helped me format this dissertation and kept me posted on graduation requirements and deadlines along with Rachel Roberts from the ESE program office. Abby serves as a one-woman publishing house for all theses and dissertations at the University of Tennessee in Knoxville. She always found time to answer every question and made herself available for consultation.

To the love of my life, Robbi Carter, who sacrificed countless evenings and weekends while I completed coursework and this dissertation, words can't describe my gratitude. An ORNL information technology systems administrator, she was instrumental in keeping my computers online and serviceable to complete this work.

PREFACE

The world of electrical engineers is composed of abstractions built upon abstractions. Abstractions like Thevenin and Norton's theorems provide the basis for circuit design and analysis. An engineer uses these abstractions to solve a problem.

Throughout my life, I lived in this world of electrical engineering. It was a great surprise to me to find that the world of physics was upside down compared to electrical engineering. Physicists see the answer and attempt to develop a question.

For example, when physicists first observed beta decay, the electron should have exhibited a monoenergetic spectrum, a single spectral line. Instead, the spectrum was continuous. Physicist Lionel Pauli postulated the question, "Where is this additional energy going?" The question was no less important than the observation to a physicist; perhaps it was more important. The question provided a framework for a new understanding of beta decay.

Since its birth, physics has repeatedly focused on observation and question postulation. With this approach, we consider how to help make neutrino detectors more compact, combining engineering and physics. Given background radiation levels, how much and what shielding would be required to provide a sufficiently quiet environment to detect antineutrinos generated from reactors?

This dissertation departs somewhat from the typical technical format. It reflects the empirical and non-empirical nature of Energy Science and Engineering, a field driven by qualitative and quantitative questions. What energy sources are likely to replace fossil fuels when they run out? How long will our global oil supplies last? How can we meet

our energy needs while protecting our environment? How much and what kinds of energy sources do we need globally? What renewable energy sources are likely available to us soon, on the research horizon, and beyond?

The introduction highlights Nobel Prize winners who contributed to understanding neutrino science. It also includes a section on Bruno Pontecorvo, who is considered by many to be a subject matter expert on neutrinos. Emmy Noether is also briefly mentioned because of her mathematical contributions. These distinguished scientists established the importance of this field of study.

What is novel about this dissertation? Successful neutrino detectors have typically been massive, requiring tons of detector material. This dissertation builds a case for a user facility to test and evaluate compact neutrino detectors. No facility like this currently exists, supported by current literature.

Periodically, researchers consider effective Z or the calculated number of protons in a unit measure of a compound. A comparison of four effective Z computer programs is applied to a specific radiation detection compound, sodium iodide thallium [NaI(Tl)], to determine correlations. The resulting data indicates discrepancies. While this comparison proved interesting, its importance for radiation detection and analysis appears to be minimal. Numerous computational tools and software toolkits are available to characterize shielding and radiation detection materials. These include manufacturer resources like Luxium's efficiency calculator (Luxium, 2024) and Monte Carlo software for particle tracking through matter including the GEometry ANd Tracking (Geant4) collaboration and Monte Carlo N-Particle Transport Code (MCNP6).

These are all parts of the technical fabric supporting legacy nuclear reactor performance and fuel characterization in future operations. However, new thorium molten salt modular reactors (MSR) in the prototype and testing phase won't require the same level of security monitoring because the fuel can't be easily weaponized.

Owing to a different isotopic weakly radioactive composition and low penetration of alpha particles for thorium [Th-232] and operational characteristics of MSRs, waste materials can have shorter-lived or smaller quantity waste products than uranium [U-235] and [U-238] in Pressurized Water Reactors (PWRs). PWRs account for about 73% of operational reactors globally. MSRs can be operated in a continuous fuel recycling mode. Fission products are continuously removed in this mode of operation (Cern, 2013). Even though thorium [Th-232] has a long half-life, about 14 billion years, it is fertile rather than fissile material.

The news isn't all good. MSR liquid fuel has a higher degree of chemical complexity than pressure water reactors, complicating isotope separation and waste management. MSR molten salt fuel is corrosive, tending to cause leakage problems in the reactor itself and waste storage containment leakage. The importance of continuing to operate legacy nuclear reactors and future molten salt reactors will become clear in the context of future global energy requirements.

ABSTRACT

Antineutrino detection and characterization promise to reduce the expense and labor required to verify legacy reactor fuel and operation. To realize this promise, the huge antineutrino detectors prevalent today, consisting of tons of active material, must be reduced to a manageable size on the order of a meter cubed. Charge-coupled and bolometric devices are the best candidates for compact antineutrino detectors.

Oak Ridge National Laboratory's high flux isotope reactor (HFIR) provides a controlled environment to establish a user facility to test compact antineutrino detectors. To this end, the Compact HIFR Antineutrino Monitoring Platform (CHAMP) project was established. The first step was to establish background radiation. This dissertation focuses on the design and implementation of the background detection system. The author drafted the research proposal, initiated, planned, executed, monitored, and controlled the project to complete the build and data collection in one month, considered record time, to meet schedule requirements at HFIR. The system was successfully constructed, and data was collected. Additional CHAMP milestones are on hold due to the Very Short Baseline Reactor Antineutrino Experiment (vIOLETA) collaboration established among twelve countries with over 200 researchers targeting the same goal as CHAMP.

The author evaluated theoretical tools to continue with the next phase of CHAMP as follows. A review of deterministic calculation for effective proton count (Z) of compounds composing sodium iodide detectors is included. Also included is an evaluation of Monte Carlo software including Geometry ANd Tracking, Version 4 (Geant4), Monte Carlo N-Particle Transport Code, Version 6 (MCNP6) coupled with

Attila, and Gamma Analysis for Dose and Risk Assessment Software (GADRAS), favoring MCNP6 including the Advanced Tool for the Transport of Ionizing Radiation (Attila). Geant4 is an open-source toolkit requiring significant computer science and C++ programming skills. MCNP6 and GADRAS are both stand-alone proprietary computer programs. GADRAS is less capable for particle transport modeling.

The author analyzed the need for future nuclear power based on projected global energy requirements as a function of projected population. Protecting the environment is critical. Nuclear power is critical in meeting energy consumption needs while safeguarding the environment.

TABLE OF CONTENTS

CHAPTER ONE INTRODUCTION AND GENERAL INFORMATION 1

The Beta Decay Conundrum 1

Detecting the Undetectable 3

The Man Behind the Scenes in Neutrino Science 9

Neutrino Sources 12

Radioactive Decay and Neutrinos 15

Betrayal: The Nucleus, Nothing Interesting Happens There 15

Structure of the atomic nucleus 15

Protons Contain Point-Like Structures 18

Reactor Antineutrino Production: The Flip Side 22

Nuclear Reactor Accidents and Public Opinion 26

Nuclear Power in a Larger Energy Context 28

CHAPTER TWO LITERATURE REVIEW 34

Light, Inverse Beta Decay 34

Candidates for Compact Antineutrino Detectors 34

Bolometric, Neutrino Detection 38

Charge, Coherent Elastic Neutrino-nucleus Scattering 38

Shrinking Neutrino Detectors: Charged Coupled Device Technology 42

Skipper Charge Coupled Device Physics 43

Skipper Charge Coupled Device Electronics 44

Detector Cavity Shielding at the High Flux Isotope Reactor 46

CHAPTER THREE MATERIALS AND METHODS 50

Compact HFIR Antineutrino Monitoring (CHAMP) 50
CHAMP Design 51
Scintillation 54
Photomultiplier Electronics 56
CHAPTER FOUR RESULTS AND DISCUSSION 60
Effective Atomic Number (Z) 60
Effective Atomic Number (Z) Calculation 62
Geant4 Requires Specialized Software Skills 69
MCNP6 and Attila 75
GADRAS Compared to MCNP6 77
CHAPTER FIVE CONCLUSIONS AND RECOMMENDATIONS 79
CHAMP Disposition and Reactor Security 79
Future Shielding for CHAMP 80
Future Shielding Analysis Tools for CHAMP 84
Energy Consumption Analysis 84
LIST OF REFERENCES AlPHABETICALLY BY YEAR 87
VITA 115

LIST OF TABLES

Table 1.1. Global nuclear reactor incidents. 29

Table 1.2. Two alternatives for total energy and per capita energy consumption in 2050. Modified from (Vanek, et al., 2012). 32

Table 4.1. NIST, Win XCOM attenuation values for carbon and fluorine. 66

Table 4.2. Substitution values for Equation 4.2. 66

LIST OF FIGURES

Figure 1.1. In Circa 1930, researchers were at a loss to explain why beta decay electron kinetic energy was distributed across a spectrum instead of a monoenergetic value (expected to be 1.182MeV). The unscaled intensity monoenergetic line from Hyperphysics, Georgia State University was added to this diagram. 2

Figure 1.2. Frederick Reines won the 1995 Nobel Prize in Physics for the first detection of antineutrinos using inverse beta decay. 4

Figure 1.3. Lederman, Schwartz, and Steinberger won the Nobel prize for discovery of the muon neutrino. 6

Figure 1.4. Ray Davis and Matoshi Koshiba won the 2002 Nobel Prize in Physics for detecting solar neutrinos. 7

Figure 1.5. Takaaki Kajita and Arthur B. McDonald were awarded the 2015 Nobel Prize in Physics for discovering neutrino oscillations, which “show that neutrinos have mass.”.....**Error! Bookmark not defined.**

Figure 1.6. Neutrinos are fundamental particles in three flavors: electron neutrinos [ν_e], muon neutrinos [ν_μ], and tau neutrinos [ν_τ] (Donev, 2017). .... **Error! Bookmark not defined.**

Figure 1.7. Known sources of neutrinos and antineutrinos. Humans are continuously bathed in neutrinos, the second most ubiquitous particle in nature next to photons (Gonzalez-Garcia, 2019). 13

Figure 1.8. Up and down quarks make up protons and neutrons, adapted from (Wright, 2019). 17

Figure 1.9. Putting pieces of the puzzle together showing nucleons were made of point-like charges (quarks). First Friedman and his group at the Stanford Linear Accelerator Center showed there were structures inside the proton and those structures had 1/2 spin. Then the CERN team found evidence of fractional charge in the structures. Modified from Looyen, 2020. 19

Figure 1.10. Callen and Gross (1973) simplified the relationship of $F_1(x)$ and $F_2(x)$ $2xF_1(x) = F_2(x)$. 21

Figure 1.11. Reactor antineutrino production. 23

Figure 1.12. The unexpected continuous energy spectrum of the electron. 23

Figure 1.13. Beta decay, finding a stable state. 25

Figure 1.14. The cost of International Atomic Energy Agency manual nuclear fuel verification. 27

Figure 1.15. According to two United Nations simulations world population is expected to peak in 2080. 31

Figure 2.1. Three ways to detect neutrinos, heat, charge, and light. 35

Figure 2.2. Principle of reactor operation verification with antineutrino monitors. The process for verifying reactor inventory integrity with antineutrinos bears similarities to biometric scans such as retinal identity verification. In retinal scans, an infrared beam traverses a person's retina (a) and the blood vessels, distinguishable by their higher light absorption (b) relative to other tissue, are mapped. The mapping is extracted and compared to a copy stored in a database (c), and if the two match, the person's identity is verified. Similarly, a nuclear reactor (g) continuously emits

antineutrinos which vary in flux and spectrum with the particular fuel isotopes undergoing fission (d). Some interact in a nearby detector (h) via inverse beta decay (e). The measured signal is compared to a reference copy stored in a database for the relevant reactor, initial fuel, and burnup (f); a sufficiently matching signal indicates that the core inventory has not been covertly altered. If the antineutrino flux of a perturbed reactor is sufficiently different from expected, a diversion can be concluded to have taken place (i) (Stewart, Abou-Jaoude, Erickson, 2019) 36

Figure 2.3. Examples of neutrino detectors, including KamLAND containing a 1000 ton mixture of mineral oil, benzene, and fluorescent chemicals. All these detectors are huge, measuring on the order of 20 m^3. 37

Figure 2.4. Antineutrino reactor inverse beta decay detectors have been used for decades. However, CCD and bolometric CEvNS detectors are more likely candidates for size reduction on the order of a meter cubed. CHAMP could provide a test chamber for these detectors at the ORNL HIFR facility. 39

Figure 2.5. A sketch of the CEvNS interaction (2022, COHERENT Collaboration). 41

Figure 2.6. CEvNS provides a couple of orders of magnitude higher cross section than inverse beta decay. 41

Figure 2.7. The initial design of a reverse biased charge-coupled device pixel, ... 45

Figure 2.8. A bandgap diagram representing the reverse biased metal oxide semiconductor (MOS) gate in depletion mode. Modified from (2024, Dholahiya). 45

Figure 2.9. The basic CCD design concept. As the gate voltages change charges are transported from left to right (Smith, 2010). Depletion regions have sometimes been

referred to as a bucket brigade similar to water buckets (depletion reqions) passing water (charge) from left to right..... 47
Figure 2.10. Buried channel CCD developed to mitigate trapping (semantecscholar.org, 2024). 48
Figure 2.11. Energy band structure for a buried-channel CCD. A potential well forms below the semiconductor-oxide interface in the n-type silicon preventing minority carrier trapping (Rottinger, 1999). 48
Figure 3.1. SOLIDWORKS design placement for 24 Saint-Gobains Model ZX4H16/2SS, 2 X 4 X 16” NaI(Tl) dectectors and lead separator plates (courtesy of Brandon Longmire). 52
Figure 3.2. The CHAMP experimental radiation background collection station located at HFIR. 53
Figure 3.3. Given the Geant 4 mono-energetic gamma ray input spectrum shown in red, the blue response function results for a Saint-Gobains model ZX4H16/2SS 2x4x16” NaI(Tl) crystal (modified from Matta, 2021). 53
Figure 3.4. The Saint-Gobains (now Luxium Solutions) model ZX4H16/2SS 2x4x16” NaI(Tl) detector on the left with it’s Geant4 graphic representation on the right. Note the orange circle denoting entry of a mono-energetic 15.0MeV gamma ray and it’s subsequent reaction with the crystal shown in green. The translucent Geant4 crystal envelope represents the detector’s steel cladding (modified from Matta, 2021). 55
Figure 3.5. A basic photomultiplier diagram. Light impinging on the photo cathode produces electrons. These are in turn multiplied by voltage attracted dynodes.

Electrons are collected at the anode representing the original radiation detected within the scintillator (Molecular Expressions, 2019). 57
Figure 3.6. Photomultiplier tube schematic used for CHAMP NaI(Tl) detectors (Fabris, 2021). 57
Figure 3.7. This double-sided printed circuit board (front and back) designed with KiCad contains the basic design in the schematic of Figure 3.6 (Fabris, 2021)…….....58
Figure 3.8. Mechanical connections for the 24 CHAMP custom photomultiplier tube bases (SolidWorks housing design provided courtesy of Paul Nogradi)..... 59
Figure 4.1. Zeff-toolkit: Mann, et al., (2016) [average of three calculations – Taylor, et Al. (2012); Manohara, et Al. (2008); Singh et Al. (2012)]..... 61
Figure 4.2. Alpha Spectra detector for this calculation is wrapped in Teflon with a protective aluminum foil cover inside an aluminum container. The figure was drawn using IronCAD. 63
Figure 4.3. NIST, Win XCOM graphs for fully specified Teflon parameters as listed.... 68
Figure 4.4. This configuration provided limited success. Geant4 demonstration programs including some modifications proved successful. However, complex geometries using three-dimensional CAD programs like SolidWorks repeatedly failed. Instigating make or an integrated development environment (IDE) provides final preparation for compiling.Qt or “cute” displays a two-dimensional image of the three-dimensional Geant4 simulation output. Although written in C++, Qt can be bound to other languages like Python. Geant4 has its own visualization options, but Qt allows for more user-friendly, customized visual representations of simulation

data. Qt also allows users to develop graphical user interfaces like simulation control panels to start, stop, and configure simulations. Data visualization using plots and graphs to represent data along with user input management with forms or dialogs is another possibility with Qt. 71
Figure 4.5. A simplified approach to incorporate Geant4 incorporating Windows 10 failed to provide a stable programming platform. 71
Figure 4.6. Programs are often created using compiled languages making use of dynamic linked libraries (Windows) or shared libraries (Linux, Unix) to run (Modified from Anton, 2017 and Hawaii.edu, 2019). 73
Figure 4.7 CMake is a cross platform build system generator (Loggini, 2020). 73
Figure 4.8. Git version control is widely used along with the GitHub service used to host Git repositories. Geant4 libraries are all available on GitHub (modified from Nemerever, 2019). 74
Figure 4.9. Geometry input using SpaceClaim and display with tecplot in Attila coupled with MCNP6 do not require large external library downloads or expertise in multiple other software programs and tools as opposed to Geant4..... 76
Figure 4.10. Responses in a 2 x 4” sodium iodide detector from a cesium 137 source (a) in a GADRAS simulation and (b) experimentally displayed using EasyPeak. 78
Figure 5.1. (a) Collimated sources reduce buildup. (b) Collimation could be incorporated in antineutrino detectors (the height and width of the detector) to reduce background radiation buildup from the reactor and detector shielding. However, some buildup would still be a factor..... 81

Figure 5.2. Shielding innovations to explore in future CHAMP development. An example of Py-MLBUF is included in the upper right corner..... 83

CHAPTER ONE
INTRODUCTION AND GENERAL INFORMATION

The Beta Decay Conundrum

The year was 1930. Scientists were perplexed by a mystery of nature; radioactive beta decay emitted electrons across a spectrum of energy. Theoretical physics predicted monoenergetic electrons, as shown in **Figure 1.1**. Where was this lost energy going? In desperation, Wolfgang Pauli theorized a new particle called the neutron. When Chadwick discovered the neutron in 1932, Enrico Fermi renamed Pauli's particle the neutrino, Italian for "little neutral one (Shef, 2013)." This neutral particle, believed to be massless, presented a problem for experimental physicists. Many top scientists, including Pauli, believed the electron neutrino could never be detected.

The theory predicted neutrinos and symmetry played a part in the hypothesis. Enter the Noether Theorem. Emmy Noether, a brilliant mathematician, helped Einstein refine his theory of general relativity (Rowe, 2021). Her theorem included symmetrical techniques used later by scientists to establish conservation laws governing neutrinos and gave scientists clues on what to look for as they searched for neutrinos.

Perhaps her most significant achievements were her dedication, determination, and selfless knowledge-sharing with students. She initially attended mathematics classes in Germany as an observer. Women in the early 1900s were not allowed to attend institutions of higher learning. For over a decade, she worked in the shadow of universities without compensation. Most people have never heard of Emmy Noether, yet history records her as one of the most brilliant mathematicians of her time.

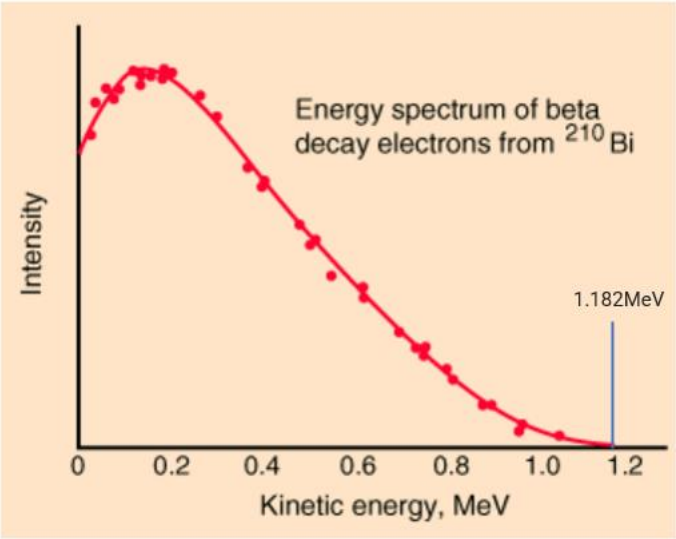


Figure 1.1. In Circa 1930, researchers were at a loss to explain why beta decay electron kinetic energy was distributed across a spectrum instead of a monoenergetic value (expected to be 1.182MeV). The unscaled intensity monoenergetic line from Hyperphysics, Georgia State University was added to this diagram.

Decades later, using 10 tons of equipment, Reines and Cowan ran the first successful antineutrino reactor experiment. Their 1956 Poltergeist Experiment marked the earliest recorded antineutrino detection (Giunti, Kim, 2007).

Detecting the Undetectable

"Those Who … Have Conferred the Greatest Benefit to Humankind."

-Alfred Nobel

Pauli was confident of the neutrino's undetectability. He cabled the funding committee for the Reines and Cowan experiment, recommending not funding their neutrino detection project (Rajasekaran, 2016). Fortunately, his cable arrived too late to affect the committee's decision. Reines and Cowan were the first to detect the antineutrino in 1954 using inverse beta decay detection. Reines received the 1995 Nobel Prize in Physics for his co-detection of the neutrino (**Figure 1.2**) (Nobel, 2014). Cowan died two decades earlier. The Nobel Committee does not award prizes posthumously. Owing to perseverance and determination, neutrino researchers have received four Nobel Prize awards in physics. The significance of these awards speaks to the importance of neutrino research.

Reines and Cowan started their Poltergeist experiment at the Hanford reactor in Washington State in 1953 (Reines, Cowan, 1953). Their method detected two gamma rays separated by 5.5 microseconds (Close, 2012). Electron-positron annihilation generated the first pulse and neutron capture in the second.

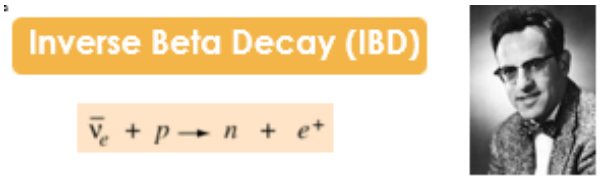


Figure 1.2. Frederick Reines won the 1995 Nobel Prize in Physics for the first detection of antineutrinos using inverse beta decay (Nobel, 2014).

The experiment moved to Savannah River, Aiken, South Carolina, for better shielding against cosmic rays. The shielding location was 11 m from the reactor 12 m underground. Shielding for Poltergeist included 4 to 6 feet of paraffin alternated with 4 to 8 inches of lead. Reines and Cowan installed a six-foot thick water shield above the detector to help shield against cosmic rays. The more correct description of the neutrino they detected would be the electron antineutrino (Close, 2012).

An interesting side note: the source of cosmic rays is unknown. Magnetic fields change the direction of these charged particles, so their reverse vector does not point to their origin. Scientists believe most Cosmic rays come from outside our galaxy (Drury, 2012). A relatively quiet environment to detect antineutrinos requires cosmic ray shielding.

In 1962, when scientists were only aware of electron neutrinos, researchers Lederman, Schwartz, and Steinberger were instrumental in using Brookhaven National Laboratory's Alternating Gradient Synchrotron to identify a new particle (**Figure 1.3**). This device generated a beam of energetic protons to produce a shower of pi mesons, which traveled 70 feet to a 5,000-ton steel wall. On their journey, they decayed into muons and neutrinos. The steel wall made of old battleship plates blocked the muons. The neutrinos, however, were unimpeded and continued into a neon-filled spark chamber detector, proving the existence of previously unknown muon neutrinos (Nobel, 2019).

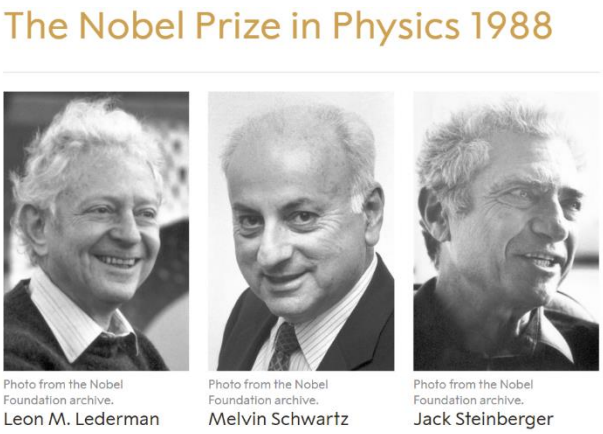


Figure 1.3. Lederman, Schwartz, and Steinberger won the Nobel prize for discovery of the muon neutrino (Nobel, 2019).

Ray Davis had regrettably attempted to detect “neutrinos” produced by a reactor. As Reines and Cowan proved, reactors produce antineutrinos. Although disheartened by what he perceived as a failure, Davis persevered. Switching from fission to fusion reactors, he successfully detected the sun’s neutrinos in 1969, winning the Nobel Prize for his work in 2002 (**Figure 1.4)**.

In 1998, Takaaki Kajita reported that neutrinos had mass after observing only half as many neutrinos coming from below the Earth as from above directly from the sun. His measurements came from the Super-Kamiokande experiment. Arthur McDonald at the Sudbury Neutrino Observatory reported neutrino oscillations in 2001, proving neutrinos have mass. In 2015, Kajita and McDonald were jointly awarded the Nobel Prize in Physics for their work (Error! Reference source not found.**)** (Nobel, 2019).

Scientists have proven neutrinos are subatomic particles that come in three flavors: electron neutrinos [ν_e], muon neutrinos [ν_μ], and tau neutrinos [ν_τ] **(**Error! Reference source not found.). An international collaboration of 54 physicists proved the existence of Tau neutrinos at the Department of Energy’s Fermi National Accelerator Laboratory (Hazi, 2007).



Davis built a pilot experiment 2,300 feet underground in a limestone mine near Akron, Ohio. In 1965, he went deeper still—to Homestake’s 4850 Level.

Figure 1.4. Ray Davis and Matoshi Koshiba won the 2002 Nobel Prize in Physics for detecting solar neutrinos (Nobel, 2019).

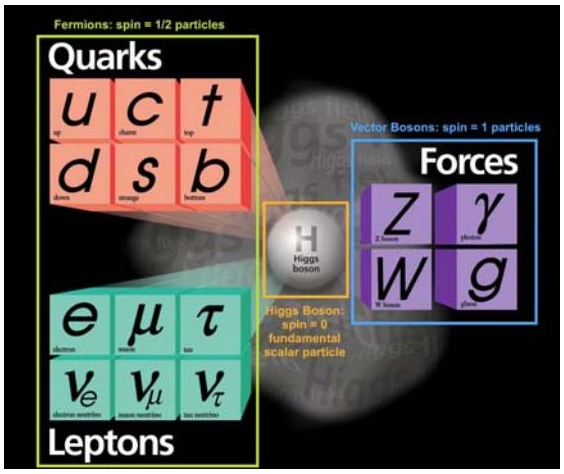


Figure 1.5. Neutrinos are fundamental particles in three flavors: electron neutrinos [ν_e], muon neutrinos [ν_μ], and tau neutrinos [ν_τ] (Donev, 2017).

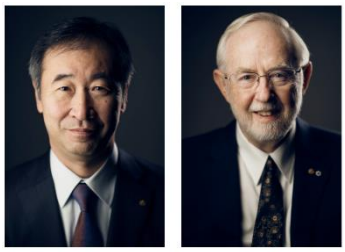


Figure 1.6. Takaaki Kajita and Arthur B. McDonald were awarded the 2015 Nobel Prize in Physics for discovering neutrino oscillations, which "show that neutrinos have mass (Nobel, 2019)."

The Man Behind the Scenes in Neutrino Science

"Great and strange ideas transcending experience often have less effect upon men and women than smaller, more tangible considerations."

- H. G. Wells, Invisible Man

Conspicuous in his absence from the previous section is Bruno Pontecorvo, a man who was as productive in his ideas about neutrino physics as his political convictions were contentious. Pontecorvo is a fascinating scientist to consider in the story of neutrino physics. Unless otherwise cited, information in this section came from (Close, 2015). Studying the scientist and his research environment is as vital as learning the science (IOM, NAS, NAE, 2009). Rarely can one find a more intriguing case study in this regard than Bruno Pontecorvo, arguably the most brilliant physicist in the history of neutrino physics. Although not explicitly related to neutrinos, Pontecorvo's observation and investigation of slow neutrons' efficacy eventually became important in nuclear power. During what has been termed the golden age of nuclear physics from the mid-1930s to the mid-1950s (Cook, 2006), science, scientists, and security clearances were popular topics. Bruno Pontecorvo was pivotal in studying particle neutrino physics theory and experimental investigation in the context of these three topics.

Born in Pisa, Italy, in 1913, Bruno was the fourth of eight children, three girls and five boys. He was considered the least intelligent of his siblings. For this reason, he may have worked harder to prove himself.

At age sixteen, he entered Pisa University, majoring in engineering. Technical drawing proved a dull subject for him. After two years, he switched to physics at La Sapienza

University in Rome. After graduation, he assisted Enrico Fermi, noting an odd difference in neutron production depending on the surface where he performed his experiments. The investigation eventually resulted in heavy water and graphite reactor materials to slow neutrons for added interaction in splitting nuclei to produce more neutrons (CERN, 2013).

Three years later, in 1936, as WWII unfolded in Italy, the political climate proved unfriendly to Jewish families like the Pontecorvos, so Bruno moved to Paris to work with Irène and Frédéric Joliot-Curie (Close, 2015). Many intellectuals preferred Russian communism to German and Axis Power Italian fascism. Among those individuals was Frédéric, who would profoundly influence Bruno, turning him into a devout communist. Bruno's political choice would one day affect his security clearance and coerce him into an unfortunate exile.

As the Germans flooded into northern France, Bruno fled south 300 miles by bicycle. He escaped WWII in Europe with his wife and daughter to Tulsa, Oklahoma, where he worked on neutron logging to identify likely oil reserves. Unknown to him, this experience would become helpful in developing the heavy water nuclear reactor at Chalk River Laboratory in Canada (Close, 2015).

The Manhattan Project acquired all the uranium and nuclear science equipment available in the United States, making Pontecorvo's development and testing of his oil logging systems impossible. In 1943, he accepted a position at Chalk River, Ontario, Canada.

The Canadians were attempting to build a heavy water reactor. Uranium had been discovered in Canada. Pontecorvo's means of identifying oil reserves also proved beneficial in searching for uranium.

During his six years at Chalk River, he was instrumental in building Onterio's Zero Energy Experimental Pile (ZEEP) and National Research Experimental (NRX) heavy water reactors, but he also developed fundamental science theories. Pontecorvo theorized these revelations (Close, 2015).

- The weak interaction is a universal force of nature.
- The muon, a heavy electron version, has a unique flavor.
- There are distinct varieties of neutrinos.
- Neutrinos oscillate between varieties.

Pontecorvo left Chalk River in January 1949, accepting a position at Harwell Atomic Energy Research Establishment in the United Kingdom. For those who had known Bruno Pontecorvo, the next few years in history became cloudy visions of unsubstantiated rumors and innuendo.

With the United States still reeling from the deceptions of various spies, including Klaus Fuchs, Harry Gold, Julius and Ethel Rosenberg, and David Greenglass, who shared classified nuclear science information with the Russians, McCarthyism left no stone unturned in its search for foreign agents (Close, 2015). Given Pontecorvo's previous dedication to communism and his friendship with Fuchs, he came under suspicion.

Neither Military British Intelligence (MI5) nor U.S. intelligence had hard evidence of any spying activity by Pontecorvo. Britain decided to transfer Pontecorvo from his government laboratory into an unclassified University faculty appointment. Before moving out of Harwell, Pontecorvo and his family took an extended European holiday in the summer of 1950 (Close, 2015).

Pontecorvo and family mysteriously disappeared that summer without a trace. In a clandestine detour, the Pontecorvos defected to Russia. From a scientific point of view, Bruno Pontecorvo's future work from the summer of 1950 forward was sequestered behind the Iron Curtain, where he received the highest Russian scientific honors.

In his elder years, he was allowed to leave the Soviet Union and gave interviews to several authors eager to tell his story. Pontecorvo described a recurring dream. In this dream, as a young man, he made a mistake in a scientific calculation, carrying the error forward throughout his future work.

He had made no such error. His restrained scientific freedom and lack of access to Western high-energy physics experimental capability restricted his research. His dream implied that he had misjudged his decision to defect to Russia, resulting in forty-three years of sequestered science.

Neutrino Sources

Refer to **Figure 1.7** courtesy of (Gonzalez-Garcia, 2019). The universe has been generating ubiquitous neutrinos since the beginning of time. Scientists estimate the Big Bang gave birth to 330 neutrinos for every cubic centimeter, each with an energy of

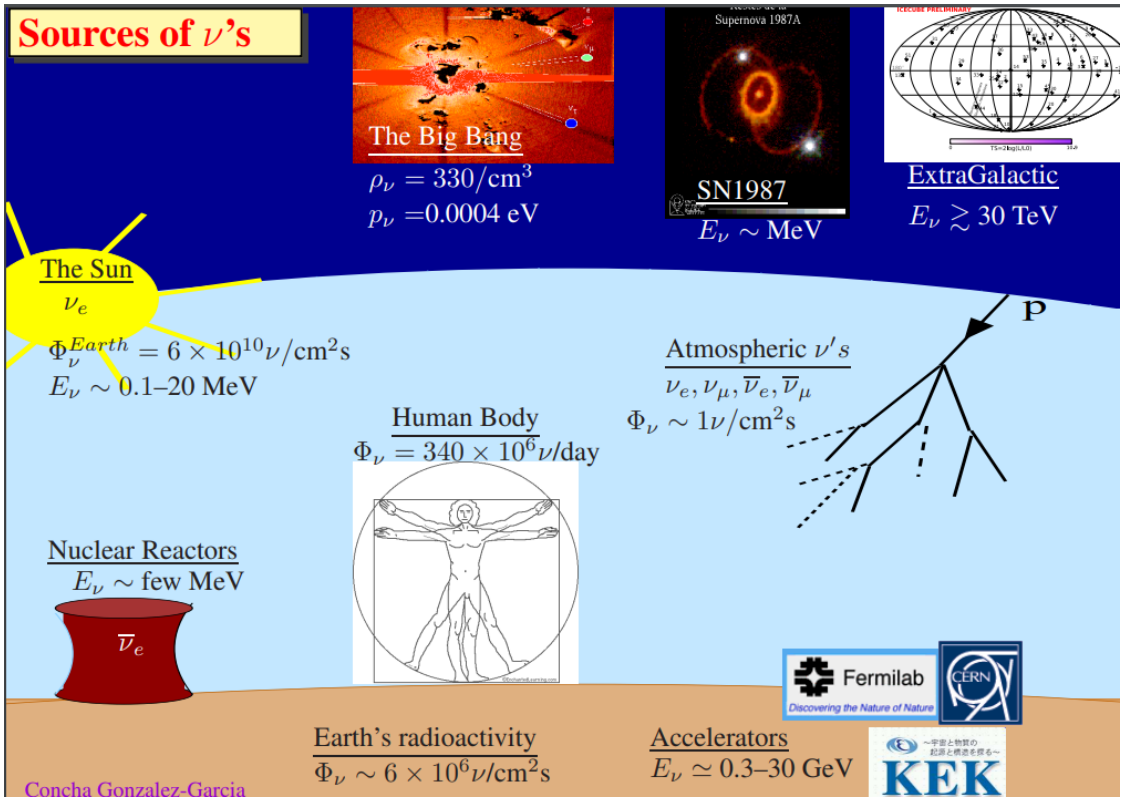


Figure 1.7. Known sources of neutrinos and antineutrinos. Humans are continuously bathed in neutrinos, the second most ubiquitous particle in nature next to photons (Gonzalez-Garcia, 2019).

0.0004 electron volts [eV]. Since the Big Bang, other celestial phenomena have continued to generate large numbers of neutrinos.

One example is a supernova, SN1987, generating neutrinos in the megaelectronvolt [MeV] range. Even more energetic neutrinos come from outside the galaxy on the order of 30 teraelectronvolt [TeV]. Cosmic rays also hit the Earth's atmosphere, interacting with atmospheric atoms and causing a cascade of neutrinos with an area flux of about one in each centimeter squared.

The source of cosmic rays is unknown. Magnetic fields change the direction of these charged particles, so their reverse vector does not point to their origin. Scientists believe most Cosmic rays come from outside our galaxy (Drury, 2012).

Closer to Earth, the sun is a constant source of 0.1-20 Mev neutrinos. Its fusion energy reaction spews out some 6×10^{10} neutrinos through every square inch of area. The Earth's natural radioactive decay elements are responsible for 6×10^{6} neutrinos per square centimeter flux.

Man's effort to duplicate the sun's fusion reaction with the International Thermonuclear Experimental Reactor (ITER) project continues to elude mankind. ITER is billions of dollars over budget and over a decade behind schedule (Seife, 2023). What are the motivations for this costly and time-consuming project? In just one hour the energy from the sun's fusion reaction hitting the earth is enough to supply all the world's power requirements for a year (NREL, 2024). Man could have clean power virtually forever.

Manufactured reactors generate antineutrinos with energy in the order of 5 MeV (Dodd, Gripaios, 2020). For high-energy neutrinos the calculated value of the cross-section for the laboratory frame of reference σ_{LAB} as follows (Fukugita, Yanagida, 2003),

$$\sigma_{LAB}\ (\nu_e + e^- \rightarrow \ \ e^- + \ \nu_e) = \ \sigma_0 \ \frac{E_{ve}}{m_e} \qquad \text{Equation 1-1}$$

Where, σ_0 = 9 x 10^{-45} cm^2 is a constant value

Reactor neutrinos have a cross section around 10^{-43} cm^2.

Adding humankind's accelerator 0.3-30 gigaelectronvolts [GeV] neutrinos into the mix, these particles bathe every human on Earth with roughly 340 x 10^6 neutrinos daily. Even still, perhaps only two or three will react within any person during their lifetime. While this low interaction is suitable for human survival, it doesn't bode well for scientists attempting to detect these ghost-like particles. The tiny cross-section, low neutrino mass, and high speed make them nearly undetectable.

Radioactive Decay and Neutrinos

Students were taught the nucleus was composed of neutrons and protons. These nucleons, together with electrons, were the elemental building blocks of all matter (Mannheim, 1986). Nuclear physics for the 1970s electrical engineering student consisted almost entirely of calculating nuclear half-live.

Betrayal: The Nucleus, Nothing Interesting Happens There

Structure of the atomic nucleus

An electrical engineering student of the 1970s studying nuclear science today could be excused from feeling betrayed by his original undergraduate college physics courses. At

that time, the atom's outer shell electrons were the focus of electrical engineering. To these students, nothing interesting happened in the nucleus for their discipline. Undergraduate engineering physics and electrical engineering in the seventies drew this picture of the atom for students. First, electrons were most important to electrical engineering. There was nothing of interest in the nucleus for mainstream electrical engineers. Engineering physics and chemistry at the time discussed decay in the most general terms, focusing on half-life calculations. For electrical engineering students the nucleus consisted of two elementary particles, the neutron and proton. During the previous decade, theoretical physicists Murray Gell-Mann and George Zweig began to question this view of the nucleus. In 1964, they proposed quarks (Allday, 2018).

An electrical engineering student in the seventies would be if he chose to delve more deeply into the physics of the nucleus presented in **Figure 1.8**. The nucleus is composed of elementary up and down quark particles. The up quark has a +2/3 electron charge. The down quark has a -1/3 electron charge. Two down and one up quarks together form a neutral charge neutron. Two up and one down quarks together form a plus one electron charge proton (Wright, 2019).

The theory became fact when Friedman, Kendall, and Taylor found evidence of quarks within protons published in 1968. Why wasn't this research integrated into the 1970s electrical engineering physics education? Gell-Mann, arguably the leader in quark theory, said quarks are fictitious at the 1972 Eighth International Conference on High Energy Physics in Geneva, Switzerland (Kaiser, 2020). Definitive research to confirm the

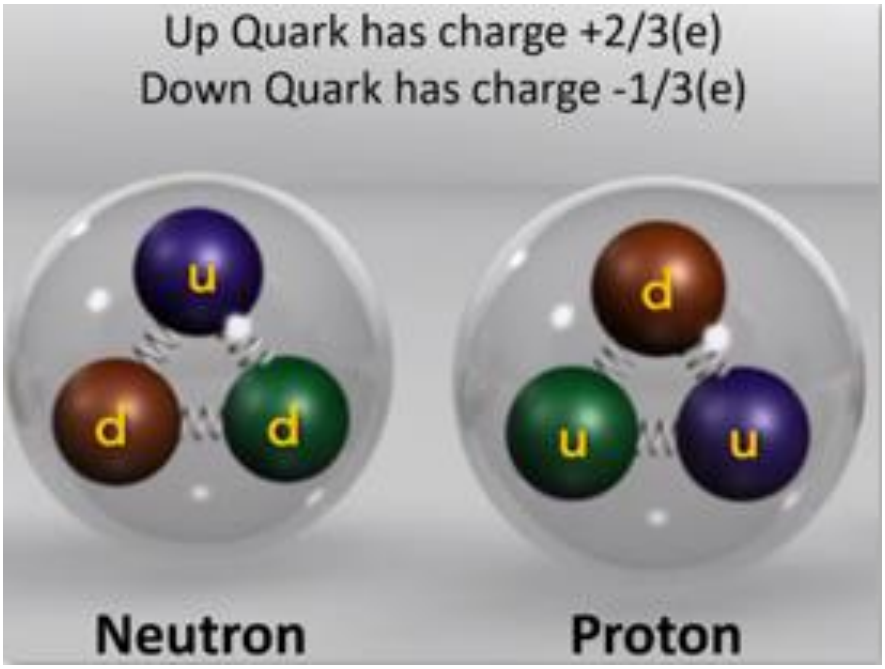


Figure 1.8. Up and down quarks make up protons and neutrons, adapted from (Wright, 2019).

existence of quarks continued into the late 1970s. Combined research developed experimentally verified quarks (**Figure 1.9**).

Protons Contain Point-Like Structures

In his 1991 Nobel Prize acceptance speech, Friedman said the primary purpose of the inelastic program was to study the electro-production of resonances as a function of momentum transfer. He describes two unexpected result***s*** of an investigation into the deep inelastic region bombarding protons with high-energy electrons.

First is weak [q^2] dependence, where q is the four-momentum transfer. Four-momentum transfer consists of a space-time vector. Energy and momentum's X, Y, and Z components comprise the four-momentum vector. Energy describes what is carried through time.

The cross-section [σ] on the vertical axis of Figure 1.9 describes the likelihood of the electron interacting with a proton. The Mott cross section [σ_{Mott}] describes Coulomb scattering off a nucleus. The Coulomb scattering law states that the force between two charged particles is proportional to the charged products and inversely proportional to the distance between them (Hernandez, 2017).

Friedman and his team expected a strong [q^2] dependence, indicating elastic scattering between the high-energy electron and proton, similar to billiard balls. In that case, the proton would be an elemental particle with no internal structure. Instead, the weak [q^2] dependence implied a structure within the proton. (Gell-Mann, 1964) and (Zweig, 1964) suggested the possibility of quarks while (Feynman, 1972) hypothesized more general

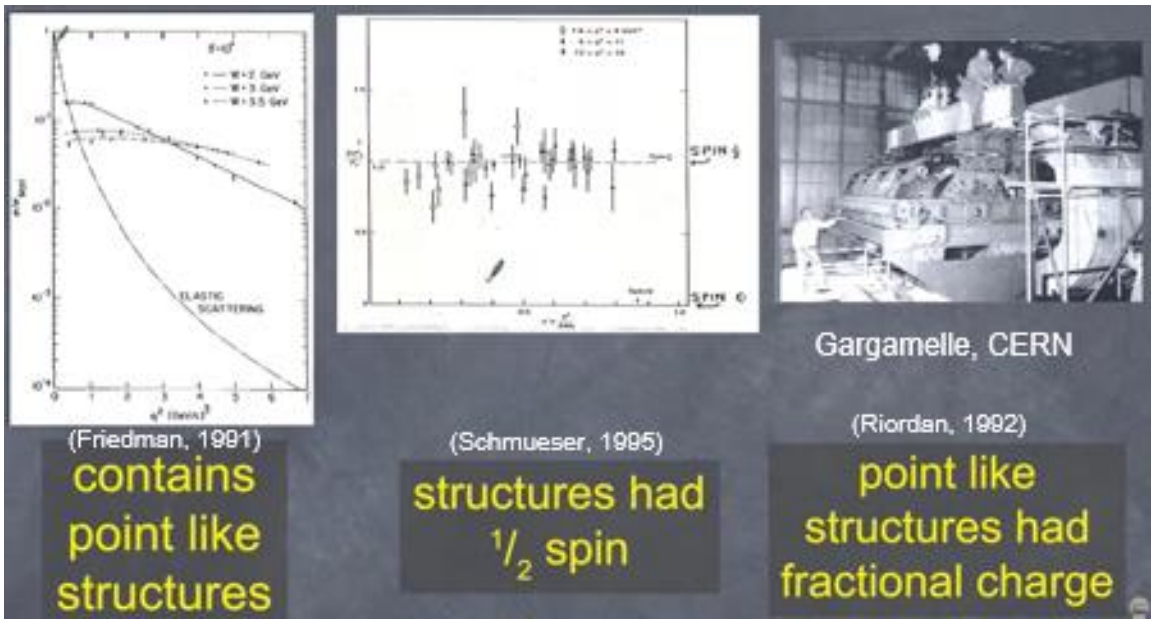


Figure 1.9. Putting pieces of the puzzle together showing nucleons were made of point-like charges (quarks). First Friedman and his group at the Stanford Linear Accelerator Center showed there were structures inside the proton and those structures had 1/2 spin. Then the CERN team found evidence of fractional charge in the structures. Modified from Looyen, 2020.

particles called partons. As late as 1972, Gell-Mann expressed little faith in the actual existence of quarks. The idea was more of a mathematical solution to unexplained experimental results. Friedman and his team were well on the way to proving the existence of quarks.

Another surprise Freeman discussed in his Nobel Prize speech was scaling as stated by the Bjorken hypothesis: at large energies and momentum transfers, the cross section depends on one variable only. The photon no longer scatters coherently off the nucleon, but solely sees point-like structures, partons (Bjorken, 1968). Bjorken characterized inelastic scattering as follows in equations 1.1 and 1.2.

$$\mathrm{m_p W_1}(\nu, Q^2) \longrightarrow \mathrm{F_1}(x) \qquad \text{Equation 1-2}$$

$$\frac{Q^2}{2\mathrm{m_p}x}\mathrm{W_2}(\nu, Q^2) \longrightarrow \mathrm{F_2}(x) \qquad \text{Equation 1-3}$$

Callen and Gross (1973) simplified the relationships further depicted in **Figure 1.10**. Deep inelastic scattering built a strong case for the existence of physical spin ½ quarks. But what about the fractional charges proposed for quarks? Krauss (2009) discusses how electron, proton scattering (Friedman, 1991) and CERN, Gargamelle neutrino, proton scattering as described by (Riordan, 1992) both supported the fractional charge theory leading to today's conception of quarks composing nucleons previously shown in Figure 1.8.

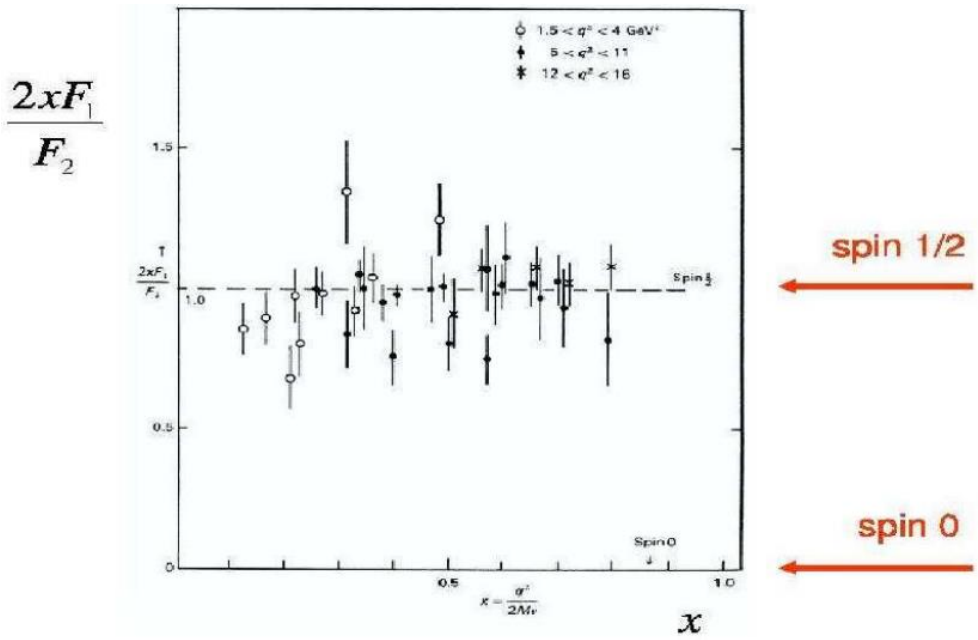


Figure 1.10. Callen and Gross (1973) simplified the relationship of $F_1(x)$ and $F_2(x)$ $2xF_1(x) = F_2(x)$.

Reactor Antineutrino Production: The Flip Side

Considering **Figure 1.11** recall [Z] is the atomic number or proton number of an atom. [A] is the atomic mass or the number of protons and neutrons together (Callen, Gross 1973). Note the difference between parent and daughter. While atomic mass remains the same the number of protons has increased by one. In other words, a neutron has flipped to become a proton.

In fission, the neutron composed of two down quarks and an up quark, flips to a proton with two up quarks and a down quark. Two primary physical laws come into play, the conservation of charge and the conservation of energy (Lang, 2013).

The greater mass of the neutron than the proton has to be accounted for. Nature's bookkeeper passes part of that mass to the expelled electron. The original theory predicted a monoenergetic electron in the reaction of **Figure 1.11**.

Experimentalists didn't see monoenergetic electrons. Instead, they measured a spectrum of lower-energy electrons (**Figure 1.12**). Where was this energy going? This was a grave problem for physicists. It appeared the conservation of energy was violated in beta decay. Linus Pauli came to the rescue when he theorized an additional particle he called the neutron in 1930. As a result, physicists were then faced with a new problem. How could they detect a particle with no charge and zero or near zero mass?

Enrico Fermi gave this idea a concrete foundation in his beta decay theory, renaming Pauli's particle, neutrino (little neutral one) in 1932. Also, in 1932 James Chadwick reported the discovery of the neutron.

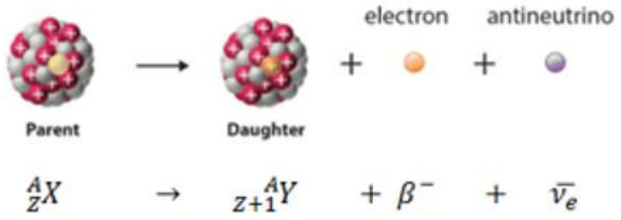


Figure 1.11. Reactor antineutrino production.

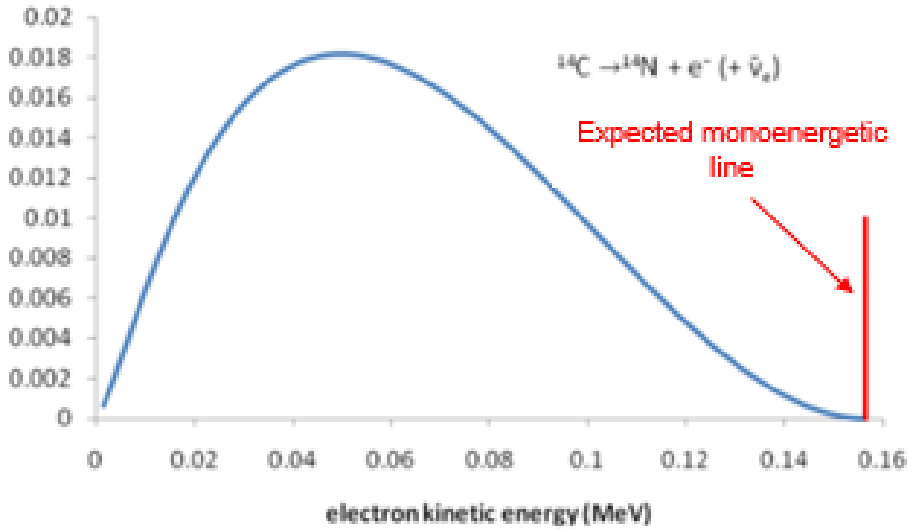


Figure 1.12. The unexpected continuous energy spectrum of the electron. Graphic provided courtesy of the T2K Experiment Team in Japan studying neutrino oscillation (T2K, 2020). The monoenergetic line is not to scale.

In a twist of nature something miraculous happens unfamiliar to humans in their classical physical world. **Figure** 1.13 attempts to shed some light on this phenomenon. Don Lincoln at the Fermi Lab explained it this way, [$\Delta E\ \Delta t \geq h/4\pi$] is relevant; however, "a W boson is a vibration of the W field and it can transfer its energy into the electron/neutrino field. Right now, we don't have a perfect understanding of the mechanism. Instead, we have a number we call the "coupling" which is a measure of the strength of the interaction" (Don Lincoln, 2021). In other words, we have a mathematical model accurately describing what we observe. However, this mathematics represents an abstraction, not a complete understanding.

Physicists often describe nuclear decay as a proton changing into a neutron. However, an up quark changes into a down quark. Saakyan (2013) and Gilmore (2008) discuss nuclear decay. The simple explanation is energy minimalization. Radioactive atoms seek their lowest energy state referred to as an energy parabola for a single element (Saakyan, 2013) or energy valley for multiple elements (Gilmore, 2008).

In beta decay, to attain a lower energy state, a down quark changes into an up quark transforming a neutron into a proton (Resag, 2018). Einstein's equation $E=mc^2$ quantitatively describes how much energy will be created in the W^- Boson field as the difference in mass between the neutron and proton (Dalager, 2024).

The vibrating W^-Boson field transfers its energy to the neutrino and electron fields, and out pops an antineutrino and an electron. These elemental particles account for most of the neutron and proton mass difference. Any excess energy provides kinetic energy to the antineutrino and electron.

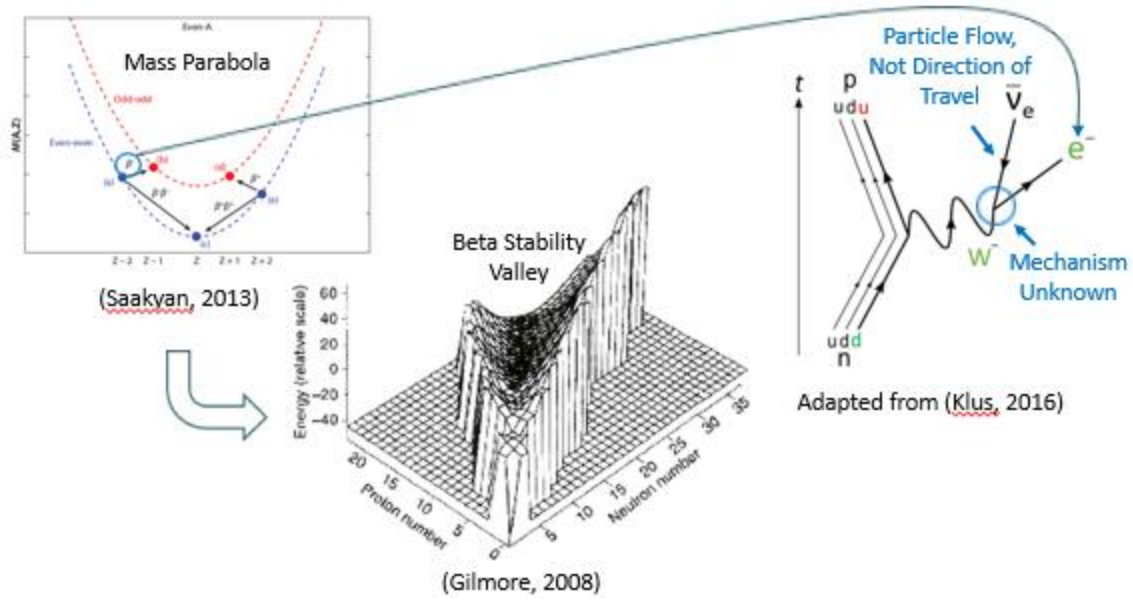


Figure 1.13. Beta decay, finding a stable state.

It’s important to recognize, these elemental particles weren’t constituents of the neutron. In other words, they weren’t originally part of the neutron. Energy and mass are two sides of the same coin. The mass difference between the neutron and proton transforms into energy (Pal, 2015). That energy is transformed into mass as an antineutrino and an electron. Leftover energy propels the two elemental particles away from the radiation decay site.

While this explanation and a few equations seem persuasive, the truth is; scientists don’t understand the mechanism behind the generation of these two elemental particles. Why is a W-Boson field vibration generated? Why not in some other field? How does the Boson energy transform into matter, the antineutrino an electron? What determines how much kinetic energy is imparted to each of these elemental particles? Are they elemental particles? These are all questions without answers. Mankind may still live in the dark ages of science and technology. There are so many unanswered questions.

Nuclear Reactor Accidents and Public Opinion

The focus so far has been directed toward legacy nuclear reactors, hinting at the possibility of using antineutrino monitoring both to determine when reactors are active and eventually to characterize fuel. Fuel characterization is a laborious and costly process necessary to ensure nuclear materials are accounted for and securely stored. Individual fuel rods must be inspected and characterized at a cost of about $156 million united states dollars annually (**Figure 1.14**).

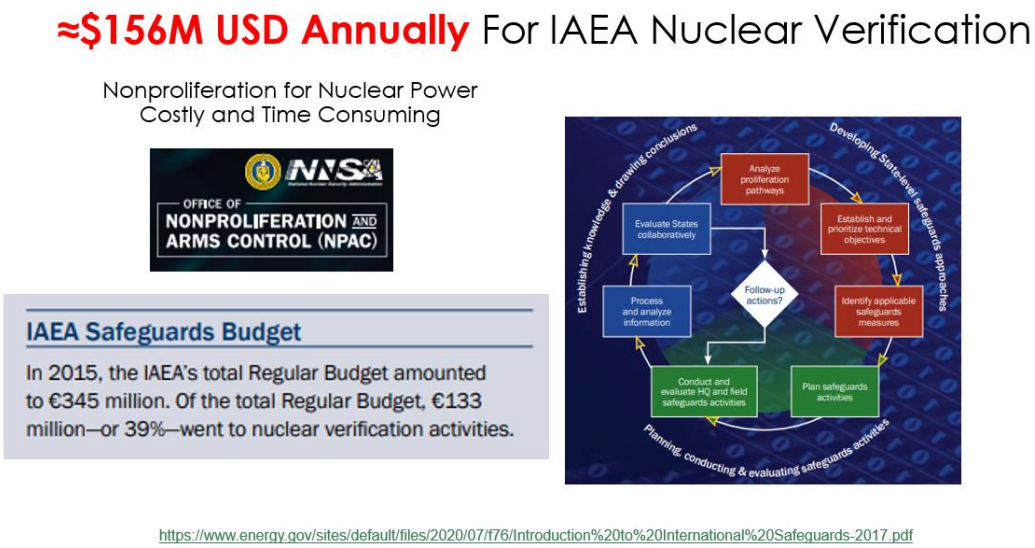


Figure 1.14. The cost of International Atomic Energy Agency manual nuclear fuel verification (Department of Energy, 2023).

Nuclear power however is publicly unpopular, especially in the United States where just over four percent of the world's population suffered almost thirty percent of global reactor incidents. Nuclear power plant incidents are big news. Like commercial aviation, incidents often receive disproportionate, sensationalized news coverage. Citizens may favor nuclear power, but most prefer not to live near reactors.

Consider the list of nuclear reactor incidents from 1948 to 2011 listed in **Table 1.1** (Marquet, 2022). The International Nuclear and Radiological Event Scale (INES) could be used to rate these incidents between zero and seven (Domenech, 2024). Arguably, three accidents were primarily responsible for developing negative public opinion. Three Mile Island and Fukushima Daiichi were INES level 5 accidents with wider consequences. These resulted in significantly releasing radioactive material impacting the environment and requiring public protection. Chernobyl was a catastrophic accident rated INES 7, a major accident with severe impacts on the environment and public health. Negative perceptions of nuclear power in the public must be overcome before nuclear power can flourish. Given the risks and high capital investment, why does the world need nuclear power?

Nuclear Power in a Larger Energy Context

Meeting future global energy consumption requirements is a complex issue. The United Nations considers climate change control to be one of its highest priorities. Energy consumption sits at the pentacle of that priority. No discussion about these issues could be complete without addressing the global population. The good news is that United

Table 1.1. Global nuclear reactor incidents (Marquet, 2022).

Year	Reactor	Location	Incident Summary
1948	Zoe	France	Near criticality accident
1952	Chalk River	Canada	Cooling system failure, major release of radioactive material
1957	Kyshtym	Russia	Nuclear waste storage explosion, major contamination
1957	Windscale	UK	Reactor fire, significant radiation release
1958	Vinca	Serbia	Criticality accident
1959	Santa Susana	USA	Core flow blockage
1960	Browning	USA	Criticality accident, no serious injuries
1961	SL-1	USA	Steam explosion kills three operators
1961	Idaho Falls	USA	Control rod ejection
1961	Submarine K-19	Russia	Primary coolant loss
1966	Fermi-1	USA	Sodium cooled fuel melting
1967	Chapelcross	UK	Magnesium cladding melting & CO2 blockage
1967	Siloe	France	Fuel plates melting
1969	Lucens	Switzerland	Partial fuel rod fusion
1969	Eaux A1	France	Coolant loss, minor radioactive gas release
1976	Bohunice A1	Czech	Coolant loss, core overheat, ≈ 1k Ci release
1979	Three Mile Island	USA	Partial meltdown, small radioactive gas release
1980	Eaux A2	France	Coolant loss, minor radioactive gas release
1983	Constituyentes RA-2	Argentina	Criticality accident, 1 death
1986	Chernobyl	Ukraine	Catastrophic explosion, widespread contamination
1989	Vandellos	Spain	Turbo-blower fire
1990	Zion	USA	Radioactive water leak
2003	Paks	Hungary	Cooling system failure, no radiation release
2011	Fukushima Daiichi	Japan	Earthquakes & tsunamis caused meltdowns in three reactors, radioactive material release

Nations simulations shown in **Figure 1.15** are predicting a peak in the world's population from the current 8 billion to about 10 billion in 2080 and a decline afterward (United Nations, 2024). This is a change in previous calculations from 2013, when the world population was projected to continue at higher levels for a longer period.

Projections of population, energy consumption, energy supply, and environmental pollution are based on assumptions of multiple variable parameters. Consider the two alternatives in **Table 1.2** (Vanek, et al., 2012). Both alternatives add up to the same total energy consumption, 631 exajoules [EJ] or 631 * 10^{18} joules implying this value is a 2050 expected limit on global energy growth for that year.

The U.S. Energy Information Administration (EIA) projects, "increasing population and income offset the effects of declining energy and carbon intensity on emissions." The projection identifies China as the primary source of energy-related carbon dioxide [CO_2] emissions through 2025 (EIA, 2023).

The International Energy Agency (IEA) published a 2021 world energy consumption of 418 EJ with a 2.2 percent growth in 2023 or about 427 EJ (Enerdata, 2024). Given these numbers, the world can expect to increase energy usage by about 48 percent over the next two and a half decades by 2025, estimated at 631 EJ. Mitigating carbon dioxide emissions will require both renewable and nuclear power additions during that timeframe (EIA, 2023).

For those who doubt man is aggravating the natural global warming cycle consider that about 97 percent of actively publishing climate scientists support consensus that man's

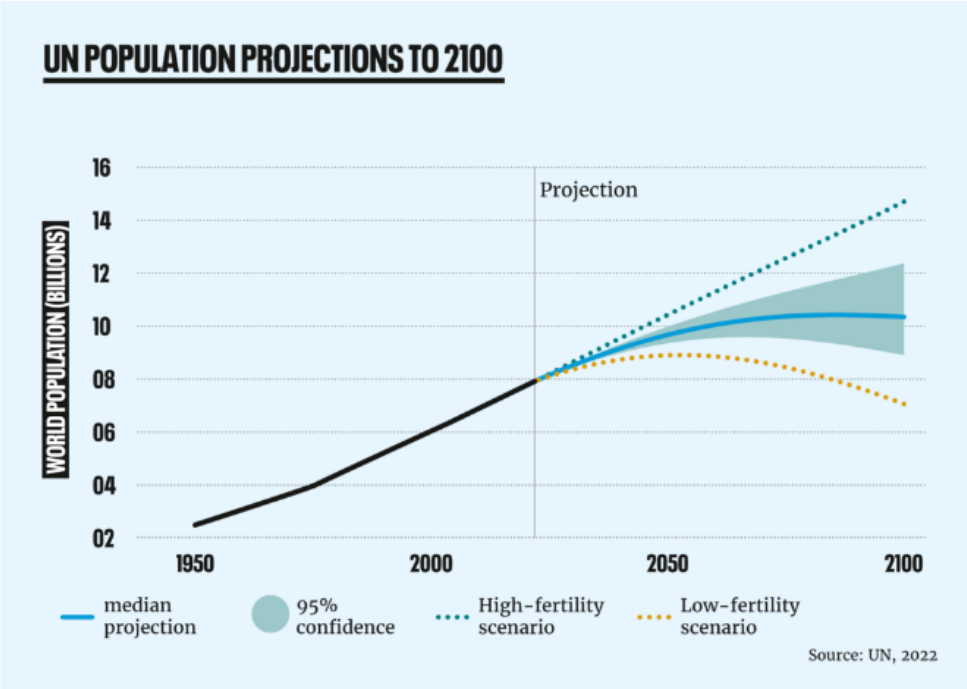


Figure 1.15. According to two United Nations simulations world population is expected to peak in 2080 (United Nations, 2024).

Table 1.2. Two alternatives for total energy and per capita energy consumption in 2050. Modified from (Vanek, et al., 2012).

Parameter	Industrial Nations	Emerging Nations
Population, 2050 (Billions)	1.2	7.7
Alternative 1 assumptions	Constant per capita consumption	Total energy remaining
Energy/capita (GJ/pers)	194	52
Energy use (EJ)	231	400
Change in energy/capita	+/- 0%	+ 34%
Alternative 2 assumptions	Decreased consumption due to efficiency	Increase energy capacity (20TW*year)
Energy/capita (GJ/pers)	100	66
Energy use (EJ)	119	512
Change in energy/capita	-48%	+71%

burning of fossil fuels is driving climate change based on 11,944 peer reviewed papers (Cook, et al., 2016). Fossil fuel combustion isn't the only contributor by man to climate change. Deforestation, land use changes, agriculture, and industrial processes are also contributors. However, the United Nations says man's use of fossil fuels including coal, oil and gas account for 75% of global greenhouse gas emissions and nearly 90% of all carbon dioxide emissions (United Nations, 2024).

CHAPTER TWO

LITERATURE REVIEW

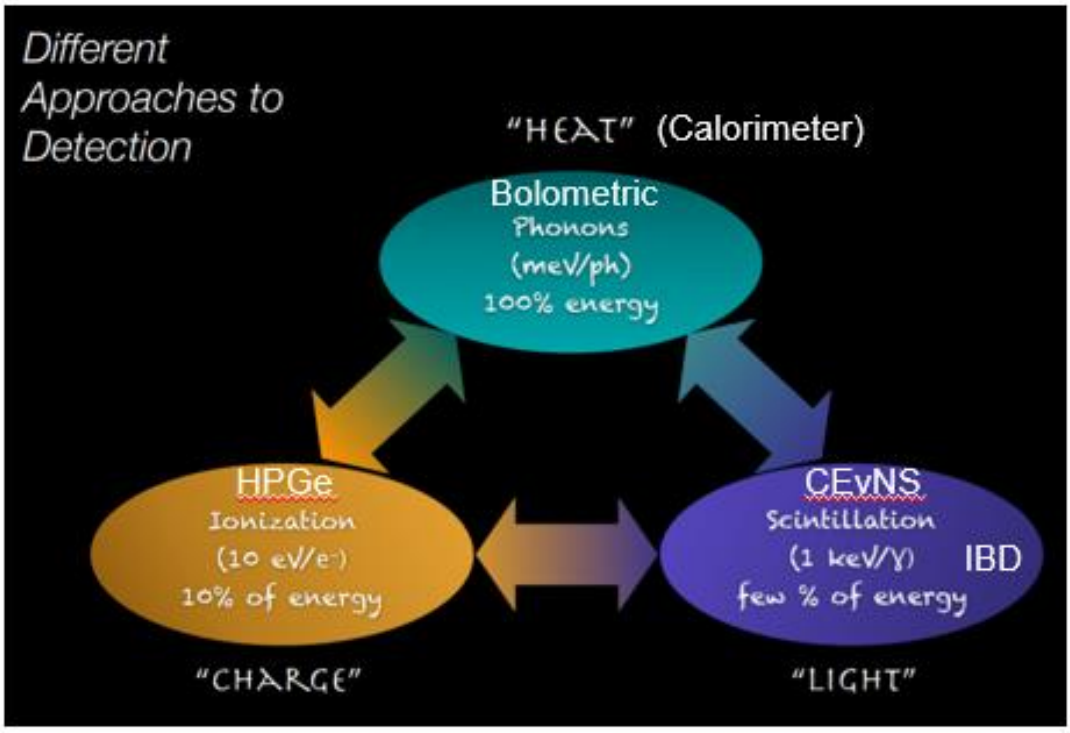
There are three primary solutions to neutrino detection. Neutrinos can be detected through light, heat, or charge (**Figure 2.1**). Bolometric detectors rely on changes in heat. The downside is the additional cryogenic equipment required. High-purity germanium detectors rely on charge. Inverse Beta decay relies on scintillation. The Reines-Cowan detector and the Coherent Elastic Neutrino Nucleus Scattering (CEvNS) detector at ORNL's Spallation Neutron Source rely on scintillation (Newby, 2020) (Miranda, et al., 2020.

Light, Inverse Beta Decay

Inverse Beta decay can be used to identify antineutrino flux and spectrum. This information can be analyzed to determine nuclear fuel quantity and composition (**Figure 2.2**). The problem is solved except for one major drawback. Most antineutrino detectors have something in common. They're huge, measured in tons of active mass (**Figure 2.3**). Note the detector material is listed in tons. Thompson (2024) describes the Super-Kamiokande neutrino detector containing 50,000 tons of water. The hope and the dream is to develop an antineutrino detector on the order of a cubic meter.

Candidates for Compact Antineutrino Detectors

Phil Barbeau from Duke University presented a lecture on the COHERENT CEvNS Experiment (2021, Barbeau). He discussed the broad scope of COHERENT and its implications. In email exchanges, Dr. Barbeau identified probable best candidate neutrino detectors for meter cubed size. He specifically mentioned two detectors: CEvNS, Charge



https://www.physics.umass.edu/acfi/sites/acfi/files/slides/cevns_umass_2019.pdf

Figure 2.1. Three ways to detect neutrinos, heat, charge, and light (Formaggio, 2019).

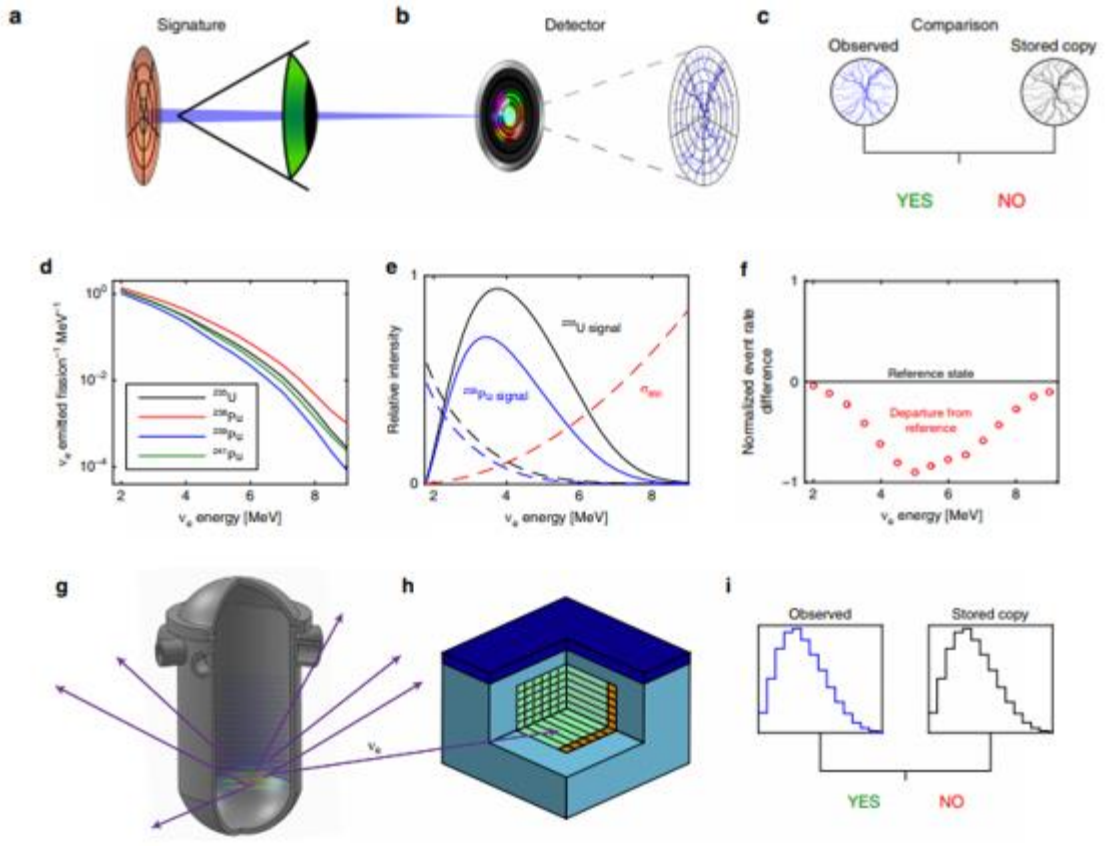
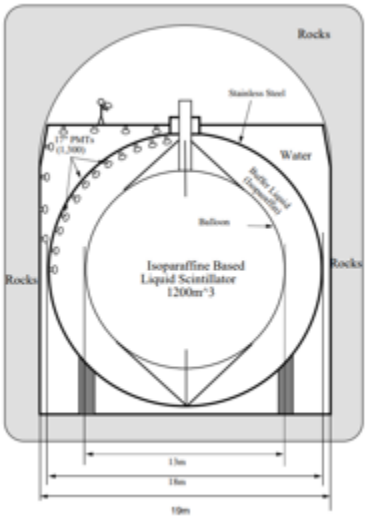


Figure 2.2. Principle of reactor operation verification with antineutrino monitors. The process for verifying reactor inventory integrity with antineutrinos bears similarities to biometric scans such as retinal identity verification. In retinal scans, an infrared beam traverses a person's retina (a) and the blood vessels, distinguishable by their higher light absorption (b) relative to other tissue, are mapped. The mapping is extracted and compared to a copy stored in a database (c), and if the two match, the person's identity is verified. Similarly, a nuclear reactor (g) continuously emits antineutrinos which vary in flux and spectrum with the particular fuel isotopes undergoing fission (d). Some interact in a nearby detector (h) via inverse beta decay (e). The measured signal is compared to a reference copy stored in a database for the relevant reactor, initial fuel, and burnup (f); a sufficiently matching signal indicates that the core inventory has not been covertly altered. If the antineutrino flux of a perturbed reactor is sufficiently different from expected, a diversion can be concluded to have taken place (i) (Stewart, et al., 2019)

Experiment	Reaction	Active mass (ton) & detector	E_{th} (MeV)	Location	Period
CHOOZ	$\bar{\nu}_e p \rightarrow e^+ n$	5 Gd-LS	1.8	Ardennes, France	1997–1998
Gösgen	$\bar{\nu}_e p \rightarrow e^+ n$	377 liter LS	1.8	Gösgen Switzerland	1985–
Double CHOOZ	$\bar{\nu}_e p \rightarrow e^+ n$	10.16 Gd-LS	1.8	Ardennes, France	2010–2015
Nucifer	$\bar{\nu}_e p \rightarrow e^+ n$	850liter Gd-LS	1.8	CEA-Saclay, France	2012
NEOS	$\bar{\nu}_e p \rightarrow e^+ n$	~1 Gd-LS	1.8	Younggwang, Korea	2015–2016
Neutrino-4	$\bar{\nu}_e p \rightarrow e^+ n$	$1.8m^3$ volume Gd-LS	~1.8	Dimitrovgrand, Russia.	2016–Present
STEREO	$\bar{\nu}_e p \rightarrow e^+ n$	Gd-LS	~2.0	Grenoble, France	2016–Present
RENO	$\bar{\nu}_e p \rightarrow e^+ n$	16 Gd-LS	1.8	Younggwang, Korea	2011–Present

(Athar, Singh, 2020)



KamLAND experiment

Figure 2.3. Examples of neutrino detectors, including KamLAND containing a 1000 ton mixture of mineral oil, benzene, and fluorescent chemicals. All these detectors are huge, measuring on the order of 20 m^3.

Coupled Device (CCD), and bolometric (Figure 2.4).

The High Flux Isotope Reactor (HFIR), located at Oak Ridge National Laboratory, operated at 85 megawatts (MW), provides the highest reactor-based neutron source for research in the United States (HFIR, 2024). By extension, this reactor also provides a rich source of antineutrinos. HFIR has a relatively short 24-day refueling cycle. This cycle offers a comparatively consistent omnidirectional stream of energetic antineutrinos.

The relatively small signal source of antineutrinos compared to other radiation encourages eliminating as many variables as possible. Since HFIR uses only highly enriched uranium-235, it provides a relatively unambiguous spectral signature.

The Compact HFIR Antineutrino Monitoring Platform (CHAMP) based in HFIR could provide a unique test chamber for advanced antineutrino detectors on the order of a meter cubed.

Bolometric, Neutrino Detection

Bolometric detectors measure energy changes as temperature variations. They are extremely sensitive and can detect small amounts of energy, making them suitable for observing the small energy depositions resulting from CEvNS events. These detectors require added bulky cryogenic equipment and are outside the scope of this research.

Charge, Coherent Elastic Neutrino-nucleus Scattering

Kate Scholberg, Department of Physics, Duke University, discusses the coherent elastic neutrino-nucleus scattering acronym (Scholberg, 2015). With several abbreviations in the literature (e.g., CNS, CNNS, CENNS), she favors CEvNS. Replacing the first “N” with a “v” for “neutrino” makes sense. “NN” means “nucleon-nucleon” to many in the nuclear

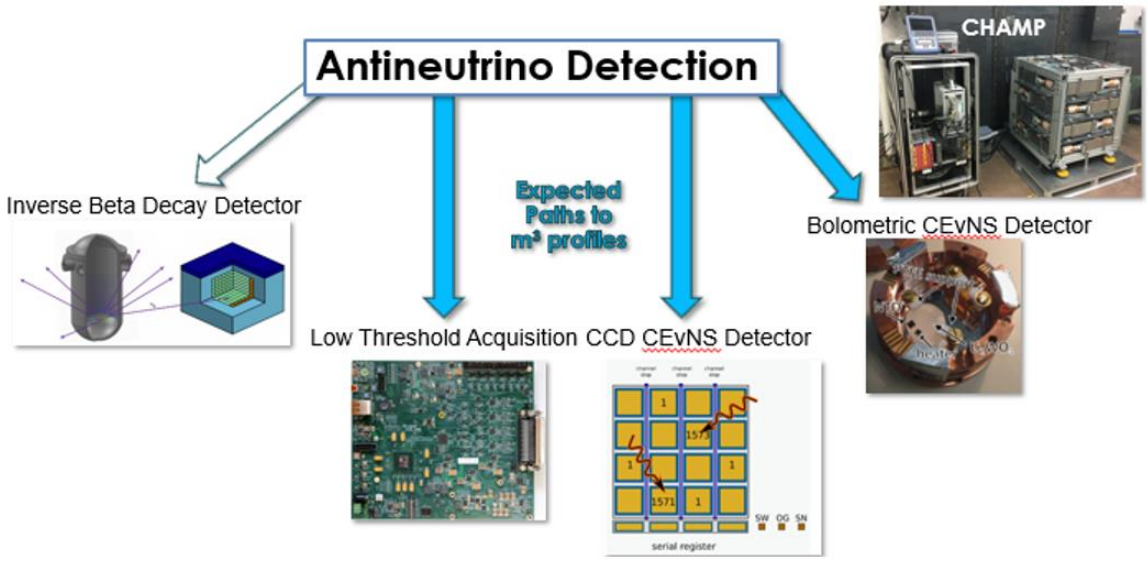


Figure 2.4. Antineutrino reactor inverse beta decay detectors have been used for decades. However, CCD and bolometric CEvNS detectors are more likely candidates for size reduction on the order of a meter cubed. CHAMP could provide a test chamber for these detectors at the ORNL HIFR facility.

physics community. CENNS is the name of an experimental collaboration. The Roman letter "ν" is readily available on ubiquitous English QWERTY Keyboards. The Greek letter "ν" is commonly used for neutrino, but is not a typical keyboard character.

Dr. Scholberg noted the Spallation Neutron Source (SNS) in Oak Ridge, TN, as an excellent neutrino source (Bolozdynys et al., 2012) for detection experiments. The SNS uses a proton beam energy of about 1 gigavolt [GeV] incident on a liquid mercury target for total power up to 1.4 megawatts [MW] and yields about 8×10^{14} neutrinos per flavor per second produced at the source. The COHERENT collaboration experiment in Neutrino Alley at the SNS made the first-light measurement of CEvNS on cesium iodide [CsI] in 2017 (COHERENT Collaboration, 2017) and the first measurement on argon in 2020 (COHERENT Collaboration, 2021). While detection physics, instrumentation, and experimental apparatus are complex, the basic CEvNS concept is simple (**Figure 2.5**) and it is a couple of orders of magnitude higher cross section than inverse beta decay (**Figure 2.6)**.

The neutrino scattering coherently off the whole nucleus results in sensitivity to the square of the total weak charge of the nucleus. This could enhance the coherent scattering cross-section by a factor of 10 to 100 when compared to neutrino-nucleon scattering (Fernandez-Moroni, 2022). Neutrinos interact with the entire nucleus in coherent scattering rather than individual nucleons (Munteanu, 2021). Elastic scattering refers to neutrinos bouncing off the nucleus without losing energy.

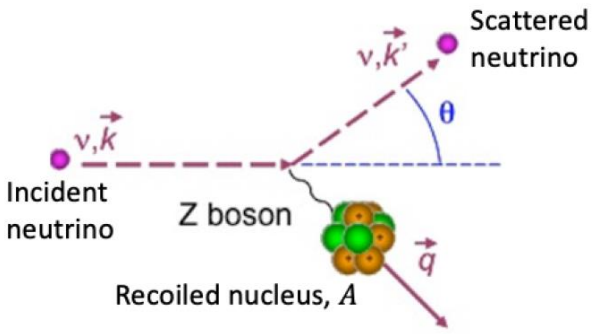


Figure 2.5. A sketch of the CEvNS interaction (COHERENT Collaboration, 2022).

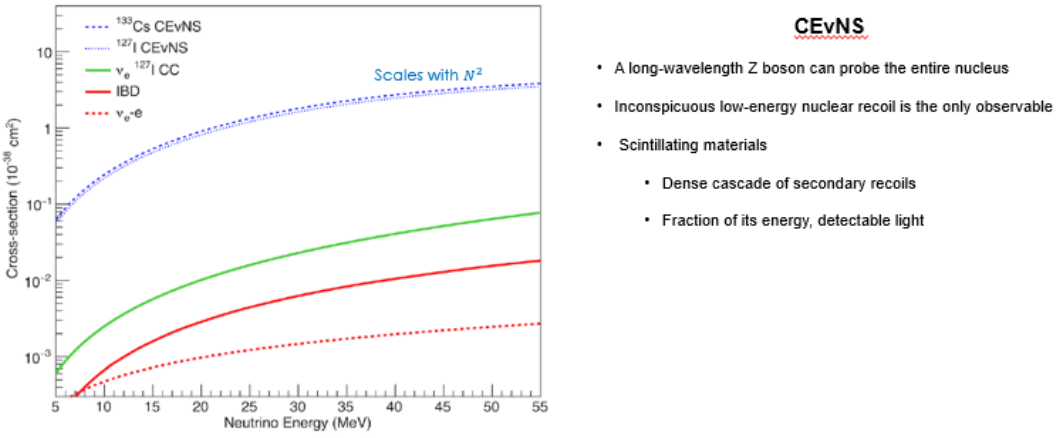


Figure 2.6. CEvNS provides a couple of orders of magnitude higher cross section than inverse beta decay (Barbeau, 2021).

Oak Ridge National Laboratory (ORNL) describes the CEvNS low energy nuclear recoil signature as it is slightly moved by the neutrino impact as an elephant recoiling after being "bumped by a mosquito (ORNL, 2024)." The formidable technical challenges described by ORNL include low detector thresholds with large target masses, incredibly low backgrounds, and an intense neutrino source.

ORNL's Spallation Neutron Source (SNS) includes neutrino alley, an experimental high-energy source producing all three currently known neutrino flavors: electron, muon, and tau. It has an energy of 1.4 megawatts [MW] and produces about 8×10^{14} neutrinos per flavor per second (Scholberg, 2015). While this experimental apparatus is quite large, it provides a first step in the development process to enable CEvNS reactor detectors on the order of a meter cubed.

Shrinking Neutrino Detectors: Charged Coupled Device Technology

Phil Barbeau, an antineutrino researcher at Duke University, had this to say about neutrino detectors: Charge-coupled device (CCD) or bolometric technology is the most promising for providing detectors in a meter cubed profile. Because of the additional cryogenic cooling equipment, bolometric detectors might be larger (Barbeau, 2021). Leaving cryogenic equipment and bolometric devices for future discussion, CCDs can achieve readout noises at the lowest fraction of electrons. To reduce dark current thermal fluctuations, the sensor is operated at a low temperature, about 140° Kelvin.

Skipper-CCD, developed at Lawrence Berkeley National Laboratory, is a p-channel CCD fabricated on high resistivity n-type silicon fully depleted at a substrate voltage of 40 V.

The sensor is up to 675 micrometers thick and composed of 15 um x 15 um square pixels (Fernandez, et al., 2024).

Skipper Charge Coupled Device Physics

Skipper CCDs detect the translation from nuclear recoil energy to ionization energy encoded by the quenching factor. The quenching factor refers to the process of converting energy from a nuclear recoil event into a detectable signal. It accounts for the fact that not all the energy transferred to the nucleus ends up as ionization; some of it can be lost in other forms of energy or affect the interaction in ways that reduce the amount of ionization produced (Fernandez et al., 2024).

Neutrinos interact with silicon nuclei in the Skipper CCD, producing a measurable charge. Skipper CCDs are particularly advantageous because they can accumulate and measure charge with extremely high precision, allowing them to detect even the faint signals produced by low-energy neutrino interactions.

As the recoiling nucleus moves through the material, it can ionize atoms. This means that it can knock electrons out of their orbits, creating electron-ion pairs. The total amount of ionization energy generated is related to the nucleus's recoil energy (Fields, 2014).

Guaranteed single-carrier accounting capability time spent reading the charge for each pixel is on the order of 10 milliseconds [ms]. This corresponds to about 0.2 electron charge [e^-] of readout noise. Because of this slow readout, active shielding cannot be used to mitigate cosmic ray background interference (Fernandez-Moroni et al., 2022).

Skipper Charge Coupled Device Electronics

Physicists Willard Boyle and George Smith were attempting to find a more affordable way of storing bits of data in computers than using magnetic bubble memory at Bell Laboratories in the mid-1960s. However, their successful charge-coupled device design in 1969 did not impact the computer industry (Smith, 2010). Instead, it revolutionized camera imaging, eventually leading to innovative solid-state particle physics detector applications.

In his Nobel Lecture, Smith made a remarkable revelation. Together, he and Boyle developed the basic idea for CCD camera technology in a one-hour brainstorming session. A week later, they built the first crude metal oxide semiconductor (MOS) prototype using photolithography techniques. Metal oxide semiconductors (MOS) provided a primary enabling technology for CCD's. This technology was also developed at Bell Laboratories by Mohamed Atalla and Dawon Kahng in 1959.

Figure 2.8 depicts the initial design. This discussion focuses primarily on biasing to develop a depletion region. A positive gate voltage (V_g), referred to as reverse bias, drives majority characters, holes in the P silicon material, away from the silicon dioxide layer, forming a depletion region if the gate voltage is not too high.

The gate voltage [V_g] bends energy levels within the CCD by an amount [qV_g] as shown in **Figure 2.7,** where q is the electron charge $1.602 \cdot 10^{-19}$ coulombs. This energy band bending represents potential energy changes experienced by electrons in the semiconductor due to the gate voltage. Unfortunately, this design had one major drawback. When charges were transferred to the next gate, some minority carriers were

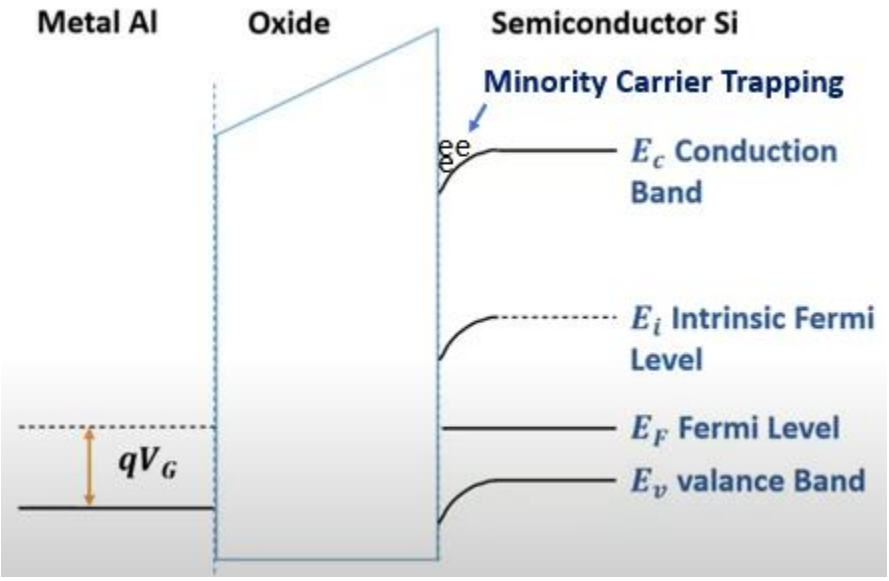


Figure 2.7. A bandgap diagram representing the reverse biased metal oxide semiconductor (MOS) gate in depletion mode. Modified from (2024, Dholahiya).

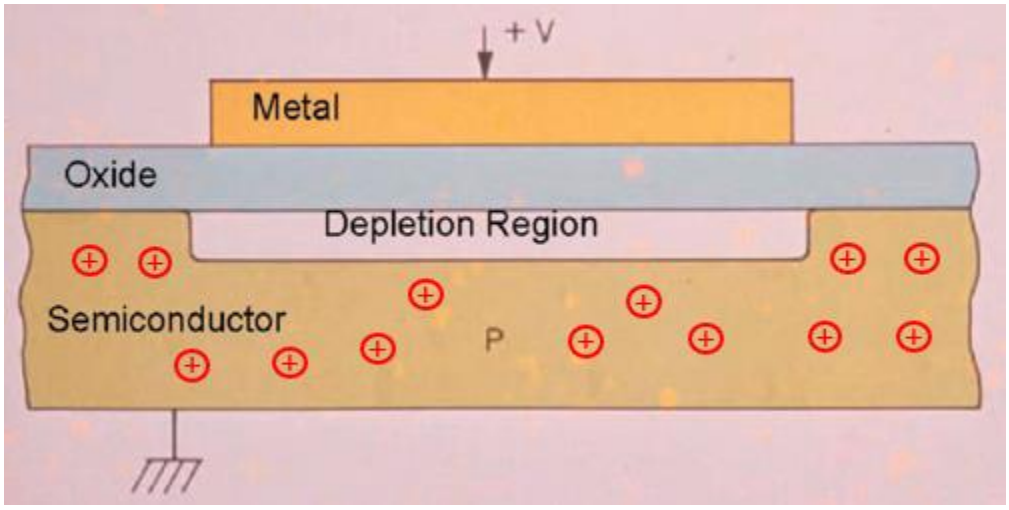


Figure 2.8. The initial design of a reverse biased charge-coupled device pixel, modified from (Smith, 2010).

trapped in the bend of the conduction band. Trapped minority carriers flowed into the next gate later, but that caused the CCD image to smear. The CCD prototype consisted of multiple metal dates over a silicon substrate separated by an insulating silicon dioxide layer. Gate voltages (V_g) vary on these multiple gates to store, transfer, and read charge packets, as shown in **Figure 2.9**. Cycling gate voltages move charges from left to right. To overcome the trapped minority carrier problem Boyle and Smith designed the buried channel CCD represented in **Figure 2.10**. Compare bandgap diagrams in **Figure 2.7** for the initial CCD design and **Figure 2.11**. For the buried channel CCD design, note how the latter drives the depletion region below the silicon dioxide layer. This prevents trapping beneath the silicon dioxide layer.

Detector Cavity Shielding at the High Flux Isotope Reactor

Lead is arguably the most common radiation shielding material for gamma rays. It has a high atomic number of 82, is relatively abundant, and is relatively inexpensive. However, density is the true determinant of the best shielding material. Lead has a density of 11.35 grams per centimeter cubed[g/cm^3]. Other elements with higher densities, therefore, provide better gamma ray shielding. These will be discussed later.

Hydrogenous materials provide shielding against neutrons because they moderate neutrons (slow them down). This process is a direct result of elastic scattering. The internal states of the particles remain unchanged (Zwiebach, 2018). The focus of neutron shielding is primarily to prevent background noise in the detector. Compact prototype antineutrino detectors should be tested as close to the reactor core as possible. This

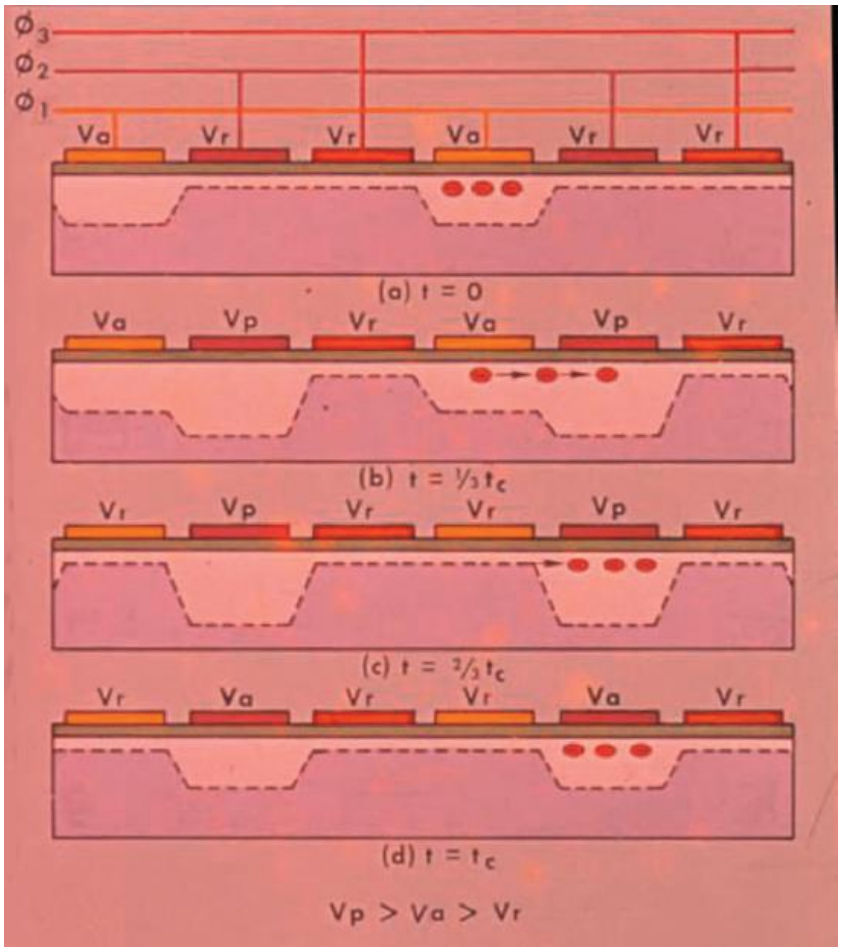


Figure 2.9. The basic CCD design concept. As the gate voltages change charges are transported from left to right (Smith, 2010). Depletion regions have sometimes been referred to as a bucket brigade similar to water buckets (depletion reqions) passing water (charge) from left to right.

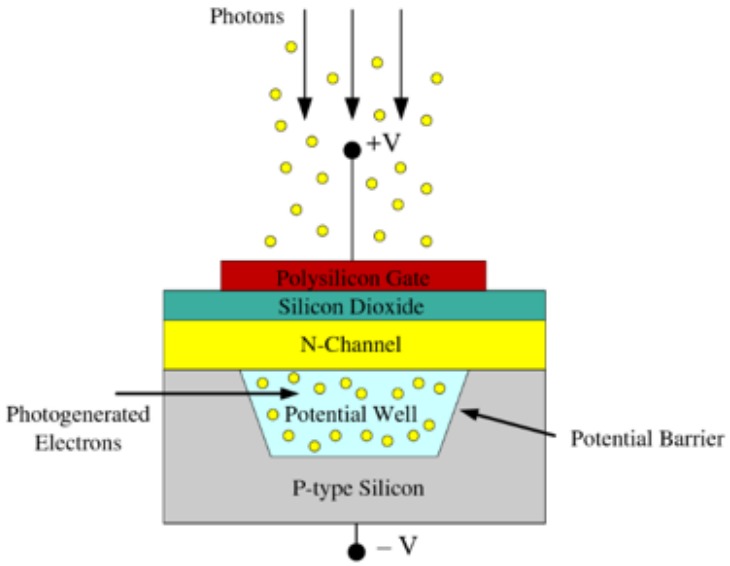


Figure 2.10. Buried channel CCD developed to mitigate trapping (semantecscholar.org, 2024).

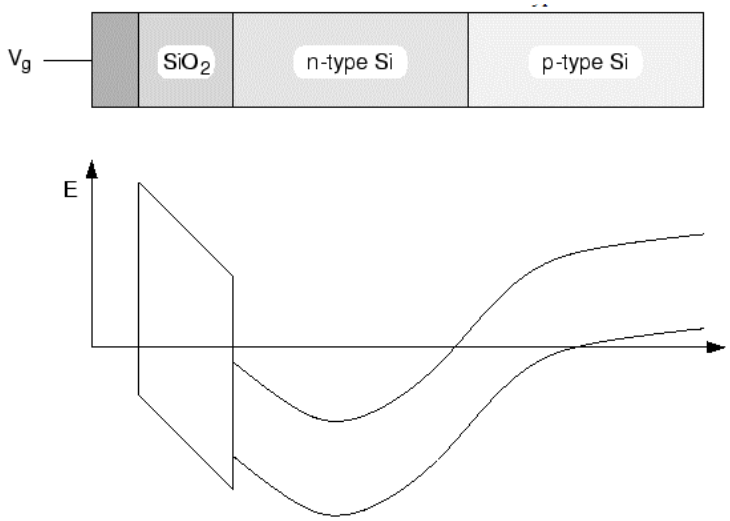


Figure 2.11. Energy band structure for a buried-channel CCD. A potential well forms below the semiconductor-oxide interface in the n-type silicon preventing minority carrier trapping (Rottinger, 1999).

allows maximum neutrino flux through the detector volume. The HFIR configuration allows for a 7 to 12 meter radial distance. This high flux comes at a cost. Reactor proximity translates into high radiation background rates. Gamma backgrounds can mimic prompt antineutrino signals. Fortunately, there is no significant high-energy neutron background at HFIR.

CHAPTER THREE

MATERIALS AND METHODS

Compact HFIR Antineutrino Monitoring (CHAMP)

The CHAMP team (including the author) completed a contract to place the background radiation collection station (**Figure 3.3**) in the HFIR facility in a short timeframe, one month. Three-dimensional data collection is complete at HFIR location 1. Two additional data acquisition locations are planned. The goal of CHAMP was to collect baseline radiation data. This radiation would need to be shielded to some undetermined degree for neutrino detection. Identifying background radiation levels is the first step. CHAMP uses 24 sodium iodide thallium-doped [Na(Tl)] scintillators. Comparing the effective atomic number (Zeff) for [NaI(Tl)] has revealed contention in radiation attenuation analysis. Some researchers have abandoned the traditional concept of Zeff altogether, favoring other parameters. The effective atomic number will be discussed further in the Results and Discussion chapter.

Since the sodium iodide thallium photomultiplier tube bases were custom-designed, emphasis will be placed on those detectors. Also, twenty-four detectors represent the larger detector volume. It is worth mentioning why CHAMP has three different types of detectors. [NaI(Tl)] has a high density and provides good scintillation properties for detecting gamma rays. These detectors offer good energy resolution for gamma spectra. Helium (HE-3) detectors are sensitive to thermal neutrons.

The liquid scintillator (EJ-309) can detect both gamma rays and neutrons providing timing resolution in good energy response. With the flashpoint of 144° C, the EJ-309 is

much less likely to be a fire hazard compared with other liquid scintillators with lower flashpoints on the order of 26 degrees Celsius [°C] (2024, Eljen).

CHAMP Design

Figure 3.1 represents a SolidWorks design including 24 sodium iodide thallium doped [NaI(Tl)] detectors and the HFIR experiment in **Figure 3.2**. Each of these Saint-Gobains detector crystals measures 2 by 4 by 16 inches. The deposition of energy in these detectors is a stochastic process. With a mono-energetic input to the crystal, the response spectrum is referred to as a response function (Matta,2021). Experimental determination of the response function is difficult because of background radiation and the fact that most gamma-ray sources are not mono-energetic. The response function can be simulated using Monte Carlo techniques (Matta, 2021). The detector response function is important because it provides a means of energy calibration, resolution, detector efficiency, background and interference, and detector performance characterization.

Figure 3.3 represents the crystal's Geant4 simulated response to a mono-energetic 15.0 megaelectronvolts [Mev] gamma ray. Pair Production dominates above approximately 2.5 MeV (Short, 2016). Note the peak at 511 keV representing two gamma rays resulting from positron-electron annihilation. When the 15.0 MeV gamma ray impacts the steel cladding, pair production produces an electron and a positron.

The small peak around 1000 keV results from complex positron-electron interactions within the material. This could include the possible formation and annihilation of positronium. The 1000 keV peak can also represent scattering in energy redistribution effects in the material.

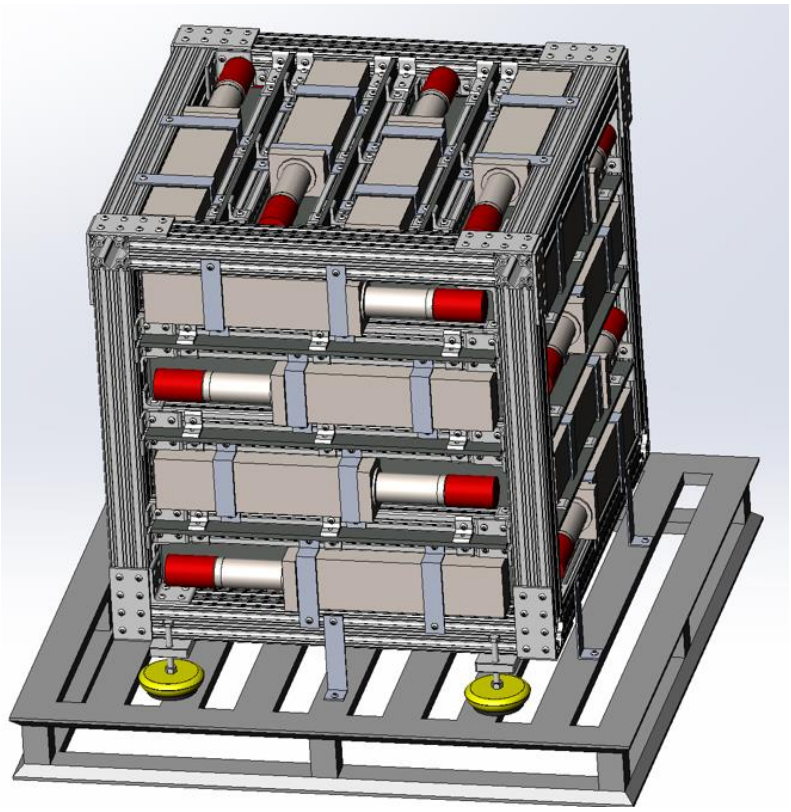


Figure 3.1. SOLIDWORKS design placement for 24 Saint-Gobains Model ZX4H16/2SS, 2 X 4 X 16” NaI(Tl) dectectors and lead separator plates (courtesy of Brandon Longmire).



Figure 3.2. The CHAMP experimental radiation background collection station located at HFIR.

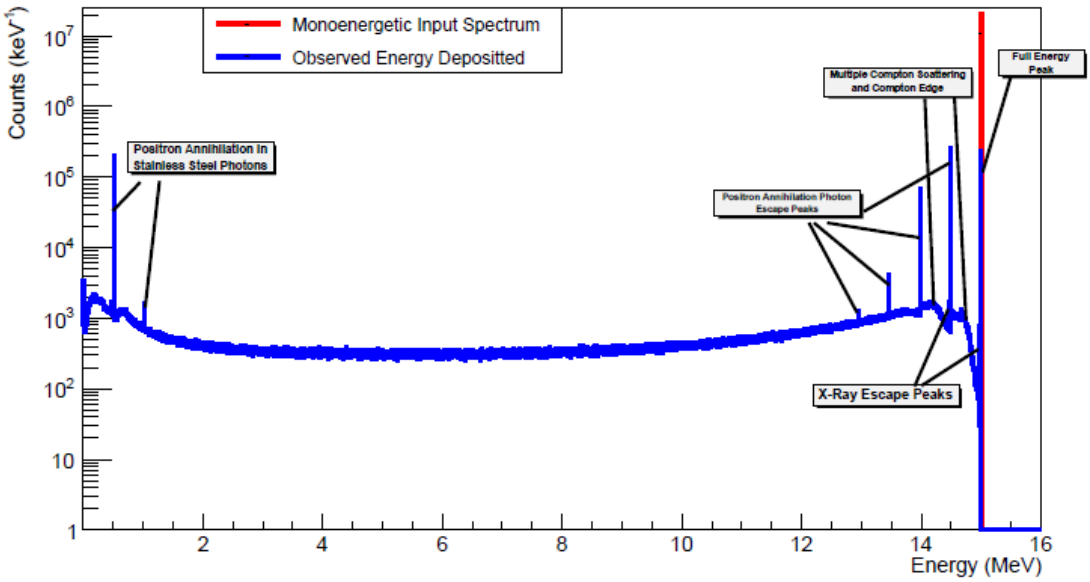


Figure 3.3. Given the Geant 4 mono-energetic gamma ray input spectrum shown in red, the blue response function results for a Saint-Gobains model ZX4H16/2SS 2x4x16” NaI(Tl) crystal (modified from Matta, 2021).

.

Positron annihilation photon escape peaks in the 13 to 14.5 MeV range include a combination of high energy photon interactions, secondary emissions, and pair production. The x-ray escape peak at approximately 14.5 MeV results from energy loss with some photons detected. The full power x-ray escape peak is likely a stainless steel cladding interaction.

Multiple Compton scattering and Compton edge effects can be interpreted as follows: The edge at about 15 MeV represents maximum energy transfer. However, the edge just below 14.5 MeV also represents high-energy photon interactions with the detector or cladding.

Figure 3.4 depicts the sodium iodide thallium detector and its Geant4 simulation of a mono-energetic 15.0MeV gamma ray and it's subsequent reaction with the crystal (Matta, 2021). The simulation included the crystal surrounded on five sides by a 0.125-inch thick stainless steel cladding. Omitting the flare and photomultiplier tube simplify the simulation but did not significantly affect the simulated response. This lack of mass will, however, cause a somewhat smaller 511keV response from pair production and Compton scattering in the stainless-steel cladding.

Scintillation

Curiosity and awareness can lead to new discoveries. In 1895, Wilhelm Roentgen noticed a glow in a nearby platino-barium cyanide crystal while firing a beam of electrons at a target inside an evacuated glass tube. This glow disappeared when Roentgen switched his electron source off. This phenomenon, later described as scintillation, is the emission of light in some materials, usually crystalline or plastic, when they absorb high-energy

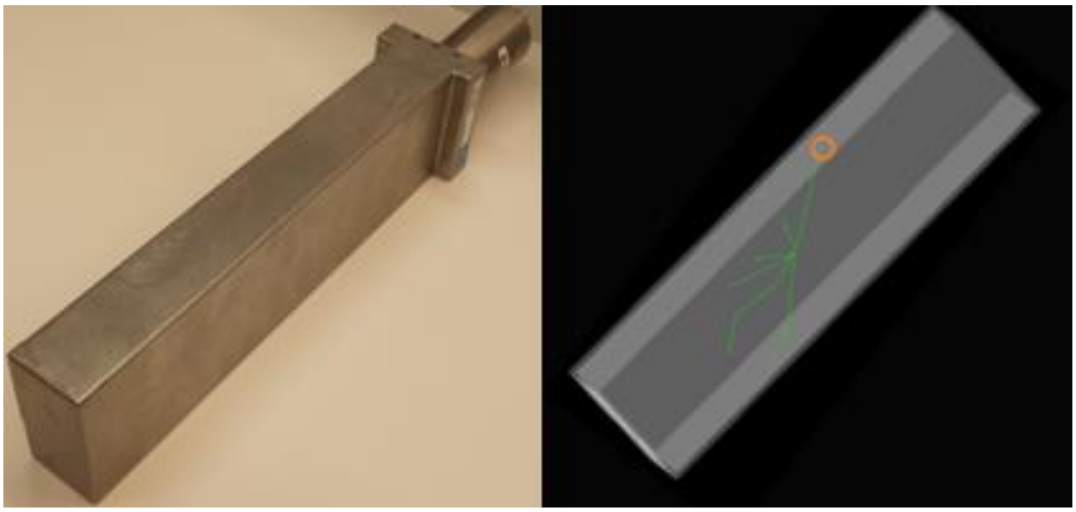


Figure 3.4. The Saint-Gobains (now Luxium Solutions) model ZX4H16/2SS 2x4x16” NaI(Tl) detector on the left with it’s Geant4 graphic representation on the right. Note the orange circle denoting entry of a mono-energetic 15.0MeV gamma ray and it’s subsequent reaction with the crystal shown in green. The translucent Geant4 crystal envelope represents the detector’s steel cladding (modified from Matta, 2021).

.

radiation. The radiation transmits some of its energy and elevates electrons temporarily to higher energy states. When these electrons return to their ground states, they dissipate excess energy in the form of light (Tsoulfanidis, Landsberger, 2015).

The Latin scintillate means to sparkle and is the origin of the word scintillation, commonly used in radiation detection terminology today. William Crookes is credited as the first to observe scintillations on a ZnS screen using alpha particles (Tsoulfanidis, Landsberger, 2015). The work of T. Sidot, F. Giesel, J. Elster, and H. Geitel laid the groundwork for Crookes' breakthrough (Kolar, Hollander, 2004). Their work and studies laid the groundwork for Crookes' observation.

Photomultiplier Electronics

Scintillation light can be captured in a photomultiplier tube as shown in **Figure 3.5**. When light hits the photocathode, the photoelectric effect generates electrons (Wright, 2017).

Each dynode from left to right has an increasingly higher positive voltage. Therefore, each dynode attracts electrons from the previous stage dynode. When these electrons hit each successive dynode, additional electrons are dislodged, multiplying exponentially along the chain of dynodes. Finally, the electrons are collected at the end of the process, representing what could be a very weak light signal.

Now consider the custom photomultiplier electronic design for the Compact HFIR Antineutrino Monitoring Platform (CHAMP) in **Figure 3.7.** The same general comments

above apply to the CHAMP design. Error! Reference source not found. depicts the

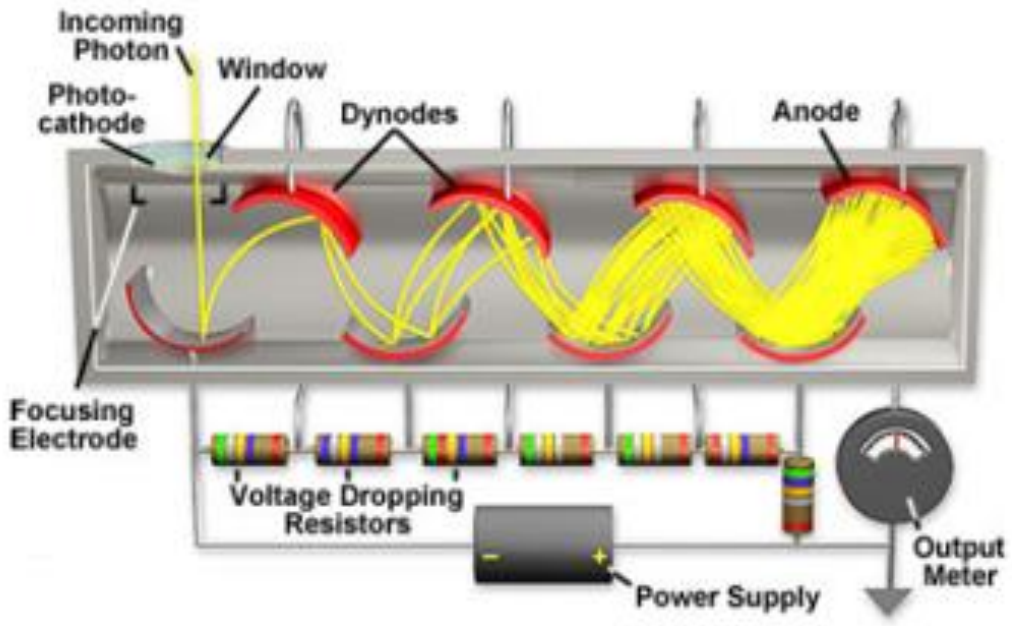


Figure 3.5. A basic photomultiplier diagram. Light impinging on the photo cathode produces electrons. These are in turn multiplied by voltage attracted dynodes. Electrons are collected at the anode representing the original radiation detected within the scintillator (Molecular Expressions, 2019).

printed circuit board implementing the schematic.**Error! Reference source not found.**

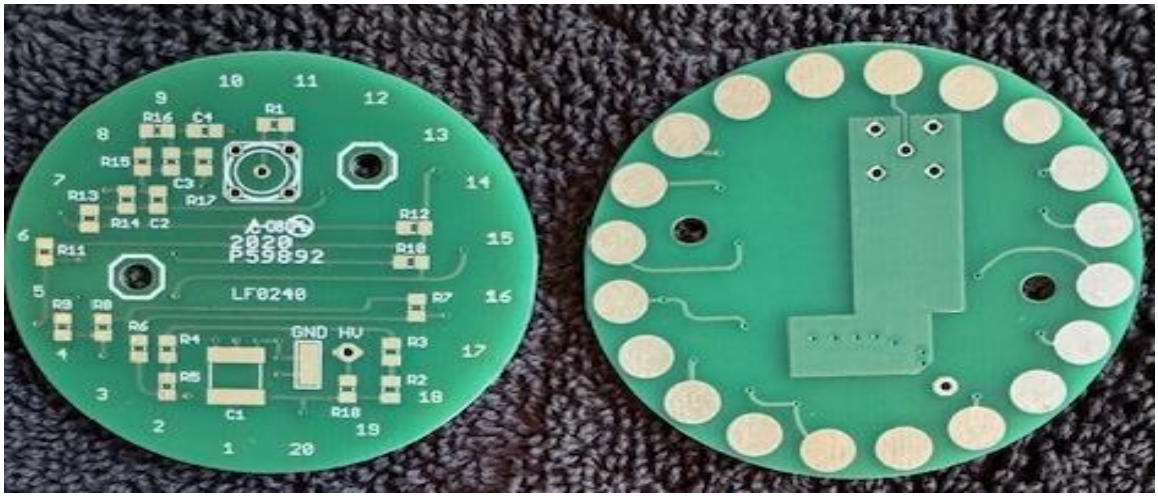


Figure 3.6. This double-sided printed circuit board (front and back) designed with KiCad contains the basic design in the schematic of Figure 3.7 (Fabris, 2021).

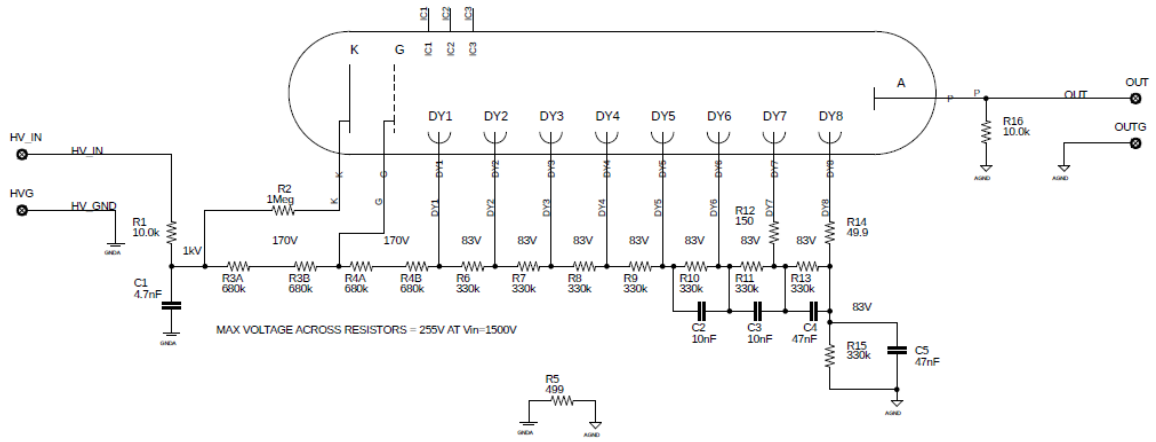


Figure 3.7. Photomultiplier tube schematic used for CHAMP NaI(Tl) detectors (Fabris, 2021).

The custom mechanical assembly for the photomultiplier tube bases is shown in **Figure 3.8** CHAMP uses twenty-four of these bases. It was more cost-effective to design and build these identical bases than to purchase commercial off-the-shelf products.

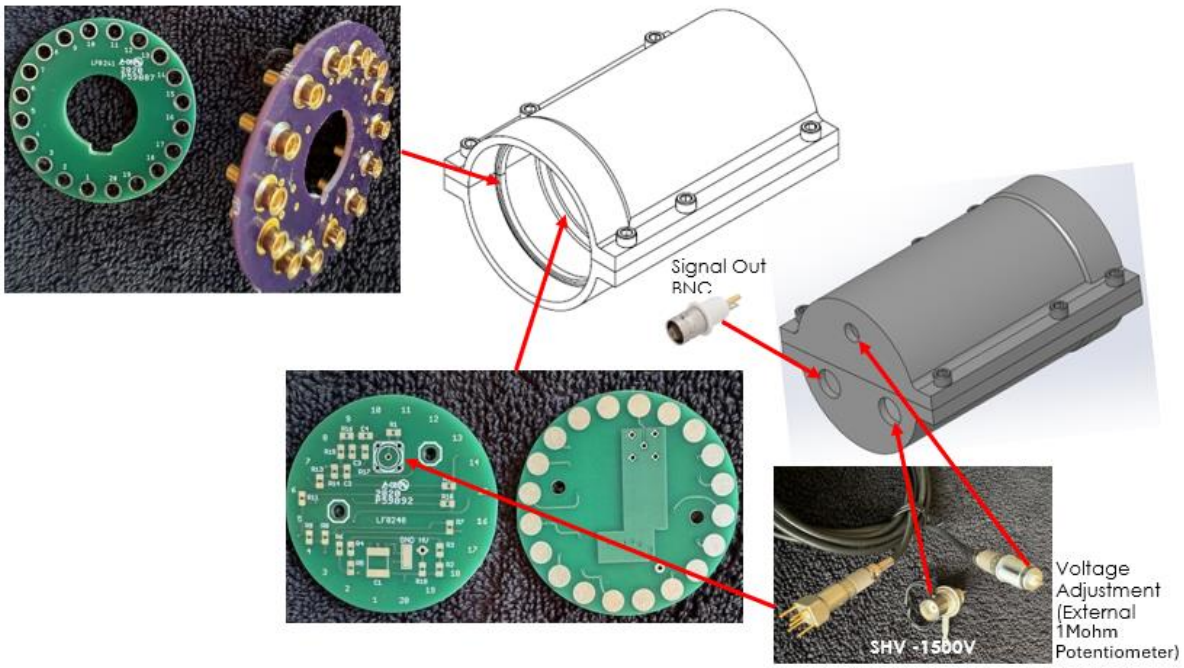


Figure 3.8. Mechanical connections for the 24 CHAMP custom photomultiplier tube bases (SolidWorks housing design provided courtesy of Paul Nogradi).

CHAPTER FOUR

RESULTS AND DISCUSSION

Radiation detector performance is a function of several parameters, including scintillation efficiency, attenuation coefficient, energy resolution, density, and volume. Since the attenuation coefficient is a function of atomic number, consideration was given to determining the effective atomic number for detector compounds. This turned out to be an interesting academic exercise, but it is not well-established in the literature. Monte Carlo techniques would likely be more accurate since they have been carefully vetted. Originally, Geant4 was intended for shielding simulation. However, the primary focus became the design and implementation of CHAMP, its experimental application, and data collection at the high-flux isotope reactor at Oak Ridge National Laboratory.

Effective Atomic Number (Z)

Figure 4.1 shows the computer analysis of four different programs designed to compute effective atomic number (Z), the effective number of protons for substances. Recall, material properties are determined by the number of protons in an atom. In other words the number of protons determines the elemental atom. Effective atomic numbers might be used to estimate the attenuation coefficient of compounds.

Consider a sodium iodide crystal doped with thallium represented as [NaI(Tl)]. Sodium iodide has a crystalline structure composed of about 17% sodium and 83% iodine. Iodine with an atomic number of 53, is far denser than sodium, with an atomic number of 11. Although thallium has the highest atomic number, 81, it doesn't contribute significantly

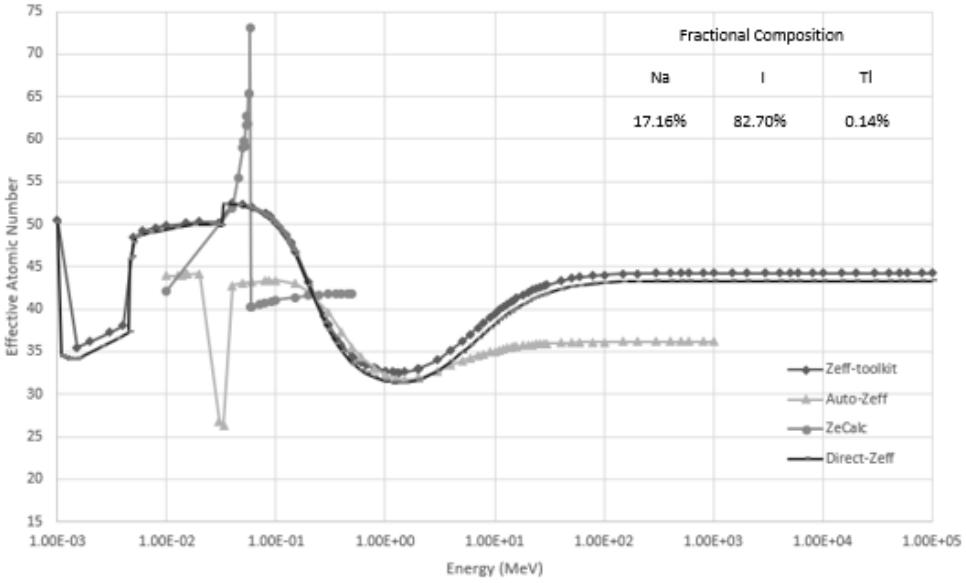


Figure 4.1. Zeff-toolkit: Mann, et al., (2016) [average of three calculations – Taylor, et al. (2012); Manohara, et al. (2008); Singh et al. (2012)]
Auto-Zeff: Taylor, et al., (2012) [based on summed fractional weighting of mass attenuation coefficient to weighted atomic number of constituent elements]
ZeCalc: Garcia, et al., (2016) Note: results contested by (Bouchard, 2016), an ungentlemanly mess
Direct-Zeff: Un and Caner (2014)

to a change in the effective atomic number because its percentage in the compound is only about 0.14 percent.Of the four programs, Zeff-toolkit (Mann et al., 2016) and Direct-Zeff (Un and Caner, 2014) appear to have similar curves. Auto-Zeff (Taylor et al., 2012) and ZeCalc (Garcia et al., 2016) have spike artifacts in their curves. Auto-Zeff was based on summed fractional weighting of mass attenuation coefficient to weight atomic number of constituent elements. ZeCalc results were contested in literature and there was no resolution.

Photoelectric absorption dominates from the work function energy up to about 245 keV (Short, 2016). Compton Scattering dominates from several hundred keV up to five MeV (Knoll, 2010). Pair Production dominates above approximately 2.5 MeV (Short, 2016). Rayleigh scattering occurs at low energy, but since this is an elastic phenomenon, all the incident and subsequent energy after collision is retained by the gamma-ray. No energy is deposited in the crystal detector.

Effective Atomic Number (Z) Calculation

Before leaving this topic, consider the direct calculation of effective atomic number. An Alpha Spectra sodium iodide detector enclosure will serve as an example. The Alpha Spectra [NaI (Tl)] detector is contained within a Teflon reflector wrapped in aluminum foil protected by an aluminum housing (**Figure 4.2**). Although aluminum photon count (Z) is readily available, along with other single elements, Teflon proton count requires some discussion.

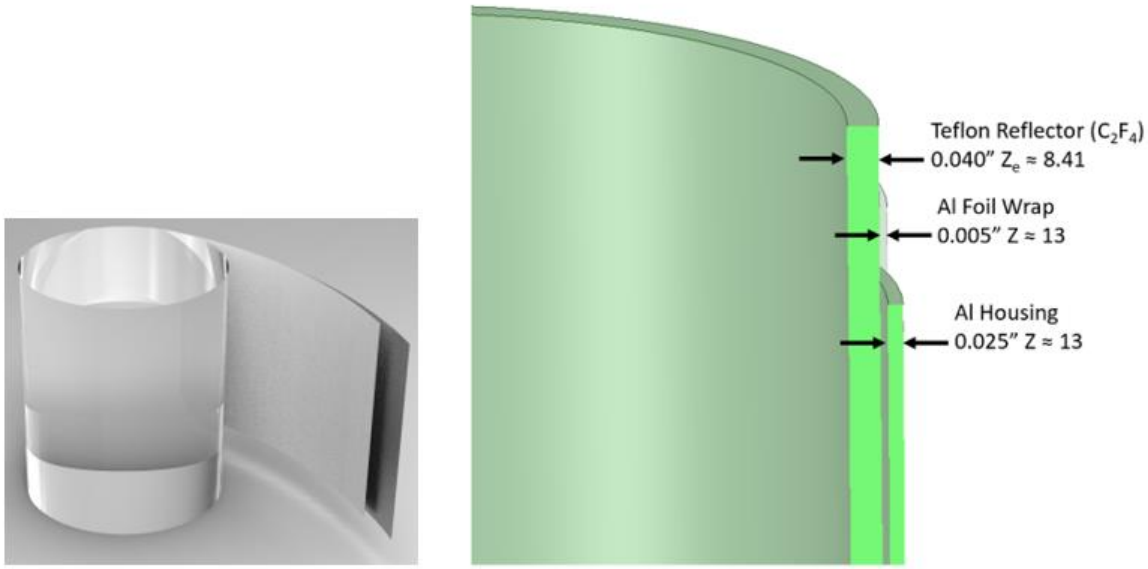


Figure 4.2. Alpha Spectra detector for this calculation is wrapped in Teflon with a protective aluminum foil cover inside an aluminum container. The figure was drawn using IronCAD.

Researchers have proposed various equations to estimate atomic number for compounds and mixtures. The earliest recorded mathematical model dates to 1946 and is used for medical X-ray technology, as shown in Equation 4-1 (Spiers, 1946).

$$Z_{eff} = \sqrt[p]{\sum_i a_i Z_i^p}$$

Where,

Z_{eff} ≡ effective atomic number

a_i ≡ relative electron fraction contributed by the i^{th} constituent atom

Z_i ≡ atomic number of the i^{th} constituent atom

p ≡ empirically determined constant

Equation 4-1

Spires' equation provided a relatively simple means for medical practitıoners to determine effective Z estimating x-ray effects on humans. The variable 'p' was somewhat arbitrary, assigned through experience and practical application. Subsequent research, arbitrary, assigned through experience and practical application. Subsequent research, equipped with computational tools not available in 1946, found this equation to be imprecise.

In 2008 Manohara, et al. described effective Z for compounds and mixtures shown in Equation 4-2.

$$= \frac{\sum f_i A_i \left(\frac{\mu}{\rho}\right)_i}{\sum f_j \frac{A_j}{Z_j} \left(\frac{\mu}{\rho}\right)_j}$$

Equation 4-2

Where,

Z_{eff} ≡ effective atomic number

f_i ≡ relative molar fraction contributed by the i^{th} constituent atom

A_i ≡ atomic mass of the i^{th} constituent atom

$\left(\frac{\mu}{\rho}\right)_i$ ≡ attenuation coefficient of the ith i^{th} constituent atom

f_j ≡ relative molar fraction contributed by the j^{th} constituent atomic electrons

A_j ≡ atomic mass of the j^{th} constituent atom

Z_j ≡ atomic number of the j^{th} constituent atom

$\left(\frac{\mu}{\rho}\right)_j$ ≡ attenuation coefficient of the ith j^{th} constituent atom

For comparison to Teflon Z_e = 8.41 provided by (Smith, 2011), energy at 100keV was chosen to provide $\left(\frac{\mu}{\rho}\right)$ for carbon and fluorine from NIST, Win XCOM in **Table 4.1**.

Smith, Martz, and Kallman optimized over a range, 30-160 keV for x-ray examination in the electronic baggage scanning program. Substituting **Table 4.2** values into Equation 4.2 gives the result in Equation 4-3.

$$Z_{eff} \approx 8.305 \text{ Teflon } (CF_2), 100 \text{ keV} \qquad \text{Equation 4-3}$$

Note the percentage difference error between $Z_e \approx 8.41$ and $Z_{eff} \approx 8.305$. If 8.41 is taken as the correct value, the percentage difference error is 1.25%. Z_{eff} as determined by Manohara, et al. for higher energy gamma rays are inferred to be a reasonable value.

Table 4.1. NIST, Win XCOM attenuation values for carbon and fluorine.

Edge	(required) Photon Energy	Scattering		☐ Photoelectric Absorption	Pair Production		Total Attenuation	
		☐ Coherent	☐ Incoherent		☐ In Nuclear Field	☐ In Electron Field	☐ With Coherent Scattering	☐ Without Coherent Scattering
	MeV	cm^2/g	cm^2/g	cm^2/g	cm^2/g	cm^2/g	cm^2/g	cm^2/g
Carbon								
	1.000E-01	3.719E-03	1.466E-01	1.031E-03	0.000E+00	0.000E+00	1.514E-01	1.476E-01
	6.000E-01	1.069E-04	8.047E-02	4.253E-06	0.000E+00	0.000E+00	8.058E-02	8.048E-02
Fluorine								
	1.000E-01	7.012E-03	1.380E-01	4.593E-03	0.000E+00	0.000E+00	1.496E-01	1.426E-01
	6.000E-01	2.060E-04	7.627E-02	1.980E-05	0.000E+00	0.000E+00	7.649E-02	7.629E-02

Table 4.2. Substitution values for Equation 4.2.

f_{ic} (carbon) ≈ 0.2402

A_{ic} (carbon) ≈ 12.01 amu

$\left(\frac{\mu}{\rho}\right)_{ic}$ (carbon) ≈ 0.1514 cm^2/g

f_{ic} (carbon) ≈ 0.25

Z_{ic} (carbon) ≈ 6

f_{if} (fluorine) ≈ 0.7598

A_{if} (fluorine) ≈ 19.00 amu

$\left(\frac{\mu}{\rho}\right)_{if}$ (fluorine) ≈ 0.1496 cm^2/g

f_{if} (fluorine) ≈ 0.75

Z_{if} (fluorine) ≈ 9

Find Z_{eff} for Teflon (CF_2) at 600 keV:

Given $\left(\frac{\mu}{\rho}\right)_{ic}$ (carbon) ≈ 0.08058 cm^2/g and $\left(\frac{\mu}{\rho}\right)_{if}$ (fluorine) ≈ 0.07649 cm^2/g and noting the fully specified NIST, Win XCOM parameter curves for Teflon in **Figure 4.3** for reference, Z_{eff} is calculated in Equation 4-4.

$$Z_{eff} \approx \frac{0.2402 * 12.01\ \text{amu} * 0.08058\frac{\text{cm2}}{\text{g}} + 0.7598 * 19.00\ \text{amu} * 0.07649\ \text{cm2/g}}{0.25 * \frac{12.01\text{amu}}{6} * 0.08058\frac{\text{cm2}}{\text{g}} + 0.75 * \frac{19.00\text{amu}}{9} * 0.07649\ \text{cm2/g}} \quad \text{Equation 4-4}$$

Resulting in,

Equation 4-5

$$Z_{eff} \approx 8.280 \ \text{Teflon (CF}_2\text{), 600keV}$$

Software like Gamma and Dose Rate Assessment Software (GADRAS) used for nuclear incidents or radiological assessments requires an estimate of the atomic number (Z). Z, or the number of protons for input, has been referred to as the effective Z, which coincidentally is also the number of electrons in an unexcited atom (Manohara, 2008).

Assume contributions to [Z_{eff}] of [Al] and Teflon based on the relative thicknesses of each. Calculations are based on gamma-ray energy of approximately 600 keV.

Assume contributions to Z_{eff} of Al and Teflon based on the relative thicknesses of each. Calculations are based on gamma-ray energy of approximately 600 keV.

$$Z_{eff} = \frac{Z_{Al}T_{Al} + Z_{Al}T_{Al;(foil)} + Z_{eff\ Teflon}T_{Teflon}}{T_{Al} + T_{Al;(foil)} + T_{Teflon}} \quad \text{Equation 4-6}$$

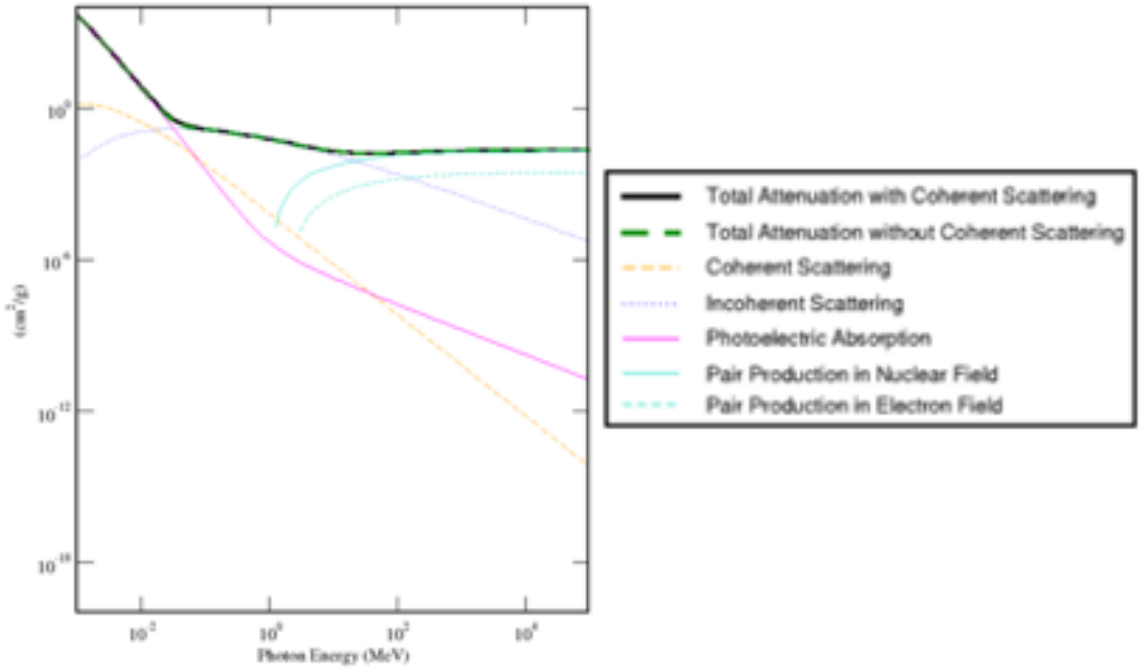


Figure 4.3. NIST, Win XCOM graphs for fully specified Teflon parameters as listed.

Where,

T_{Al} = 0.025” or 0.064 cm

$T_{Al(foil)}$ = 0.005” or 0.013 cm

T_{Teflon} = 0.040” or 0.102 cm

and,

$Z_{eff\ Teflon} \approx 8.280$

$Z_{Al} \approx 13$

$$Z_{eff(enclosure)} = Z_{Al}T_{Al} + Z_{Al}T_{Al;(foil)} + \frac{Z_{eff\ Teflon}T_{Teflon}}{T_{Al} + T_{Al;(foil)} + T_{Teflon}}$$ Equation 4-7

$$Z_{eff(enclosure)} = \frac{13 * 0.064\ \text{cm} + 13 * 0.013\ \text{cm} + 8.280 * 0.102\ \text{cm}}{0.064\ \text{cm} + 0.013\ \text{cm} + 0.102\ \text{cm}}$$ Equation 4-8

$$Z_{eff(enclosure)} = 10.31$$ Equation 4-9

Geant4 Requires Specialized Software Skills

Geometry ANd Tracking, Version 4 (Geant4) is a Monte Carlo toolkit developed at the Conseil Européen pour la Recherche Nucléaire (CERN) and translated into English by the European Organization for Nuclear Research. The software allows users to define limited geometry for shielding and detectors. It simulates particle tracks through matter including scattering. Physics interactions are accounted for including electromagnetic, hadronic, and decay processes (CERN, 2023). Geant4 is a complex toolkit with

dependencies requiring working knowledge across multiple software tools, C++, Git, GitHub, CMake, and Ubuntu, to name a few.

Geant4 provides a core library with central functions for particle tracking and interaction simulations. The main libraries of Geant4 include geometry, materials, tracking, physics, event and run management, visualization, user interface, and output and data handling. Within Geant4, geometry specifications proved to be the most challenging aspect. Several prototype software tools have been developed to input computer-aided design geometry into Geant4. However, a significant number of other software tools must be included to run Geant4. Each of these tools requires significant computer science knowledge.

A simplified Geant4 configuration approach proved to be unsuccessful. After multiple attempts to incorporate this configuration, the platform was still unstable. The host computer operated behind a firewall at Oak Ridge National Laboratory **(Figure 4.5)**. The instability was likely due to multiple factors. Upload and download connections affecting online components and Geant4 updates were limited by network restrictions. Geant4 requires access to external libraries limited by the firewall. Strict user permissions limit the installation or execution of Geant4 components. Resource allocation was likely also an issue.

A dedicated personal computer connected directly to the Internet proved successful using a Ubuntu Linux-based operating system, **Figure 4.4**. Ubuntu is a Linux kernel (core system resource and communication management) Debian derived operating system. Geant4 demonstration programs ran successfully using this configuration. New users in

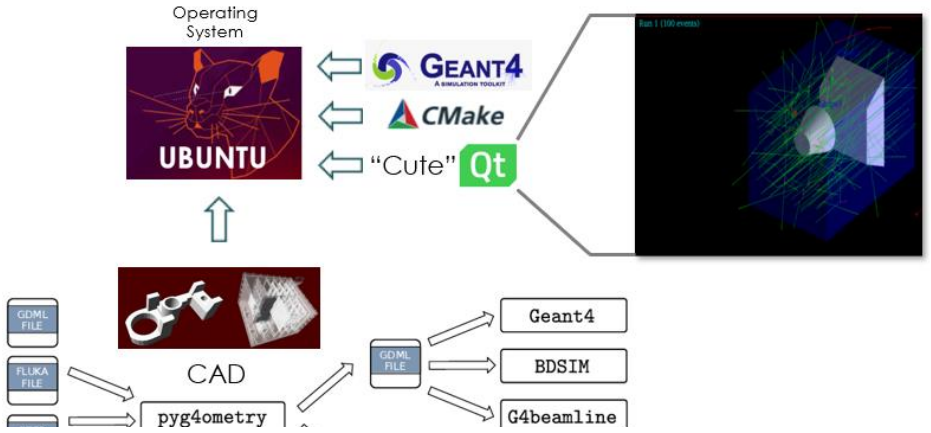


Figure 4.4. This configuration provided limited success. Geant4 demonstration programs including some modifications proved successful. However, complex geometries using three-dimensional CAD programs like SolidWorks repeatedly failed. Instigating make or an integrated development environment (IDE) provides final preparation for compiling.Qt or "cute" displays a two-dimensional image of the three-dimensional Geant4 simulation output. Although written in C++, Qt can be bound to other languages like Python. Geant4 has its own visualization options, but Qt allows for more user-friendly, customized visual representations of simulation data. Qt also allows users to develop graphical user interfaces like simulation control panels to start, stop, and configure simulations. Data visualization using plots and graphs to represent data along with user input management with forms or dialogs is another possibility with Qt.



Figure 4.5. A simplified approach to incorporate Geant4 using Windows 10 behind the ORNL firewall failed to provide a stable programming platform.

Geant4 are encouraged to modify existing demonstrations for customized applications like the detector response shown in **Figure 3.4**.

Even basic radiation transport analysis in the Geant4 toolkit requires knowledge and application of multiple tools and programming capabilities. Since Geant4 libraries are primarily programmed in C++, simulations require C++ compiling as shown in **Figure 4.6**.

CMake is an open-source, platform-independent scripting language used to manage and build software projects, **Figure 4.7** (Loggini, 2020). Before compiling, CMake is configured using a CMakeLists.txt file to specify source files, libraries, and compilation options. Running CMake then generates build files for the appropriate environment.

Along with the somewhat daunting Geant4 toolkit libraries users also have to learn the Git version control system (**Figure 4.8**) its GitHub cloud server and related programs, such as Visual Studio Code (VSCode), an open-source Microsoft code editor.

Without version control like Git software teams have no way of knowing which changes have been approved for release. Worse, team members may create incompatible changes in two or more unrelated pieces of software resulting in execution errors (Shapiro, 2019). Git is distributed so the entire project and history is on each programmer's machine and, as a result, is faster than centralized version control where the project resides on a single server. Programmers working alone can benefit from the changes logged in history and structure for version control.

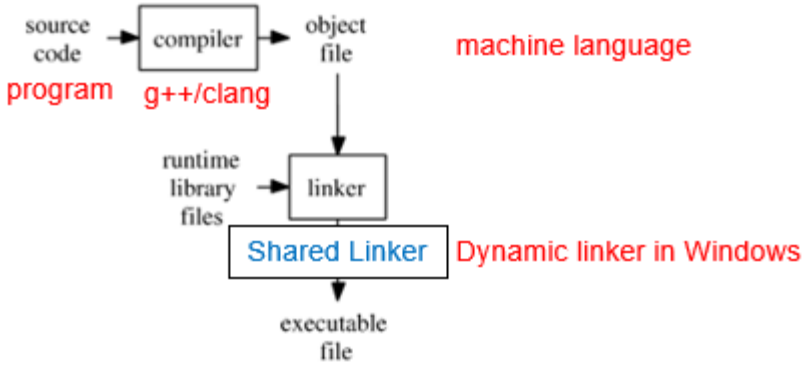


Figure 4.6. Programs are often created using compiled languages making use of dynamic linked libraries (Windows) or shared libraries (Linux, Unix) to run (Modified from Anton, 2017 and Hawaii.edu, 2019).

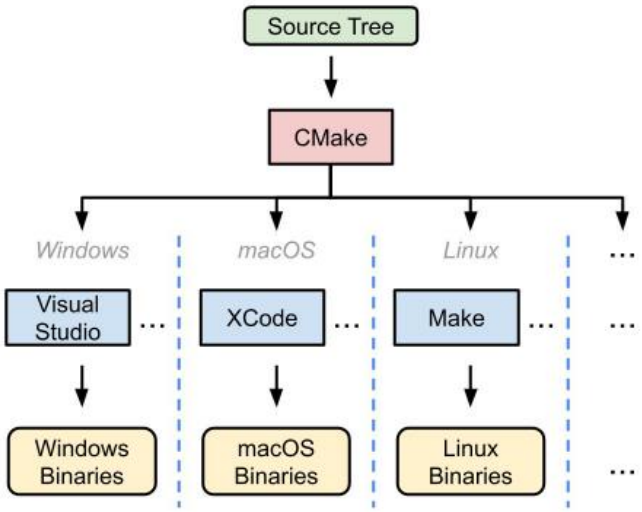


Figure 4.7 CMake is a cross platform build system generator (Loggini, 2020).

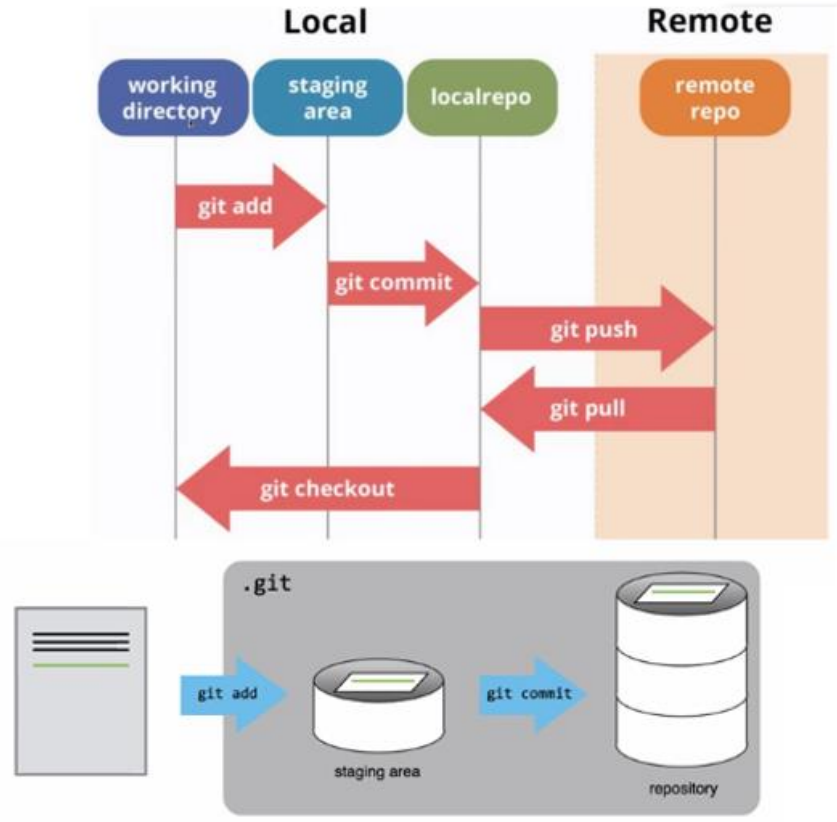


Figure 4.8. Git version control is widely used along with the GitHub service used to host Git repositories. GEANT4 libraries are all available on GitHub (modified from Nemerever, 2019).

More complicated geometrical configurations developed in three-dimensional computer-aided design (3D CAD) programs like SolidWorks require special software skill sets. Attempted geometry input from SolidWorks into Geant4 repeatedly failed using pyg4ometry (Walker, et al., 2021). With additional funding, this simulation capability could be further investigated or contracted for future project work.

MCNP6 and Attila

Monte Carlo N-Particle Transport Code, Version 6 (MCNP6) was developed in the 1970s at Los Alamos National Laboratory (LANL). The first release was in 1983. MCNP6 simulates neutron, photon, and electron transport. The program allows for complex geometries, but input is laborious and error-prone. One attempted solution to the complex geometry problem is the Attila deterministic software program (**Figure 4.9**).

While the Geant4 toolkit requires a host of downloads and computer science expertise across multiple tools, MCNP6 is a self-contained software program. The complex geometry input and display problem can be streamlined by coupling another self-contained Attila program to MCNP6. The Attila program contains Parasolid and tecplot both transparent to the user. Parasolid enhances complex geometry modeling for Attila. While tecplot provides data visualization, postprocessing, customizable graphs, data export, and reporting.

During a three-day Attila seminar the author produced the visualization output displayed in **Figure 4.9.** The cesium 137 source (Cs-137) emits beta and gamma radiation. Color coded gamma radiation flux is displayed around two 2x2 and four 2x4 Alpha Spectra sodium iodide thallium detectors.

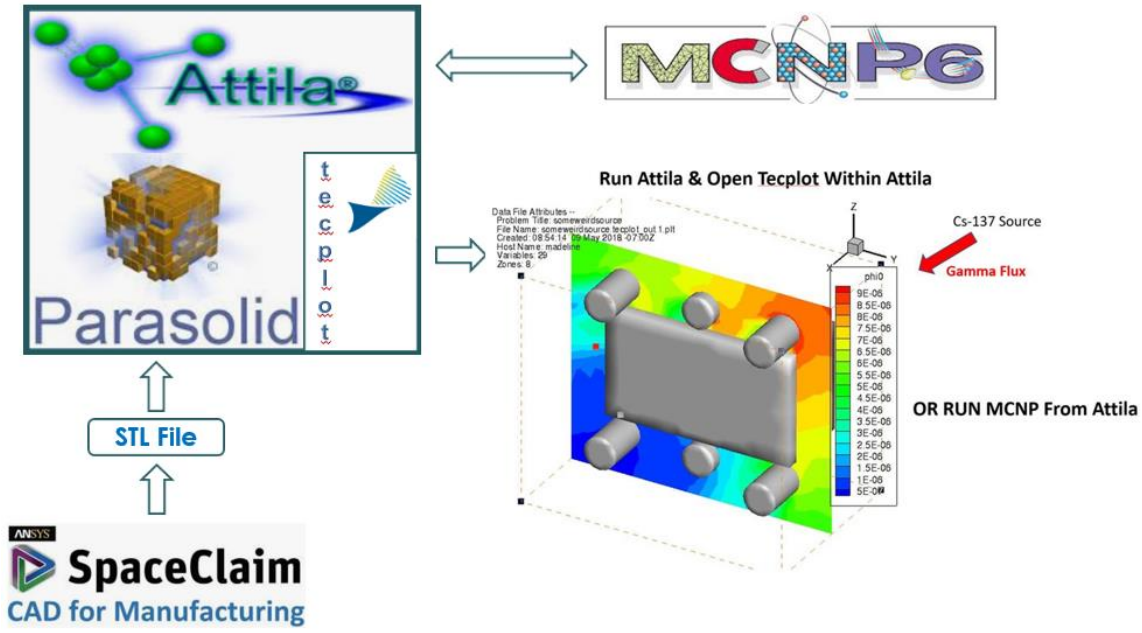


Figure 4.9. Geometry input using SpaceClaim and display with tecplot in Attila coupled with MCNP6 do not require large external library downloads or expertise in multiple other software programs and tools as opposed to Geant4.

GADRAS Compared to MCNP6

It's worth noting the correlation using Gamma Analysis for Dose and Risk Assessment Software (GADRAS) with experimental data collected using this configuration **in Figure 4.10**. Among other uses GADRAS provides simulated responses of gamma detectors. GADRAS has shown good agreement with MCNP6 with the exception of hydrogenous or large quantity moderating shielding (Klasky, et al., 2016).

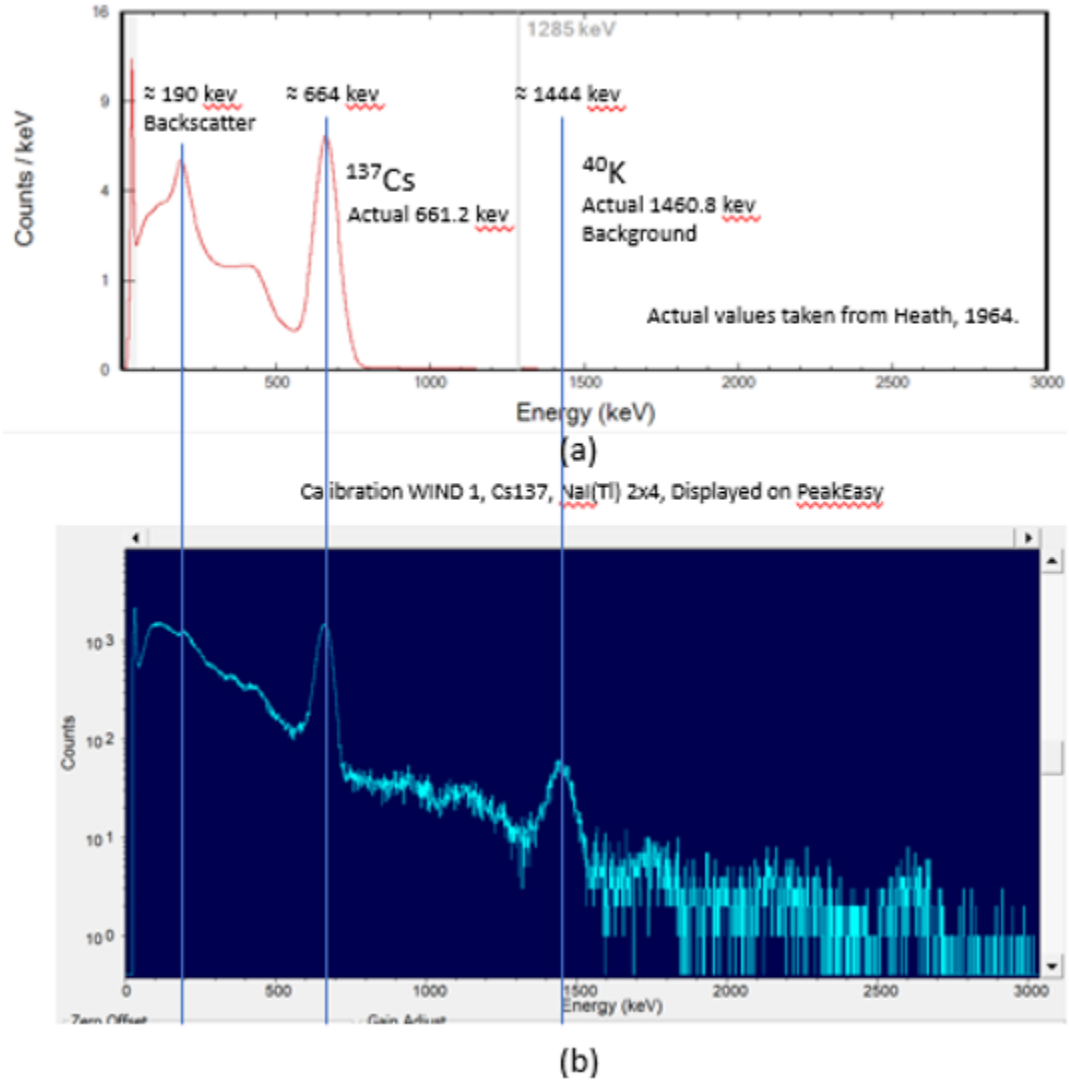


Figure 4.10. Responses in a 2 x 4" sodium iodide detector from a cesium 137 source (a) in a GADRAS simulation and (b) experimentally displayed using EasyPeak.

CHAPTER FIVE

CONCLUSIONS AND RECOMMENDATIONS

CHAMP Disposition and Reactor Security

CHAMP was successfully designed and implemented as the main focus of this dissertation. Background data has been collected from the High Flux Isotope Reactor (HFIR) at ORNL. Characterization of background data and optimization of shielding remain to be implemented. This chapter will focus primarily on recommendations for future work.

The $180K CHAMP project has in a sense been “scooped” by the $5.3M Very Short Baseline Reactor Antineutrino Experiment (vIOLETA) collaboration (vIOLETA, 2024). Although vIOLETA isn’t technically intended to be a user facility for antineutrino detection and experimentation like the future vision of CHAMP, it does provide a complete experimental package including a customized lower energy threshold skipper CCD.

Twelve countries, including the United States, comprise the collaboration with over two hundred researchers. The detection apparatus will be placed eight and twelve meters away from the center of the Atucha 2 Nuclear Power Plant reactor core in Argentina. vIOLETA kicked off in 2022 and has planned collaborative projects indefinitely beyond 2025.

The Atucha 2 Nuclear Power Plant is a pressurized heavy water reactor (PHWR) with thermal power of approximately 2160 megawatts thermal [MWt] and electrical power of 745 megawatts [MW] (Corzo, et al., 2016). The reactor uses natural uranium fuel and

began commercial operation in 2014. Heavy water deuterium oxide [D2O] serves as both a coolant and a moderator. This is how the reactor sustains a nuclear chain reaction using natural uranium.

Compare these specifications to HFIR at ORNL. HFIR is a forced air-cooled research reactor running on low-enriched uranium (LEU), enriched to about 20 percent U-235. The reactor uses water as a moderator and produces about 85 megawatts of power. Verifying fuel rod inventory requires labor and materials totaling about $156 million per year. The process requires sampling and dismantling rods, weighing individual fuel pellets, and using gamma spectroscopy or neutron radiography to verify fuel condition and quality.

Antineutrino detection offers the promise of a lower cost alternative. Changes in antineutrino flux may one day indicate changes in fuel composition or theft of fuel rods. Antineutrino science promises the possibility of new nondestructive testing capability for nonintrusive verification. Characterization of nuclear fuel by monitoring antineutrino emissions can one day determine the amount and type of nuclear fuel in use. Existing physical and procedural safeguards may be augmented by antineutrino detectors to enhance security.

Future Shielding for CHAMP

The characterization of buildup factor is well-known (Basu,2019). Buildup is an empirical value included to allow for scattered background energy which might have otherwise missed the detector. The goal is to mitigate buildup factor. **Figure 5.1** includes a graphic representation of buildup. It also provides an equation for gamma-ray intensity,

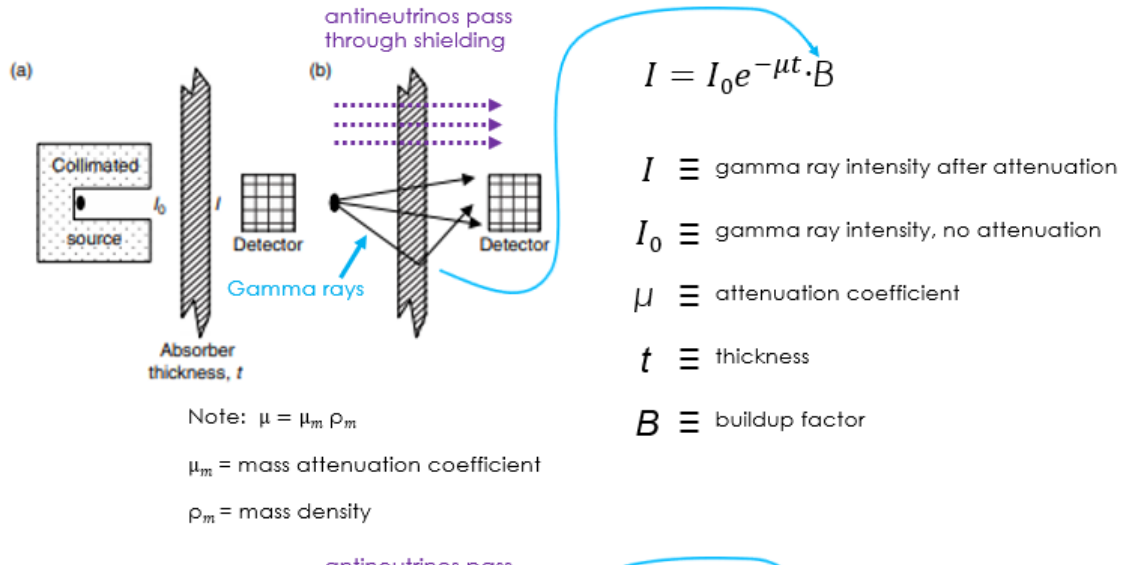


Figure 5.3. (a) Collimated sources reduce buildup. (b) Collimation could be incorporated in antineutrino detectors (the height and width of the detector) to reduce background radiation buildup from the reactor and detector shielding. However, some buildup would still be a factor (adapted from Gilmore, 2008).

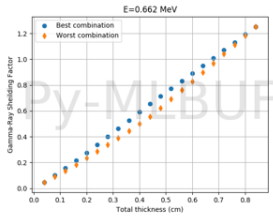
including a factor for buildup (Gilmore, 2008). A Python program for Multi-Layered Buildup (Py-MLBUF) should be available soon to allow on-line buildup calculations (2021, Mann).

There are a number of physical properties of gamma-ray shielding to explore (**Figure 5.4**). Here are a few: additive manufactured composition and geometry, mitigation of build-up factor, low to high Z layering, and sensitivity analysis of volumetric coefficients aiming to increase density.

Metal powder additive manufacturing could be used to produce novel shielding materials. Although cobalt 59 and depleted uranium would provide superior shielding both pose health risks.

A rhenium-tungsten alloy would be a good choice with a density between 19.3 and 21.0 grams per centimeter squared [g/cm^2]. The two metals together have improved mechanical properties, good thermal stability, and resistance to thermal shock. Along with high density, this combination allows for thinner material application without compromising structural integrity due to its improved mechanical properties. References are provided in **Figure 5.4** four other properties with the exception of geometry. The notion of deflecting gamma radiation in the way light is reflected by a mirror is unlikely. Shielding typically works by absorption and scattering, but scattering angles are typically statistical in changing the path. This makes controlled reproducible deflection difficult if not impossible.

Shielding Innovations



- Additive manufacturing, novel element mixtures
  - Tungsten (Z=74) 19.3 g/cm^3 manufactured with
    - Rhenium (Z=75) 21.0 g/ cm^3
    - Tantalum (Z=73) 16.6 g/cm^3
    - Hafnium (Z=72) 13.1 g/cm^3
    - Cobalt (Z=27) 8.9 g/cm^3
      - Cobalt 59 is the only stable Co isotope. Any neutron flux makes it Colbalt 60.
      - Health risk if improperly handled.
    - Bi2O3 composite, poly (methyl methacrylate) (PMMA) (Cao, et. Al., 2020)
  - Depleted uranium would be outstanding, but it's mildly pyrophoric.
  - Mechanical properties, gamma-ray shielding, tungsten composites (Wu, et. Al., 2020)
- Geometry (deflect gamma rays)
- Multiple layers (mitigate buildup)
  - low-Z/high-Z bilayer systems (Basu, et. Al., 2021) (McCaffrey, et. Al., 2009) (Ely, et. Al. 2008)
  - https://pymlbuf.pythonanywhere.com/
- Density enhancement (cryogenic, electrical) (ORNL, 2013)
  - Piezoelectric coefficient magnetostrictive effect

$$\frac{1}{V}\left(\frac{\partial V}{\partial E}\right)_T = \frac{1}{V}\left(\frac{\partial^2 G}{\partial p\,\partial E}\right) \qquad \frac{1}{V}\left(\frac{\partial V}{\partial B}\right)_T = \frac{1}{V}\left(\frac{\partial^2 G}{\partial p\,\partial B}\right)$$

Figure 5.4. Shielding innovations to explore in future CHAMP development. An example of Py-MLBUF is included in the upper right corner.

Future Shielding Analysis Tools for CHAMP

In comparing simulation software MCMP6 coupled with Attila provided the most successful results. Two obvious drawbacks are MCMP6's proprietary software and the high cost of Attila, about $30,000.

The Geant4 toolkit offers a more customized approach since is open source. With the customization also comes a higher level of computer science knowledge and skill required to successfully implement the toolkit. Geant4 input geometry format is Geometry Description Markup Language (GDML) (CERN, 2020). Complex geometry input using prototype pyg4ometry software failed but Irakli Garishvili at ORNL reports previous success with Computer-Aided Design Mesh (CADMesh) (Poole, 2012). Other possible prototype geometry input tools include SolidWorks to GDML (SW2GDML) (Vuosato, 2017), and Graphical User Interface Mesh (GUIMesh) (Pinto, 2019),

Energy Consumption Analysis

The composition of global energy consumption affects the world's environment. A study by Cook et al. reported 97 percent of actively publishing climate scientists support the consensus that man's burning of fossil fuels is driving climate change based on 11,944 peer-reviewed papers (Cook, et al., 2016).

The United Nations prioritizes energy consumption because it affects climate change and the world's environment. Population is a parameter included in energy consumption calculations. United Nations simulations predict a peak in the world's population from the current 8 billion to about 10 billion in 2080 and a decline afterward (United Nations, 2024). Considering population growth, worldwide energy consumption in 2023 of about

427 exajoules (EJ) or 427 * 10^{18} (Enerdata, 2024) has been estimated to increase about 48 percent to 631 EJ by 2050 (Vanek, et al., 2012).

Legacy nuclear power will continue to provide global energy while protecting the environment. One issue with large nuclear power plants producing on the order of 1200 megawatts (MW) of electrical power is the waste during off-peak hours. Six small Modular Reactors (SMRs) on the order of 200 MW can mitigate this problem. Operating in parallel, the SMR design allows load following to respond to grid demand.

One interesting possibility is retrofitting existing coal-fired plants with small modular reactors. An analysis from Poland recommended replacing a 460 MW supercritical coal-fired unit with a 320 MW SMR designed by Kairos Power (Bartela, et al., 2021).

The promise of fusion reactors remains elusive. In December 2022, researchers successfully produced a 1.54 (Q = 1.54) energy surplus fusion reaction at the National Ignition Facility (NIF), Lawrence Livermore National Laboratory (LLNL), California (Ahu-Shawareb, et al., 2024). Q refers to the fusion energy output divided by the laser energy input required to produce the fusion reaction. It is essential to recognize laser energy input is not the total electrical grid input energy needed for a fusion reactor. A higher grid energy would be required.

Oak Ridge National Laboratory has teamed up with the Tennessee Valley Authority and the Type One company to convert a closed coal-fired power plant, the Bull Run steam plant, into a fusion-powered prototype plant when one of the first fusion reactors becomes available. The project is in the early stages of plant acquisition and is still in the

proposal stage. A Q value 5.00 has been calculated as a necessary and sufficient energy surplus to make electrical production viable (Dow, 2024).

LIST OF REFERENCES ALPHABETICALLY BY YEAR

E. Fermi, "An Attempt at a Theory of "Beta" Ray Emission," Ricerca Scientifica, 4 (2), pp. 491-495, 1933.

H. Bethe and R. Peierls, The "Neutrino," Nature vol 133, p. 532, 1934.

H. A. Bethe, “Energy Production in Stars,” Physical Review, vol. 55, no. 1, pp. 103–103, Jan. 1939, doi: https://doi.org/10.1103/physrev.55.103.

E. Fermi, [1] E. Fermi, Nuclear Physics. Chicago, IL: University of Chicago Press, 1949.

C. L. Cowan, F. Reines, F. B. Harrison, E. C. Anderson, and F. N. Hayes, “Large Liquid Scintillation Detectors,” *Physical Review*, vol. 90, no. 3, pp. 493–494, 1953.

F. Reines and C. L. Cowan, “Detection of the Free Neutrino,” *Physical Review*, vol. 92, no. 3, pp. 830–831, 1953.

F. Reines and C. L. Cowan, “The Neutrino,” *Nature*, vol. 178, pp. 446–449, 1956.

Danby, G., et al. “Observation of high-energy neutrino reactions and the existence of two kinds of neutrinos.” *Physical Review Letters*, vol. 9, no. 1, 1962, pp. 36–44, https://doi.org/10.1103/physrevlett.9.36.

G. Zweig (17 January 1964). "An SU(3) Model for Strong Interaction Symmetry and its Breaking" (PDF). CERN Document Server. CERN-TH-401.

G. Zweig (21 February 1964). "An SU(3) Model for Strong Interaction Symmetry and its Breaking: II". *CERN Document Server*. doi:10.17181/CERN-TH-412. CERN-TH-412.

M. Gell-Mann (1964). "A Schematic Model of Baryons and Mesons". *Physics Letters*. 8 (3): 214–215. Bibcode:1964. PhL..8..214G. doi:10.1016/S0031-9163(64)92001-3.

B. Pontecorvo, “Neutrino Experiments and the Question of Leptonic-Charge Conservation,” *Old and New Problems in Elementary Particles*, pp. 251–261, 1968.

J. Friedman, H.W. Kendall (1968). "Deep Inelastic Electron Scattering." Physical Review Letters, 30(14), 694.

Bahcall, John N. “Neutrinos from the sun.” *Scientific American*, vol. 221, no. 1, 1969, pp. 28–37, https://doi.org/10.1038/scientificamerican0769-28.

J. D. Bjorken, *Phys. Rev. 179, 1547 (1969); In a private communication, Bjorken told the MIT-SLAC group about scaling in 1968.*R.P. Feynman, *(1969). "The Behavior of Hadron Collisions at Extreme Energies". High Energy Collisions: Third International Conference at Stony Brook, N.Y. Gordon & Breach. pp. 237–249. ISBN 978-0-677-13950-0.*

R. P. Feynman, “Very High-Energy Collisions of Hadrons,” *Physical Review Letters*, vol. 23, no. 24, pp. 1415–1417, Dec. 1969, doi: https://doi.org/10.1103/physrevlett.23.1415.

R. P. Feynman, “The parton picture of elementary particles,” *Proceedings of the International Conference on High-Energy Physics*, XVI, Chicago, Illinois, 1972 (Vol. 2, p. 12).

D. Z. Freedman, “Coherent effects of a weak neutral current,” *Physical Review D*, vol. 9, no. 5, pp. 1389–1392, 1974.

G. Charpak, et al., (1974). "Observation of single high-transverse-momentum electrons in the CERN-SPS." Physics Letters B, 50(2), 459-462.

H. Briand, , et al. (1974). "Observation of Particles with Large Transverse Momentum in 400 GeV Proton-Nucleus Collisions." Physical Review Letters, 33(22), 1406.

R. Davis and C. Evans, "Report on the Brookhaven Solar Neutrino Experiment," Chemistry Department* Brookhaven National Laboratory, 1976.

J. M. McKenzie, “Development of the semiconductor radiation detector,

” *Nuclear Instruments and Methods*, vol. 162, no. 1–3, pp. 49–73, Jun. 1979, doi: https://doi.org/10.1016/0029-554x(79)90706-7.

B. Pontecorvo, "Fifty Years of Neutrino Physics," Neutrino Physics and Astrophysics, Fioni (ed.), 1982.

W. L. Dunn and F. O'Foghludha, *Defense Nuclear Agency*, Washington, DC, rep., 1984.

P. D. Mannheim, “Symmetry and spontaneously broken symmetry in the physics of elementary particles,” *Computers & Mathematics with Applications*, vol. 12, no. 1–2, pp. 169–183, Jan. 1986, doi: https://doi.org/10.1016/0898-1221(86)90149-5.

R.L. Willett, et al., "Phys. Rev. Lett. 59,” 1776 (1987).

B. L. Cohen, *The nuclear energy option: an alternative for the 90s*. New York: Plenum, 1990.

F. Duncan, *Rickover and the nuclear navy: the discipline of technology*. Annapolis, MD: Naval Inst. Pr., 1990.

H. W. Kendall, “Deep inelastic scattering: Experiments on the proton and the observation of scaling,” vol. 63, no. 3, pp. 597–614, Jul. 1991, doi: https://doi.org/10.1103/revmodphys.63.597.

J. I. Friedman, “Deep inelastic scattering: Comparisons with the quark model,” *Reviews of Modern Physics*, vol. 63, no. 3, pp. 615–627, Jul. 1991, doi: https://doi.org/10.1103/revmodphys.63.615.

R. E. Taylor, “Deep inelastic scattering: The early years,” *Reviews of Modern Physics*, vol. 63, no. 3, pp. 573–595, Jul. 1991, doi: https://doi.org/10.1103/revmodphys.63.573.

M. Riordan, “The discovery of Quarks,” *Science*, vol. 256, no. 5061, pp. 1287–1293, May 1992. doi:10.1126/science.256.5061.1287

S. T. Petcov "On B Pontecorvo Contributions to Weak Interaction and Neutrino Physics," CERN, 1994

P. Schmueser, *Feynman graphs and gauge theories for experimental physicists*, 2nd ed., vol. 295. Berlin, Germany: Springer, 1995.

F. Reines, “The neutrino: from poltergeist to particle,” *Reviews of Modern Physics*, vol. 68, no. 2, pp. 317–327, 1996.

S. Kobayashi, et al., “Tungsten alloys as radiation protection materials,” *Nuclear Instruments and Methods in Physics Research Section A: Accelerators, Spectrometers, Detectors and Associated Equipment*, vol. 390, no. 3, pp. 426–430, 1997.

Staff, "The Reines-Cowan Experiments, Detecting the Poltergeist," Los Alamos Science, Number 25, 1997.

D. K. Ershov, “Biological action of antineutrino radiation from nuclear reactors at nuclear power plants,” *Atomic Energy*, vol. 85, no. 1, pp. 515–516, 1998.

D. Nicolò, “The neutrino-oscillation experiment at the CHOOZ nuclear power plant, ” *Progress in Particle and Nuclear Physics*, vol. 40, pp. 263–264, 1998.

M. Rottinger, “4.1 Charge-Coupled Devices,” *Tuwien.ac.at*, 1999. https://www.iue.tuwien.ac.at/phd/rottinger/node31.html (accessed Aug. 07, 2024).

NOVA, "*The Ghost Particle: Dancing With Neutrinos*," vol. 33, no. 12, PBS, 1999.

P. Truscott, et al. “Geant4-a New Monte Carlo Toolkit for Simulating Space Radiation Shielding and Effects.” *2000 IEEE Radiation Effects Data Workshop. Workshop Record. Held in Conjunction with IEEE Nuclear and Space Radiation Effects Conference (Cat. No.00TH8527)*, doi:10.1109/redw.2000.896281.

J. R. Janesick, *Scientific Charge-Coupled Devices*. 20Th Street, Bellingham, Wa 7-Usa Spie, 2001.

A. Bernstein, et al., “Nuclear reactor safeguards and monitoring with antineutrino detectors,” *Journal of Applied Physics*, vol. 91, no. 7, pp. 4672–4676, 2002.

F. Lei, et al., “MULASSIS: a geant4-based multilayered shielding simulation tool,” IEEE Transactions on Nuclear Science, vol. 49, no. 6, pp. 2788–2793, 2002.

M Fukugita and T Yanagida, *Physics of neutrinos and applications to astrophysics*. Berlin ; New York: Springer, 2003.

P. Lipari, Introduction to Neutrino Physics, Universita di Roma, 2003.

A. B. McDonald, et al., “Astrophysical neutrino telescopes,” *Review of Scientific Instruments*, vol. 75, no. 2, pp. 293–316, 2004. doi:10.1063/1.1642740

J. Carrier, et al., “Validation of Geant4, an object-oriented Monte Carlo toolkit, for simulations in medical physics,” *Medical Physics*, vol. 31, no. 3, pp. 484–492, 2004.

J. Gleick, Isaac Newton. New York: Vintage Books, 2004.

K. Amako,. “Geant4 In Production: Past, Present and ... - Indico.cern.ch.” *CERN Geant4*, GERN, 15 Dec. 2004, https://indico.cern.ch/event/420849/contributions/1884463/attachments/880765/1236879/G4History.pdf.

Z. Kolář and W. den Hollander, “2003: A centennial of spinthariscope and scintillation counting,” *Applied Radiation and Isotopes*, vol. 61, no. 2–3, pp. 261–266, Aug. 2004, doi: https://doi.org/10.1016/j.apradiso.2004.03.056.

R. F. Casten, *Nuclear structure from a simple perspective*. Oxford: Oxford University Press, 2005.

N. D. Cook, *Models of the atomic nucleus: with interactive software*. Berlin ; New York: Springer, Cop, 2006.

A. Hazi, “2006 Physics and Advanced Technologies In the News,” Lawrence Livermore National Laboratory, CA, Apr. 2007. Available: https://digital.library.unt.edu/ark:/67531/metadc889626/m2/1/high_res_d/909644.pdf

Anon, “Tungsten Alloys Supersede Lead in Nuclear Medicine,” *Materials & Design*, vol. 28, no. 5, p. 1745, 2007.

C. Giunti and C. W. Kim, *Fundamentals of neutrino physics and astrophysics*. Oxford: Oxford University Press, 2007.

J. Allison, “Facilities and Methods: Geant4 – A Simulation Toolkit.” *Nuclear Physics News*, vol. 17, no. 2, 2007, pp. 20–24., https://doi.org/10.1080/10506890701404297.

J. E. Turner, *Atoms, radiation, and radiation protection*. Weinheim: Wiley-Vch, 2007.

A. Bernstein, et al., “Monitoring the thermal power of nuclear reactors with a prototype cubic meter antineutrino detector,” *Journal of Applied Physics*, vol. 103, no. 7, p. 074905, 2008.

A. de Gouvea and J. Jenkins, “Physical Range Of Majorana Neutrino Mixing Parameters,” *Physical Review D*, vol. 78, 2008.

G. Gilmore, *Gamma-ray Spectrometry*, Wiley, 2008.

J. H. Ely, et al., “Shielding and Build-up Considerations for Radiation Detection,” *2008 IEEE Nuclear Science Symposium Conference Record*, vol. N02-465, 2008.

N. S. Bowden, “Reactor monitoring and safeguards using antineutrino detectors,” *Journal of Physics: Conference Series*, vol. 136, no. 2, p. 022008, 2008.

S. Abe, et al., “Precision Measurement of Neutrino Oscillation Parameters with KamLAND,” *Physical Review Letters*, vol. 100, no. 221803, 2008.

A. Bernstein, et al., “Nuclear Security Applications of Antineutrino Detectors: Current Capabilities and Future Prospects," ARXIV, 2009.

F. Krauss, “Deep-inelastic scattering and the structure of protons Introduction to particle physics Lecture 7,” 2009. Accessed: May 26, 2024. [Online]. Available: https://www.ippp.dur.ac.uk/~krauss/Lectures/IntroToParticlePhysics/Lecture7.pdf

Institute of Medicine, National Academy of Engineering, National Academy of Sciences, and C. on, *On Being a Scientist*. National Academies Press, 2009.

J. A. Gowan, *The "W" Intermediate Vector Boson and the Weak Force Mechanism*. 2009 [Online]. Available: https://arxiv.org/html/physics/0008025. [Accessed: 28-Apr-2021].

J. P. McCaffrey, et al., "Optimizing Non-Pb Radiation Shielding Materials Using Bilayers." *Medical Physics*, vol. 36, no. 12, 2009, pp. 5586–5594., doi:10.1118/1.3260839.

N. S. Bowden, et al., "Observation of the isotopic evolution of pressurized water reactor fuel using an antineutrino detector," *Journal of Applied Physics, 105(6), 064902, 2009.*

Cacuci, "Handbook of Nuclear Engineering," Ch. 11 J. Shultis, "Nuclear Shielding," Springer, 2010.

Constantin, Magdalena, et al. "Linking Computer-Aided Design (CAD) to Geant4-Based Monte Carlo Simulations for Precise Implementation of Complex Treatment Head Geometries." *Physics in Medicine and Biology*, vol. 55, no. 8, 2010, https://doi.org/10.1088/0031-9155/55/8/n03.

G. E. Smith, "Nobel Lecture: The invention and early history of the CCD," *Reviews of Modern Physics*, vol. 82, no. 3, pp. 2307–2312, Aug. 2010, doi: https://doi.org/10.1103/revmodphys.82.2307.

F. Simon, "*Aspekte der modernen Kosmologie,*" Max-Planck-Institut fur Physik, Excellence Cluster Universe, presentation, 2011

F. Thomson, “Part III Particle Physics Lectures Home Page,” 2011. *www.hep.phy.cam.ac.uk*. https://www.hep.phy.cam.ac.uk/~thomson/partIIIparticles/ (accessed May 19, 2024).

Fabri, A., and S. Pion. “CGAL - The Computational Geometry Algorithms Library.” *Proceedings 17th ACM SIGSPATIAL*, 2011.

G. C. Holst and T. S. Lomheim, *CMOS, CCD sensors and camera systems*. Winter Park, Fl. Jcd Publ. U.A, 2011.

Guatelli, S., et al. “Introduction to the gGeant4 Simulation Toolkit.” *AIP Conference Proceedings*, 2011, https://doi.org/10.1063/1.3576174.

M. Thomson, “Handout 5 : Electron-Proton Elastic Scattering Electron-Proton Scattering (e -q o e -q),” 2011. Accessed: May 19, 2024. [Online]. Available:https://www.hep.phy.cam.ac.uk/~thomson/partIIIparticles/handouts/Handout_5_2011.pdf

M. Thomson, “Handout 6 : Deep Inelastic Scattering e -p Elastic Scattering at Very High q 2,” 2011. Available: https://www.hep.phy.cam.ac.uk/~thomson/partIIIparticles/handouts/Handout_6_2011.

M. Thomson, “Symmetries and the Quark Model,” 2011. https://www.hep.phy.cam.ac.uk/~thomson/partIIIparticles/handouts/Handout_7_2011.

A. Bolozdynya *et al.*, “Opportunities for Neutrino Physics at the Spallation Neutron Source: A White Paper,” Nov. 2012.

C. M.Poole, et al., “A CAD Interface for Geant4.” *Australasian Physical & Engineering Sciences in Medicine*, vol. 35, no. 3, 2012, pp. 329–334., https://doi.org/10.1007/s13246-012-0159-8.

F. E. Close, *Neutrino*. Oxford: Oxford University Press, 2012.

F. Vanek, et al., *Energy Systems Engineering: Evaluation and Implementation, Second Edition*. McGraw Hill Professional, 2012.

J. W. Tester, *Sustainable Energy : choosing among options,* S.L.: Phi Learning, 2012.

L. O. Drury, “Origin of cosmic rays,” *Astroparticle Physics*, vol. 39–40, pp. 52–60, 2012. doi:10.1016/j.astropartphys.2012.02.006

Shaver, M.W. et al. "Transport Test Problems for Radiation Detection Scenarios," PNNL-21736, 2012.

Cern, “Thorium Energy for the World,” Proceedings of the ThEC13 Conference, Globe of Science and Innovation, Geneva, Switzerland, October 27-31, 2013.

G. Fidecaro, "Bruno Pontecorvo and his Inverse β Process to Detect Neutrinos," 2013.

K. Lang, *Essential Astrophysics*. Berlin, Heidelberg Springer, 2013.

M. P. Foxe and I. Jovanovic, “Low-energy ionization yield in liquid argon for a coherent neutrino-nucleus scatter detector,” dissertation, 2013.

R. Saakyan, "Two-Neutrino Double-Beta Decay," Annu. Rev. Nucl. Part. Sci., pp. 503- 529, 2013.

Shef, “Neutrinos and Neutrino Oscillations,” *Shef.ac.uk*, 2013. https://www.hep.shef.ac.uk/cartwright/pubweb/neutrinos_advanced.html

N. Fields, “Development Of A Low Threshold Detector For The Observation Of Coherent Elastic Neutrino-Nucleus Scattering,” Dissertation, University Of Chicago, 2014. Accessed: Oct. 11, 2024. [Online]. Available: https://www.proquest.com/docview/1647745354

R. Hargraves, “The Passion of Alvin Weinberg,” *The Breakthrough Institute*, 05-Feb-2014. [Online]. Available: https://thebreakthrough.org/issues/energy/the-passion-of-alvin-weinberg. [Accessed: 05-Jan-2021].

S. Yip, *Nuclear Radiation Interactions*. World Scientific Publishing Company, 2014.

C. Rofer, “Why did the US abandon a lead in reactor design?” *Physics Today*, 2015.

D. Lindley, “*Landmarks*—Discovery Of A 2nd Kind Of Neutrino,” *Physics*, vol. 8, 2015. doi:10.1103/physics.8.75

F. E. Close, *Half-Life: The Divided Life Of Bruno Pontecorvo, Physicist Or Spy*, New York, NY: Basic Books, A Member Of The Perseus Books Group, 2015.

J. M. Donev, “Neutrino Nobel Prize overview,” in *University of Calgary, 2015*.

K. Scholberg, "Coherent elastic neutrino-nucleus scattering." J. Phys: Conf. 606 012010, 2015.

N. Tsoulfanidis and S. Landsberger, *Measurement and detection of radiation*. Boca Raton, FL: CRC Press, 2015.

P. B. Pal, *An introductory course of particle physics*. Boca Raton, Fl: Crc Press, 2015.

E. Recami, “Majorana, The Neutron, And The Neutrino: Some Elementary Historical Memories,” Hadronic Journal, vol. 40, no. 149, 2017.

F. An, et al., "The detector system of the Daya Bay reactor neutrino experiment." Nuclear Instruments and Methods in Physics, 2016.

G. Rajasekaran, "The Story of the Neutrino," 2016

J. Cook *et al.*, “Consensus on consensus: a synthesis of consensus estimates on human-caused global warming,” *Environmental Research Letters*, vol. 11, no. 4, p. 048002, Apr. 2016, doi: https://doi.org/10.1088/1748-9326/11/4/048002.

Jillre, “UML class diagrams: Reference - visual studio 2015,” *Visual Studio 2 Microsoft Docs*, 2016. [Online]. Available: https://docs.microsoft.com/en-us/previous-versions/visualstudio/visual-studio-2015/modeling/uml-class-diagrams-reference?view=vs-2015. [Accessed: 22-Feb-2022].

M. Archer, “Three-way Coupled Pendulum & Neutrinos | What the Physics,” *YouTube*. Oct. 06, 2016. [YouTube Video]. Available: https://www.youtube.com/watch?v=YqVF3NSc5xg

M. F. L'Annunziata, *Radioactivity: Introduction and history, from the quantum to quarks*. Elsevier Science, 2016.

M. Klasky, et al., “MCNP and GADRAS Comparisons,” Los Alamos National Laboratory, Apr. 2016.

Perkins, D. H., Early steps towards quarks and their interactions using neutrino beams in CERN bubble chamber experiments. *The European Physical Journal H, 41*(2), 157–164, (2016). https://doi.org/10.1140/epjh/e2016-70016-2

S. Brewster, “Is the neutrino its own antiparticle?,” Fermilab/SLAC *symmetry magazine, 2016*. [Online].

Available: https://www.symmetrymagazine.org/article/is-the-neutrino-its-own-antiparticle. [Accessed: 02-Dec-2020].

S. F. Corzo, D. E. Ramajo, and N. M. Nigro, “CFD model of a moderator tank for a pressure vessel PHWR nuclear power plant,” *Applied Thermal Engineering*, vol. 107, pp. 975–986, Aug. 2016, doi: https://doi.org/10.1016/j.applthermaleng.2016.07.034.

A. G. Wright, *The photomultiplier handbook*. Oxford: Oxford University Press, 2017.

B. J. Scholz, “First Observation of Coherent Elastic Neutrino-Nucleus Scattering,” dissertation, 2017.

E. Recami, “Majorana, The Neutron, And The Neutrino: Some Elementary Historical Memories,” *Hadronic Journal*, vol. 40, no. 149, 2017.

H. Klus, *How We Came to Know the Cosmos: Light and Matter*. The Star Garden, 2017.

J. Donev, "Neutrino Nobel Prize Overview," presentation, 2017

J. Tiffenberg *et al.*, “Single-Electron and Single-Photon Sensitivity with a Silicon Skipper CCD,” vol. 119, no. 13, Sep. 2017, doi: https://doi.org/10.1103/physrevlett.119.131802.

M. Anton, “Dynamic or Shared Libraries - Minas Anton - Medium,” *Medium*, Aug. 09, 2017. https://medium.com/@minas_anton/dynamic-or-shared-libraries-2805cb4fb410 (accessed Oct. 16, 2024).

NNSA, *Introduction to International Safeguards*. NNSA, 2017.

P. Hernandez, “Neutrino Physics,” arxiv.org, 2017.

Tolias, P. “Analytical Expressions for Thermophysical Properties of Solid and Liquid Tungsten Relevant for Fusion Applications.” *Nuclear Materials and Energy*, vol. 13, 2017, pp. 42–57., doi:10.1016/j.nme.2017.08.002.

Vuosalo, C, et al. “A Tool to Convert CAD Models for Importation into Geant4.” *Journal of Physics: Conference Series*, vol. 898, 2017, p. 042024., https://doi.org/10.1088/1742-6596/898/4/042024.

A. L. Lund and P. K. Romano, “Implementation and Validation of Photon Transport in OpenMC,” 2018.

A. Sadique, “UML class diagram explained with C++ Samples,” *CPP Code Tips*, 19-Jul-2018. [Online]. Available: https://cppcodetips.wordpress.com/2013/12/23/uml-class-diagram-explained-with-c-samples/. [Accessed: 02-Mar-2022].

D. Forero, “Standard and non-standard neutrino physics at reactor experiments,” presentation, 2018.

D. McAlister, "Gamma Ray Attenuation Properties of Common Shielding Materials," Lisle, IL, rep., 2018.

F. Close, *Antimatter*. Oxford, Oxford University Press, 2018.

G. Allison, “Nuclear Terrorism: Did We Beat the Odds or Change Them?,” *Prism*, vol. 7, no. 3, May 2018.

J. Allday, *Quarks, Leptons and The Big Bang: Second Edition*, Milton: CRC Press, 2018.

J. C. Bryan, *Introduction to Nuclear Science*. CRC Press, 2018.

J. Resag and Springerlink (Online Service, *Feynman and His Physics: The Life and Science of an Extraordinary Man*. Cham: Springer International Publishing, 2018.

K. Scholbert, "CEvNS and NINs: Observation of Coherent Elastic Neutrino-Nucles Scattering," Presentation, 2018.

N. Allemandou, et al., “The STEREO Experiment,” IOP Publications, 2018

N. Macfadden, et al., “Development and Validation of a Geant4 Radiation Shielding Simulation Framework,” 2018.

Anon, “Molecular Expressions Microscopy Primer: Digital Imaging in Optical Microscopy - Concepts in Digital Imaging - Photomultiplier Tubes,” Fsu.edu, 2019. https://micro.magnet.fsu.edu/primer/digitalimaging/concepts/photomultipliers.htmlC.

B. Zwiebach, MIT Open Course Ware, “L19.1 Elastic scattering defined and assumptions,” *YouTube*, Feb. 14, 2019. https://www.youtube.com/watch?v=GZzrMyY01tE (accessed Aug. 17, 2024).

C. Gonzalez-Garcia, "Introduction to the Physics of Massive Neutrinos I," International PhD Summer School on Neutrinos, 2019

C. Giunti, “Precise Determination of the 235U Reactor Antineutrino Cross Section per Fission,” *Journal of Physics: Conference Series*, vol. 1216, p. 012016, 2019.

C. Stewart, A. et al., “Employing antineutrino detectors to safeguard future nuclear reactors from diversions,” *Nature Communications*, vol. 10, no. 1, 2019.

D. Akimov, et al. Observation of coherent elastic neutrino-nucleus scattering. Science, 357(6356):pp. 1123-1126, 2019. URL http://science:sciencemag:org/content/357/6356/1123 (2017).

D. Lincoln, “Why does light slow down in water?,” *YouTube*. Feb. 20, 2019. [YouTube Video]. Available: https://www.youtube.com/watch?v=CUjt36SD3h8

F. Deppisch, *A Modern Introduction to Neutrino Physics*. San Rafael, CA: Morgan & Claypool Publishers, 2019.

Hawaii.edu, 2019. http://www2.hawaii.edu/~takebaya/ics111/process_of_programming/process_of_programming.html

I. Economics & Peace, Global Terrorism Index, rep., 2019.

I. Jovanovic, “Reactor Monitoring using Coherent Elastic Neutrino- Nucleus Scattering,” in *MTV Kickoff Meeting*, 2019.

J. Ashenfelter and et Al., “Measurement of the Antineutrino Spectrum from 235U Fission at HFIR with PROSPECT,” *Physics Letters B*, Jul. 2019

J. Formaggio, "Ricochet, Probing Reactor Neutrinos Through Coherence," MIT, 2019.

J. Hader and N. Whitman, “Attila and MCNP6.2 Validation with the JASPER-IHX Benchmark for Sodium-Cooled Fast Reactor Shielding Applications,” *Transactions of the American Nuclear Society - Volume 121,* 2019.

J. Shapiro, “What is version control,” *Atlassian,* 2019. https://www.atlassian.com/git/tutorials/what-is-version-control

J. Yee, *EWT, Introduction to Energy Wave Theory,* 2019. https://www.youtube.com/watch?v=4VxZDcwFG94

K. Mahmoud, et al., “Gamma-ray shielding characteristics and exposure buildup factor for some natural rocks using MCNP-5 code,” *Nuclear Engineering and Technology*, vol. 51, no. 7, pp. 1835–1841, 2019.

K. S. Mann, “Investigation of gamma-ray shielding by double layered enclosures,” *Radiation Physics and Chemistry*, vol. 159, pp. 207–221, 2019.

L. Biron, *How do you make the world's most powerful neutrino beam?, Fermilab/SLAC Symmetry Magazine, 2019.* [Online]. Available: https://news.fnal.gov/2019/11/how-do-you-make-the-worlds-most-powerful-neutrino-beam/. [Accessed: 02-Dec-2020].

M. Loverde, *Neutrino Properties from Cosmology,* Stony Brook University, 2019

M. Nemerever,“Git, GitHub, & Workflow Fundamentals,” *DEV Community*. 2019. https://dev.to/mollynem/git-github--workflow-fundamentals-5496

M. V. D. Ende, et al., “Stand-off nuclear reactor monitoring with neutron detectors for safeguards and non-proliferation applications,” *Nature Communications*, vol. 10, no. 1, 2019.

Nobel, “All Nobel Prizes,” *NobelPrize.org*, 2019. https://www.nobelprize.org/prizes/lists/all-nobel-prizes/

P. Basu et al., “Gamma-ray buildup factors for conventional shielding materials and buildup factors computed for tungsten with a thickness beyond 40 mean free paths,” *Applied Radiation and Isotopes*, vol. 154, p. 108864, 2019.

Pinto, M., and P. Gonçalves. “Guimesh User's Manual," circa 2019.

Pinto, M., and P. Gonçalves. “Guimesh: A Tool to Import Step Geometries into Geant4 via GDML.” *Computer Physics Communications*, vol. 239, 2019, pp. 150–156., https://doi.org/10.1016/j.cpc.2019.01.024.

R. Carr, "Can Neutrino Detectors Strengthen the Nonproliferation Regime?," 2019. https://www.youtube.com/watch?v=RaZOfDQCYGM

A. Aliane, et al., “First test of a Li2WO4(Mo) bolometric detector for the measurement of coherent neutrino-nucleus scattering,” *Nuclear Instruments and Methods in Physics Research Section A: Accelerators, Spectrometers, Detectors and Associated Equipment*, vol. 949, p. 162784, 2020.

A. Bernstein, et al., “Colloquium: Neutrino detectors as tools for nuclear security,” *Reviews of Modern Physics*, vol. 92, no. 1, Mar. 2020, doi: https://doi.org/10.1103/revmodphys.92.011003.

A. F. Woolf and J. D. Werner, The U.S. Nuclear Weapons Complex: Overview of Department of Energy Sites, Congressional Research Service, vol. R45306. 2020.

A. Haghighat, et al., "Observation of Reactor Antineutrinos with a Rapidly Deployable Surface-Level Detector," Physical Review Applied 13, 11 Mar 2020.

C. Chavez *et al.*, “A solution for future single-electron-counting fast-readout Skipper-CCD experiments: high channel density front-end electronics design and noise performance analysis,” Nov. 2020, doi: https://doi.org/10.1117/12.2580121.

Fermi Lab, "Skipper CCD for observing neutrinos from nuclear reactors," Presentation, 2020.

H. Almazan, et al., “Accurate Measurement of the Electron Antineutrino Yield of U235 Fissions from the STEREO Experiment with 119 Days of Reactor-On Data,” *Physical Review Letters*, vol. 125, no. 201801, 2020.

I. Garishvilli, “Developing A Platform For Compact Neutrino Experiments For Non-Proliferation At HFIR ,” in *LDRD*, 2020.

J. E. Dodd and B. M. Gripaios, *The ideas of particle physics*, New York: Cambridge University Press, 2020.

J. Janesick, Skipper CCD Plans, Cern, 2020. https://indico.cern.ch/event/885463/attachments/1983434/3310704/COFI_skipperPlans

J. Link, et al., "The Curious History of Neutrinos and Nuclear Reactors," Nuclear News, Dec. 2020.

J. Newby, "NuToolsORNL, Introduction to Neutrino Detectors," ORNL, 2020.

L. Labit, “Latest results of the STEREO experiment,” in *STEREO Collaboration*, 2020.

M. Klute, Neutrino Physics, MIT, 2020.

M. S. Athar and S. K. Singh, The physics of neutrino interactions. “Neutrino Sources and Detection of Neutrinos,” pp. 669–707, Cambridge: Cambridge University Press, 2020.

N. J. AbuAlRoos, et al., “Tungsten-based material as promising new lead-free gamma radiation shielding material in nuclear medicine,” *Physica Medica*, vol. 78, Oct. 2020.

O. Kilicoglu and H. Tekin, “Bioactive glasses and direct effect of increased K2O additive for nuclear shielding performance: A comparative investigation,” *Ceramics International*, vol. 46, no. 2, pp. 1323–1333, 2020.

O. Miranda, et al., “Implications of the first detection of coherent elastic neutrino-nucleus scattering (CEvNS) with liquid Argon,” *Journal of High Energy Physics*, vol. 2020, no. 5, 2020.

P. Looyen, “The standard model: what’s the evidence for the quark?,” www.youtube.com, 2020. https://www.youtube.com/watch?v=HPoGMpO6Z6o

Physics Explained, “What is Compton Scattering?,” *YouTube*. Apr. 10, 2020. [YouTube Video]. Available: https://www.youtube.com/watch?v=rGy7nsC8O_Y

R. Loggini, “CMake in Visual Studio,” *Riccardo Loggini*, May 17, 2020. https://logins.github.io/programming/2020/05/17/CMakeInVisualStudio.html

S. Boyd, Neutrino Oscillations, Warwick Dept. of Physics, 2020.

ScienceClic English, “Quantum Field Theory visualized,” *YouTube*. Oct. 31, 2020. [YouTube Video]. Available: https://www.youtube.com/watch?v=MmG2ah5Df4g

T. Akindele, “Applied Antineutrinos for Nonproliferation,” in *UTK Nuclear Engineering Seminar*, 07-Oct-2020.

T2k-experiment.org, 2020. https://t2k-experiment.org/

Wu, Yin, et al. “Mechanical Properties and Gamma-Ray Shielding Performance of 3d-Printed Poly-Ether-Ether-Ketone/Tungsten Composites.” *Materials*, vol. 13, no. 20, 2020, p. 4475., doi:10.3390/ma13204475.

Y. Song et al.., “Research on fast intelligence multi-objective optimization method of nuclear reactor radiation shielding,” vol. 149, pp. 107771–107771, Dec. 2020, doi: https://doi.org/10.1016/j.anucene.2020.107771.

All Lectures, International PhD Summer School on Neutrinos, 2021.

ANS, The U.S. Nuclear R&D Imperative, rep., 2021.

C. Scott, *Professional CMake: A Practical Guide 10th Edition*. 2021.

D. E. Rowe, *Emmy Noether – Mathematician Extraordinaire*. Springer Nature, 2021.

D. Lincon, "Beta Decay, Mystery or Not," 2021

G. Cancelo, et al., “Low threshold acquisition controller for Skipper charge-coupled devices,” *Journal of Astronomical Telescopes Instruments and Systems*, vol. 7, no. 01, Jan. 2021, doi: https://doi.org/10.1117/1.jatis.7.1.015001.

G. Fernandez-Moroni, et al., “The physics potential of a reactor neutrino experiment with Skipper CCDs: measuring the weak mixing angle,” *Journal of High Energy Physics*, vol. 2021, no. 3, 2021.

IEA, “Final consumption – Key World Energy Statistics 2021 – Analysis,” *IEA*, 2021. https://www.iea.org/reports/key-world-energy-statistics-2021/final-consumption

J. Matta, ORNL-PROSPECT Technical Report 3: Simulation of large volume NaI(Tl) detectors and decomposition of their spectra, rep., 2021.

K. Scholberg, "Coherent Elastic Neutrino-Nucleus Scattering," International PhD Summer School on Neutrinos, 2021.

L. I. Munteanu, “Towards the measurement of CP violation in neutrino oscillations with the T2K experiment,” Dissertation, Université Paris-Saclay, 2021. Accessed: Nov. 14, 2024. [Online]. Available: https://theses.hal.science/tel-03474937/document

Ł. Bartela, et al., “Techno-Economic Assessment of Coal-Fired Power Unit Decarbonization Retrofit with KP-FHR Small Modular Reactors,” *Energies*, vol. 14, no. 9, p. 2557, Apr. 2021, doi: https://doi.org/10.3390/en14092557.

Luxium, “Scintillation Detector Operating Manual CRYSTALS Handling And Care Installation Troubleshooting Important Note On The Safe Handling of NaI(Tl) Crystal Material Contents,” 2021.

Available:https://www.luxiumsolutions.com/sites/default/files/2021-09/Scintillation-Operating-Manual.pdf

M. Andriamirado and et Al., “Improved Short-Baseline Neutrino Oscillation Search and Energy Spectrum Measurement with the PROSPECT Experiment at HFIR,” *Physical Review D*, vol. 103, no. 032001, 2021.

M. K. Hansda, S. Mammen, “3Dgshield: A New 3d Gamma Ray Shielding Code for Arbitrary Source and Shield Geometry Based on Point Kernel Technique.” *Annals of Nuclear Energy*, vol. 159, 2021, p. 108352., doi:10.1016/j.anucene.2021.108352.

O. Ruchayskiy, "Neutrinos as a key to a unified theory of particle physics and cosmology," International PhD Summer School on Neutrinos, 2021

P. Barbeau, “COHERENT Elastic Neutrino Nucleus Scattering (CEvNS).” 11 Jan 2021

P. Barbeau, *Small Size Antineutrino Detector*, Email, 09-Apr-2021.

“Quantum Electrodynamics and Feynman Diagrams,” *www.youtube.com*. 2021. https://www.youtube.com/watch?v=X-FEU4mQWtE

R. Nathuram, “Photon Attenuation Characteristics Of Radiation Shielding Materials," Mumbai, India, rep. P-6a-327, 2021

S. D. Walker, et al., “Pyg4ometry: a Python library for the creation of Monte Carlo radiation transport physical geometries,” *Physics Comp*, 2021.

U. Oregon, "*Particle Physics.*" Lecture, 2021

Y. Song, et al., “A novel multi-objective shielding optimization method: DNN-PCA-NSGA-II,” *Annals of Nuclear Energy*, vol. 161, p. 108461, Oct. 2021, doi: https://doi.org/10.1016/j.anucene.2021.108461.

C. R. Chavez, F. Chierchie, M. Sofo-Haro, J. Lipovetzky, G. Fernandez-Moroni, and J. Estrada, “Multiplexed Readout for an Experiment with a Large Number of Channels Using Single-Electron Sensitivity Skipper-CCDs,” *Sensors*, vol. 22, no. 11, pp. 4308–4308, Jun. 2022, doi: https://doi.org/10.3390/s22114308.

COHERENT Collaboration, "The COHERENT Experimental Program," 2022.

G. Fernandez-Moroni *et al.*, “The physics potential of a reactor neutrino experiment with Skipper-CCDs: searching for new physics with light mediators,” ˜ *The œJournal of high energy physics/˜ The œjournal of high energy physics*, vol. 2022, no. 2, Feb. 2022, doi: https://doi.org/10.1007/jhep02(2022)127.

G. Moroni, *et al.*, “Skipper Charge-Coupled Device for Low-Energy-Threshold Particle Experiments above Ground,” *Physical review applied*, vol. 17, no. 4, Apr. 2022, doi: https://doi.org/10.1103/physrevapplied.17.044050.

I. Garishvilli, “Towards developing Compact HFIR Anti-neutrino Monitoring Platform (CHAMP) ,” in Presentation, 2022.

J. T. Matta, “The Need for Speed: Keeping Pace with Science’s Ever-Growing Thirst for Data,” in *Seminar*, 28-Jan-2022.

L. Barak, et al., “Characterization of Single-Electron Events Using a Skipper Charge-Coupled Device,” *Physical Review Applied*, vol. 17, no. 014022, pp. 014022-19, Jan. 2022, doi: https://doi.org/10.1103/PhysRevApplied.17.014022.

S. Marguet, *A Brief History of Nuclear Reactor Accidents*. 2022.

UML Association vs aggregation vs composition. [Online]. Available: https://www.visual-paradigm.com/guide/uml-unified-modeling-language/uml-aggregation-vs-composition/. [Accessed: 15-Feb-2022].

B. Heffron, Neutrino Physics at a Research Reactor: Backgrounds and Analysis, UTK, 2023.

CERN, “Book For Application Developers — Book For Application Developers 11.1 documentation,” *geant4-userdoc.web.cern.ch.*, 2023. https://geant4-userdoc.web.cern.ch/UsersGuides/ForApplicationDeveloper/html/index.html

Chat GPT, "Relate Alpha, Beta, and Gamma Radiation to Strong, Weak, and Electromagnetic Forces,” 2023.

Department of Energy, “Department of Energy,” *Energy.gov*, 2023. https://www.energy.gov/

G. Barenboim, "Neutrino physics (theory & phenomenology)," 1 of 3, 2023. https://www.youtube.com/watch?v=IHNx6XR9B-E

G. Barenboim, "Neutrino physics (theory & phenomenology)," 3 of 3, 2023. https://www.youtube.com/watch?v=lrC073NO4qY&list=PLUqyF3MCZTaWv6t9rJ7Br9qj005dPoFcM&index=13

“International Energy Outlook 2023 - U.S. Energy Information Administration (EIA),” *www.eia.gov*. https://www.eia.gov/outlooks/ieo/narrative/index.php

M. Zheng, et al., “Nuclear power developments in China and the world,” 2023. *ANS*. [Online]. Available: https://www.ans.org/news/article-4748/nuclear-power-developments-in-china-and-the-

world/?mkt_tok=MDk5LVlMVS02MzAAAAGKsslV_sVhBUiGe_ei-dtkVJdvpbDV-IklYb6X2ufC0L6NyjGBROY3ZeAW2yxHEIdGdbAkQEtqCdikQiOKEochM6oFgrVG8MTDkND. [Accessed: 24-Mar-2023].

Neils Bohr Neutrino Summer School, 2023. https://www.youtube.com/playlist?list=PLUqyF3MCZTaWv6t9rJ7Br9qj005dPoFcM

Y. Q. Chen and B. H. Yan, "The technology of shielding design for nuclear reactor: A review," *Progress in Nuclear Energy*, vol. 161, p. 104741, Jul. 2023, doi: https://doi.org/10.1016/j.pnucene.2023.104741.

A. Kupco, "Quarks, Partons, and Quantum Chromodynamics Lecture 6," in *Proton structure and parton model*, May. 8, 2024

Andrey K, "Particle Resonance and Resonance Width," *YouTube*, May 03, 2014. https://www.youtube.com/watch?v=usc0YGmEmYc (accessed May 18, 2024).

Chat GPT, "use quantum field theory to explain how a W- Boson decays into an electron and neutrino," 2024

Enerdata, "World Energy Consumption Statistics," *Enerdata.net*, 2024. https://yearbook.enerdata.net/total-energy/world-consumption-statistics.html

H. Abu-Shawareb *et al.*, "Achievement of Target Gain Larger than Unity in an Inertial Fusion Experiment," *Physical Review Letters*, vol. 132, no. 6, Feb. 2024, doi: https://doi.org/10.1103/physrevlett.132.065102.

H. Dholakiya, Engineering Funda, “Engineering Funda,” *YouTube*. 2024. Accessed: Aug. 03, 2024. [YouTube Video]. Available: https://www.youtube.com/watch?v=6OZLl689pi0

H. Domenech, *Nuclear Materials*. CRC Press, 2024.

Hamamatsu, “Photomultiplier Tubes And Assemblies For Scintillation Counting & High Energy Physics,” 2024. Available: https://www.hamamatsu.com/content/dam/hamamatsu-photonics/sites/documents/99_SALES_LIBRARY/etd/High_energy_PMT_TPMZ0003E.pdf

HFIR, “High Flux Isotope Reactor | Neutron Science at ORNL,” 2024. *neutrons.ornl.gov*. https://neutrons.ornl.gov/hfir

International Centre for Theoretical Sciences, “Elastic and Deep Inelastic Scattering (Lecture 1) by V. Ravindran,” *YouTube*, Jan. 29, 2024. https://www.youtube.com/watch?v=sSbAKRQCfRk (accessed May 18, 2024).

J. Dow, “This company wants to turn a Tennessee coal plant into a fusion reactor,” *Electrek*, Feb. 21, 2024. https://electrek.co/2024/02/21/this-company-wants-to-turn-a-tennessee-coal-plant-into-a-fusion-reactor/ (accessed Oct. 30, 2024).

Luxium, “Efficiency calculator,” *Luxiumsolutions.com*, 2022. https://luxiumsolutions.com/efficiency-calculator (accessed Sep. 22, 2024).

M. Perini, et al., “Technical description,” *vIOLETA Experiment*. https://www.violetaexperiment.com/skipper-ccd/technical-description-1 (accessed Jul. 18, 2024).

M. Thomson and Cambridge University Press, *Modern particle physics*. Cambridge: Cambridge University Press, version 10, 2024.

O. Dalager, “Measurement of the θ13 Neutrino Mixing Angle at Daya Bay via Neutron Capture on Hydrogen,” Dissertation, University of California, Irvine, 2024. Accessed: Oct. 11, 2024. [Online]. Available: https://www.proquest.com/docview/3059241242

OpenAI, “Skipper CCDs detect the translation from nuclear recoil energy to ionization energy,” *ChatGPT*, 2024. https://chatgpt.com/

ORNL, “What is CEvNS – COHERENT | ORNL,” *coherent.ornl.gov*. https://coherent.ornl.gov/what-is-cevns/ (accessed Jul. 06, 2024).

United Nations, “Causes and effects of climate change,” *United Nations*, 2024. https://www.un.org/en/climatechange/science/causes-effects-climate-change

United Nations, “World Population Prospects 2024, Summary of Results”, 2024.

Wikipedia, "Mathematical formulation of the Standard Model," 2024

VITA

Robert J. Carter was born in Atlanta, Georgia, 1953 and moved to Tennessee at six. After graduating from Fulton High School in Knoxville, he attended the University of Tennessee and graduated with honors in 1978 with a Bachelor of Science in Electrical Engineering. Mr. Carter worked for Bell Telephone and International Business Machines in semiconductor development before joining the United States Air Force.

Colonel Carter served as a mission crew commander in the Advanced Range Instrumentation Aircraft, 4950th Test Wing, Wright-Patterson Air Force Base (WPAFB), Ohio supporting the Department of Defense and National Aeronautics and Space Administration (NASA) manned and unmanned space launches and reentry. After completing undergraduate flying training in T-37 and T-38 aircraft at Reese Air Force Base, Lubbock, Texas, Colonel Carter flew CT-39, C-12F, Airborne Warning and Control (AWAC), and Boeing 707 aircraft. During his Air Force flying career, he continued working part-time at the Flight Dynamics Laboratory, WPAFB, Ohio. He graduated with the highest honors, earning a Master of Science in Electrical Engineering from a combined curriculum at Ohio State University and the University of Dayton in 1985.

Transferring from active duty to the reserves, Colonel Carter flew for United Airlines in the Boeing 727, 737, and 747 while serving as an electrical engineer in the Air Force Reserve. He worked with the Aerospace Corporation, Los Angeles Air Force Station, California, NASA, and Langley-Research and Development Center, Virginia. Colonel Carter served as the senior reservist to the Science and Technology Air Vehicles

Development Directorate, WPAFB Ohio, and Air Force Liaison to Oak Ridge National Laboratory (ORNL), Tennessee, completing his 16th year of employment as a staff engineer.

Colonel Carter graduated from the Federal Law Enforcement Training Center, Artesia, New Mexico, in 2002 following the September 11, 2001, terrorist attacks on the United States. He served as a part-time Federal Flight Deck Officer (FFDO) and technical consultant to the Department of Homeland Security for fourteen years.

While employed by ORNL, Colonel Carter became the first part-time PhD candidate in the University of Tennessee's Energy Science and Engineering cohort program. He continues to split his time between two groups at ORNL: Electronics and Embedded Systems and Nuclear Material Detection and Characterization. Colonel Carter retired from the Air Force in 2013 and then from United Airlines and FFDO in 2018.